Towards Deep Sea Mining – Impact of mining activities on benthic pelagic coupling in the Clarion Clipperton Fracture Zone

Dissertation

Zur Erlangung des akademischen eines Doktors der Naturwissenschaften

-Dr. rer. nat.-

Im Fachbereich Geowissenschaften der Universität Bremen

Benjamin Gillard

Bremen
July 2019

Die vorliegende Arbeit wurde in der Zeit von November 2015 bis Juli 2019 an der MARUM – Zentrum für Marine Umweltwissenschaften der Universität Bremen und Jacobs University Bremen erarbeitet.

Autor: **Benjamin Gillard, M.Sc.**

MARUM- Zentrum für Marine Umweltwissenschaften

Universität Bremen

Jacobs University

Datum des Promotionskolloquiums: 29 November 2019

Gutachter: **Prof. Dr. Morten H. Iversen**

MARUM - Zentrum für Marine Umweltwissenschaften

Universität Bremen

AWI- Alfred-Wegener-Institut für Polar und Meeresforschung

Prof. Dr. Andrea koschinsky

Jacobs University

“Challenges are what make life interesting; overcoming them is what makes life meaningful”

Ralph Waldo Emerson

SUMMARY

As the worldwide metal demand is drastically increasing, and the metal supply are limited, countries and industries have prospected the deep-sea for their precious resources. Polymetallic nodules form on the seafloor and are rich in metals such as manganese, cobalt, and copper. Due to their economic potential, polymetallic nodules have been targeted for mining during the past three decades. The highest nodule's abundance so far has been found in the Clarion Clipperton Zone (CCZ) where currently 16 license areas have been issued for exploration only. Very limited information is available to assess the anthropogenic impact of mining activities on this fragile ecosystem. The main objective of this dissertation is to evaluate the impact of sediment plumes released during mining activities on the benthic and pelagic environment.

The oceanographic description of the eastern German License area (CCZ) indicated that surface waters were influenced by nutrient-enriched water coming from the Mexican coastal area. During winter a depleted transitional zone appeared between these water masses and the highly productive water of the equatorial region. The vertical particle distribution was investigated using a combination of high definition camera images and CTD sensors. Specific water characteristics such as the oxygen minimum zone (OMZ) was identified and appeared to be strongly correlated to particulate matter alteration, distribution and transfer to greater depths. Overall, median particle sizes are small (77µm), and bigger particles (>300 µm) were rarely encountered.

Polymetallic nodules occur in the CCZ abyssal plains which are made of fine siliceous ooze sediments (d_{50}= ± 20 µm). The anticipated impact of mining activities was tested by reproducing variable sediment plumes concentration (35–500 mg·L^{-1}) and turbulence rate (0–10.4 s^{-1}). The most rapid sediment plume flocculation was found using a high sediment discharge (500 mg·L^{-1}) combined with a turbulent shear rate of ≥ 2.4 s^{-1}. The modeling results simulating four days of plume release suggested that mining under "normal" flow conditions (± 4 cm·s^{-1}) would result in a relatively fast deposition of particles, thus restricting the blanketing effect to a relatively small fall-out area (up to 4 km downstream). Setting such sediment plumes requirements (sediment concentration and turbulence rate) should, therefore, be considered for the design of the mining collector exhaust pipe. To date, the work in this thesis represents the most advanced and complete dataset freely available to everyone.

The bacterial community associated with the sediment plume was investigated using a cultivation-based approach. In total, 40 fast-growing bacterial strains belonging to 13 fast-growing bacterial species were identified. Based on their phenotypic characterization and heavy metals resistance, three potential organisms were found to be potential model systems for future ecological studies. Intra-species variabilities were not only found in phenotypic profiles but also in heavy metal tolerance although the taxonomic marker 16s rRNA sequences were almost identical. We proposed the use of API strips and partial-enrichment media that can easily be implemented on-board for rapid and cost-effective monitoring of deep-sea mining plume dispersion using microbial dissemination analyses. In this context, heavy-metal resistance analysis provides new scope for future research on Mn^{2+} resistance pathways and their role in microbial dispersion from anthropogenic impacts on deep-sea environments.

The exploitation of deep-sea resources is developing faster than policies are established and still requires extensive exploration. A precautionary approach based on environmental awareness and the history of similar activities suggest that deep-sea mining will have an impact on the marine environment. However, if mining is approved, the studied impacts will play a crucial role in regulating the mining activities. Overall, this thesis complements the scientific efforts made by describing the deep-sea environment and provide valuable knowledge on how to reduce the environmental impacts from sediment plumes released during mining activities in the CCZ.

ZUSAMMENFASSUNG

Durch die drastisch steigende, weltweite Nachfrage an Metallen und die gleichzeitig begrenzte Verfügbarkeit sind die Rohstoffresourcen der Tiefsee in den Fokus von Ländern und Industrie gerückt. Polymetallische Knollen, die sich am Meeresboden bilden, sind reich an Metallen wie Mangan, Kobalt und Kupfer und wurden auf Grund ihres wirtschaftlichen Potentials in den letzten drei Jahrzehnten als mögliche Ressource untersucht. Die weltweit höchste Dichte wurde bisher in der Clarion Clipperton Zone (CCZ) gefunden, wo bis heute 16 Lizenzgebiete ausschließlich zur Erkundung vergeben wurden. Um die anthropogenen Auswirkungen des Abbaus auf das empfindliche Ökosystem einschätzen zu können, liegen der Wissenschaft derzeit nur begrenzt Informationen vor. Das Hauptziel dieser Dissertation war es, die Auswirkungen der beim Abbau freigesetzten Trübungswolke auf die benthische und pelagische Umwelt zu bewerten.

Die ozeanographische Beschreibung des östlichen deutschen Lizenzgebietes zeigte, dass das Oberflächenwasser vom nährstoffreichen Wasser der mexikanischen Küste beeinflusst wird. Im Winter entsteht eine nährstoffarme Übergangszone zwischen diesen Wassermassen und der hochproduktiven äquatorialen Zone. Zur Untersuchung der vertikalen Partikelverteilung wurden HD Kameraaufnahmen kombiniert mit CTD Sensordaten verwendet. Hierbei wurden spezielle Eigenschaften der Wassersäule wie zum Beispiel die Sauerstoffminimumzone identifiziert und es zeigte sich, dass diese stark abhängig sind von Partikelalteration und –verteilungen sowie von dem Transport in die Tiefe. Insgesamt war der Median der Partikelgrößen eher klein (77 µm) und größere Partikel (>300 µm) kamen selten vor.

Polymetallische Knollen kommen in der Tiefseeebene der CCZ mit Kieselschlamm vor (d_{50} = ± 20 µm). Um den potentiellen Einfluss vom Abbau der polymetallischen Knollen zu testen wurde verschiedene Trübungswolkkonzentrationen (35–500 mg·L^{-1}) und Turbulenzraten (0–10.4 s^{-1}) reproduziert. Eine sehr schnelle Aggregation dieser Tiefsee-Sedimente in einer durch Tiefseebergbau produzierten Trübewolke fand bei Labor-Experimenten mit Original-Sedimenten des Arbeitsgebietes bei hohen Partikelkonzentrationen (500 mg L^{-1}) in Kombination mit Scherraten von ≥ 2.4 s^{-1} statt. Modelberechnungen zum Verteilungsverhalten der Trübungswolke über einen simulierten Zeitraum von vier Tagen zeigten, dass die Ablagerung der beim Knollenbau entstehenden Partikel unter „normalen“ Strömungsbedingungen (± 4 cm s^{-1} stromabwärts)

relativ schnell geschehen und sich damit der sogenannte Blanketing Effect (Sediment-Bedeckungseffekt) auf eine relativ kleine Fläche beschränken würde (bis zu 4 km Entfernung). Diese Bedingungen (Sedimentkonzentration und Turbulenz) sollten deshalb bei der Konstruktion des Kollektors speziell für den Sedimentauslass berücksichtigt werden. Aktuell beinhaltet diese Arbeit den detailliertesten und vollständigsten frei zugänglichen Datensatz.

Die sich in der Trübungswolke befindenden Bakterien wurden mit Hilfe von Kultivierungsexperimenten untersucht. Insgesamt wurden 40 schnell wachsende Bakterienstämme von 13 verschiedene Bakterienspezies identifiziert, von denen bis zu drei für zukünftige öko-toxikologische Untersuchungen in Frage kommen. Intraspezifische Variationen wurden nicht nur im Phänotyp sondern auch in der Schwermetalltoleranz beobachtet, obwohl die taxonomischen 16s rRNA Sequenzen fast identisch waren. Wir schlagen vor mit Hilfe von API Strips und teilangereicherten Nährmedien mikrobielle Analysen an Bord durchzuführen, um ein schnelles und kostengünstiges Monitoring der Sedimentdispersion beim Tiefseebergbau zu ermöglichen. In diesem Zusammenhang hat sich gezeigt, dass die Untersuchung der Mn^{2+} resistenten Stoffwechselwege und ihrer Rolle in der mikrobiellen Dispersion durch anthropogene Auswirkung auf die Umwelt der Tiefsee, ein weiteres Forschungsfeld darstellt. Unsere Genomanalyse deutet auf das Vorhandensein von Efflux-Systems hin, welcher Gegenstand zukünftiger transkriptomischer oder proteomischer Untersuchungen sein könnten.

Die technologische Entwicklung zur Nutzung von Tiefseeressourcen verläuft momentan schneller als die Erstellung von Richtlinien für den Tiefseebergbau, welche noch weitere umfangreiche Untersuchungen erfordert. Unter Berücksichtigung des Vorsichtsprinzips im Hinblick auf mögliche Umweltschäden und bisheriger Erfahrungen mit ähnlichen Aktivitäten sollte kein Tiefseebergbau stattfinden. Wenn der Abbau dennoch genehmigt wird, können die bisher erhobenen Daten entscheidend dazu beitragen entsprechende Richtlinien zu entwickeln. Insgesamt ergänzt diese Arbeit den wissenschaftlichen Beitrag zur Erforschung der Tiefsee und zeigt Möglichkeiten auf, wie die Auswirkungen der beim Abbau in der CCZ freigesetzten Trübungswolken verringert werden können.

ACKNOWLEDGMENTS

First of all, I would like to thank my thesis supervisors: Morten Iversen, Laurenz Thomsen, Matthias Ullrich, and Nicolas Nowald. This work would not have been possible without your support, guidance, and fruitful discussions. As a multidisciplinary research project, I continue to be astonished by your invaluable knowledge and expertise in your respective fields. You were all great mentors and have taught me very different approaches and work styles that I believe made me the open-minded scientist that I am today. I want to express my gratitude to Laurenz Thomsen for taking me under his wing at the OceanLab. You showed me the world of particle dynamic and provided me with a fantastic working environment. Three years later, I am still there and looking forward to all the things to come. You gave me the opportunity and time to develop many instruments in close collaboration with engineer and technician, which taught me many skills that are often missing in the scientific world.

Many other people substantially contributed to this thesis. I would like to thank my co-authors (Damianos Chatzievangelou, Rob Harbor, Kaveh Purkiani and Annemiek Vink), the scientific group of marine resource of BGR Hannover and crew of the R/V SONNE cruise. Without your effort and support, this work would have most probably not existed.

To my colleagues and friends at the OceanLab, Microbiology laboratory and SeaPump groups: Dr. Song Wang, Damianos Chatzievangelou, Dr. Charly Kleint, Annika Moje, Dr. Sophie Paul, Dr. Dennis Krämmer, David Ernst, Clara Flintrop and many others. What a lovely time we spend together, it was great getting to know you all. It was a blast!

Thanks to all my closest friends and family for your support, encouragement, and being there for me all those years.

Finally, dear Jo, thank you so much for sharing my life and your love every day. You always took care, supported and recalling me back to the real world over those years.

Benjamin Gillard
Bremen, June 2019

ABBREVIATIONS

BBL	Benthic boundary layer
CCZ	Clarion Clipperton fracture zone
Chla	Chlorophyll-a
CTD	Conductivity temperature density
DFC	Digital floc camera
DOC	Dissolved organic carbon
DW	Deep water
ESD	Equivalent spherical diameter
ESV	Equivalent spherical volume
HYCOM	Hybrid coordinate ocean model
LCPW	Lower Circumpolar Water
LISST	Laser in-situ scattering and transmissometry
MB	Marine broth
MIC	Minimal inhibitory concentration
MUC	Multiple corer
NEC	North equatorial current
NECC	North equatorial counter current
NPDW	North Pacific Intermediate Water
NPIW	North Pacific Intermediate Water
NPP	Net primary productivity
OMZ	Oxygen minimum zone
PCR	Polymerase chain reaction
POC	Particulate organic carbon
SST	Sea surface temperature
TML	Thermocline layer
TSW	Tropical surface water
TZCF	Transition zone chlorophyll front
WA	Working area

Contents

LIST OF PAPERS

Manuscript I

Gillard, B., Harbour, R. P., Nowald, N., Thomsen, L., Iversen, M.H., From the surface to the seafloor: vertical profile of particulate matter in the Clarion Clipperton fracture zone (eastern-central Pacific). In preparation for submission to *Progress in Oceanography*.

Manuscript II

Gillard, B., Purkiani, K., Chatzievangelou, D., Vink, A., Iversen, M.H. and Thomsen, L., 2019. Physical and hydrodynamic properties of deep sea mining-generated, abyssal sediment plumes in the Clarion Clipperton Fracture Zone (eastern-central Pacific). Elem Sci Anth, 7(1), p.5. DOI: http://doi.org/10.1525/elementa.343

Manuscript III

Gillard B, Chatzievangelou D, Thomsen L and Ullrich MS (2019) Heavy-Metal-Resistant Microorganisms in Deep-Sea Sediments Disturbed by Mining Activity: An Application Toward the Development of Experimental in vitro Systems. Front. Mar. Sci. 6:462. DOI: 10.3389/fmars.2019.00462

1 INTRODUCTION

1.1 Deep-sea mining and minerals resources

Over the last decades, the worldwide demand for metals and rare earth elements has drastically intensified, especially from rapidly expanding countries, such as India and China. These extreme market demands are mainly explained by technological advancement, green energy transition, and worldwide expanding civilization (Beyond mining, 2011). Due to the limited metal suppliers, a possible shortage in the near future have pushed industries and countries to prospect for enriched mineral deposits from the deep-sea environment (Hein et al., 2013).

The presence of deep-sea ores on the seafloor has been known for more than a century. Three types are currently being considered as potential resources due to their economic potential (Figure 1; Hein et al., 2013; Miller et al., 2018): ferromanganese crust (on seamounts; Hein and Koschinsky, 2014), massive sulfides (beneath hydrothermal vents; Boschen *et al.*, 2013) and polymetallic nodules (on the seafloor; focus of this Ph.D. thesis). However, the relatively stable market price as well as the slow technological advancements for processing the associated minerals have resulted in low mining activities since the 1980s. During the past decade, underwater technology has improved considerably, rendering deep-sea mining profitable.

Since 1994, the International Seabed Authority (ISA) has managed the regulation and control of all mining-related activities in international waters, beyond the exclusive economic zones (EEZ). This intergovernmental agency has reinforced regulations and imposed to assess the potential environmental impact of mining activities before any exploitation may begin.

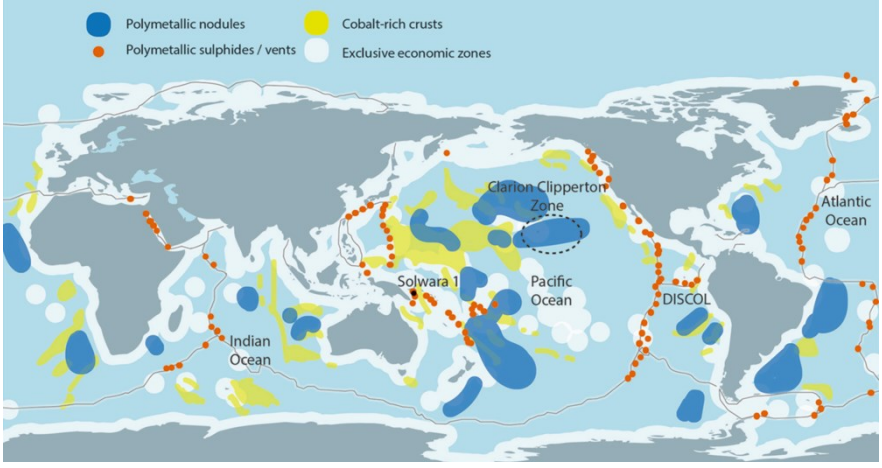

Figure 1. Global map showing the location of the three primary marine mineral deposits (Miller *et al.*, 2018).

1.1.1 Polymetallic nodules

Polymetallic nodules were discovered in 1868 during the H.M.S. Challenger expedition, (Figure 2a). Nodules are marine concretions ranging from 1 – 12 cm (Kuhn et al., 2017), mainly composed manganese andiron oxides as well as copper (~1%), nickel (~1.3%) and cobalt (0.2) (Hein and Koschinsky, 2013). They may occur on the abyssal seafloor of every ocean at a depth between 4000 and 6000 m, where the water is oxic and sedimentation rate is less than 10 mm/Kyr (Gollner et al., 2017). Their genesis (Figure 2b) is not fully understood, but results in metal precipitation around a nucleus (e.g., fish bones, shark tooth or any hard substrate) of two types:

- Hydrogenetic growth (1– 5 mm/myr; Koschinsky, Winkler and Fritsche, 2003) , in which the metals are precipitated from the water column.
- Diagenetic growth (up to 250 mm/myr; Von Stackelberg, 2000), in which the metals are precipitated from the sediment pore waters.

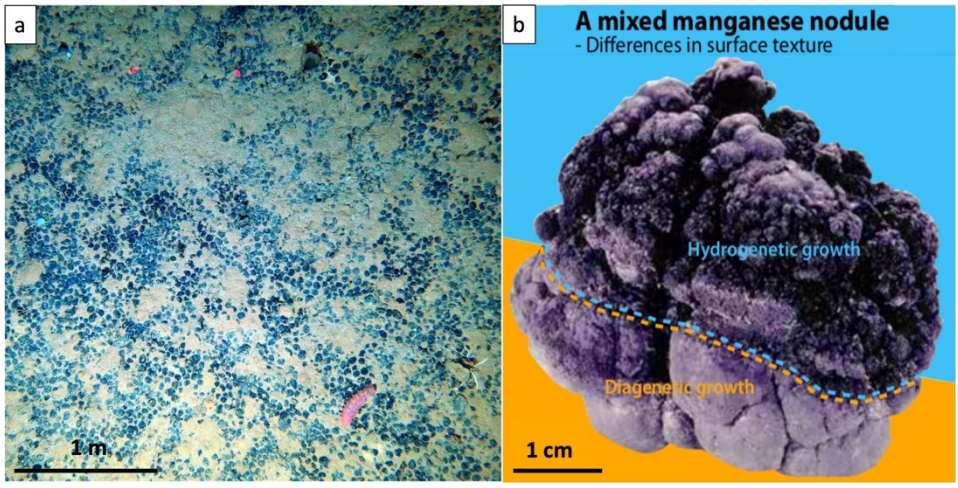

Figure 2. Deep sea polymetallic nodules.
(a) North Pacific seafloor showing nodules field in the Clarion Clipperton Zone. Photograph from the Bundesanstalt für Geowissenschaften und Rohstoffe. **(b)** Nodule formation process (Hein & Petersen, 2013).

Their metal content varies between locations and depends on water properties and growth mechanisms of the nodules. Overall, the average growth of polymetallic nodules is 10 – 20 mm per million years (Kuhn et al., 2017), which make them one of the slowest geological formations on earth. The highest nodule concentration (metal-rich) is found in the "manganese nodule belt" in the Clarion Clipperton Zone (CCZ, north equatorial Pacific; Figure 1) with a dry weight estimation of 21,100 million tones (ISA, 2010).

1.1.2 Study site

The Clarion Clipperton zone (CCZ) is located in the north-eastern equatorial Pacific, with an extent of 4.5 million km² (Figure 3). The area is bordered by the Clarion fracture (North) and Clipperton fracture (South). The bottom topography is formed of numerous seamounts, NW - SE ridge systems but mostly made of flat abyssal plains at a depth of 4000 - 5000 m. The sediment is characterized by siliceous ooze and mud (Berger, 1976), an oxygen penetration depth of 1 – 4.5 m (Mewes et al., 2016; Volz et al., 2018), a calcite compensation depth at around 4600 m depth (Verlaan et al., 2004) and an extreme low sedimentation rate of 1–2 mg C_{org}/m^2 d (Vanreusel *et al.*, 2016; Figure 7). Due to the extensive nodule coverage and their high metal contents, the International Seabed Authority has issued, to date, 16 licenses for exploration (Figure 3), indicating a strong interest of mining companies and countries.

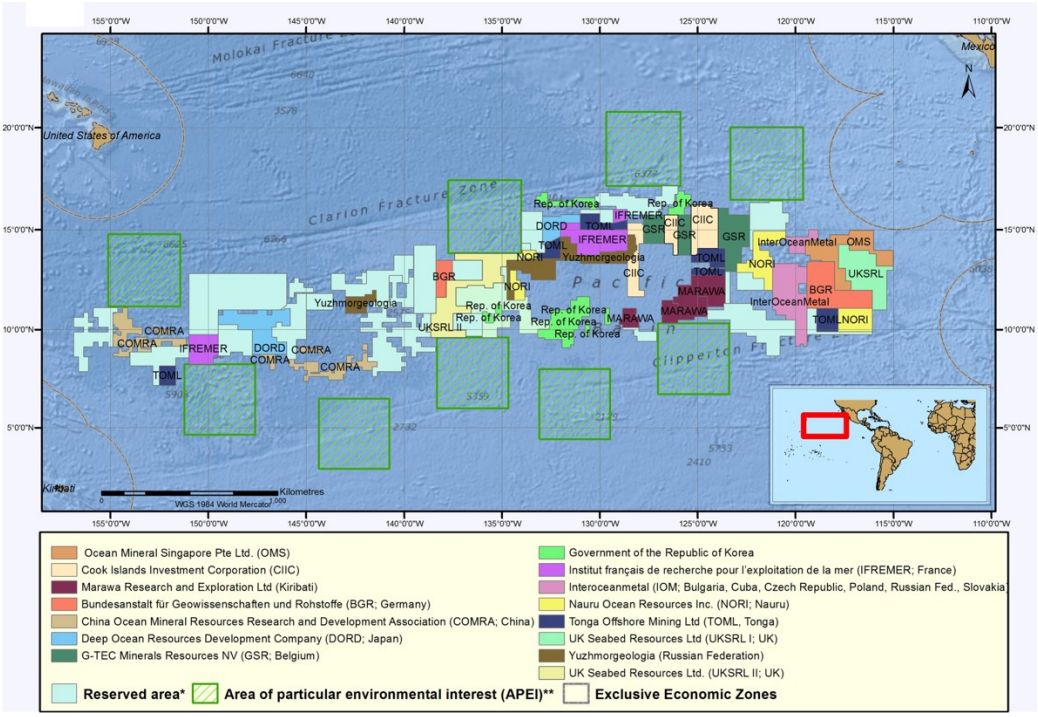

Figure 3. Polymetallic nodules exploration areas in the Clarion Clipperton fracture zone. (ISA, 2014)

1.1.3 Deep-sea mining technology

Due to technological limitations, only a few mining trials have successfully extracted nodules from the seafloor but did pave the way for the next generation of deep-sea mining nodule collectors. In 1978, two pilot mining tests were conducted by the Mining Inc. (OMI) and the Ocean Mining Associates (OMA) in the North equatorial Pacific

using the first described hydraulic collector system (Ozturgut et al., 1981). The system uses a water jet to lift the nodules from the seafloor using low pressure and scouring action (Figure 4c, d). The latest collector design and the most technologically advanced system was launched in September 2018 by Global Sea Mineral Resources (GSR, Belgium, Figure 4b). The collector prototype, with a dimension of 12 x 4.7 x 4.5m (length x width x height) and a nominal speed of 0.5 m/s, does not include any rising system to the surface ocean yet and can be divided into four major's components:

(1) Nodule collector head: that will harvest nodules using a water jet pump system (Figure 4a, b, c, d) with flow velocity control system and sensors to position the collector's head (e.g., altimeter).

(2) Propulsion system: a two-caterpillar propulsion system specifically design for deep-sea floor.

(3) Nodule separator and exhaust system: Once collected, nodules and sediment will move up inside the collector. Gravity will separate nodules from water/sediment and collected in a bucket. Discharge of sediment will be at the back of the collector towards a diffusor-exhaust.

(4) Vehicle: that comprise the frame and all components for the system functioning.

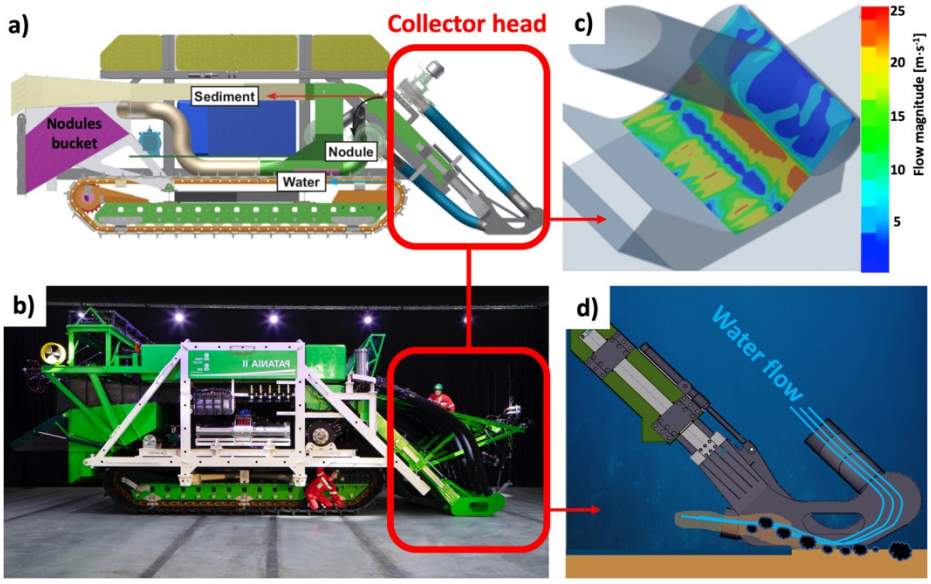

Figure 4. Deep sea mining collector Patania II.

(a) Schematic drawing of the crawler. **(b)** Launched of Patania II September 2018. **(c)** Collector head system showing water jets flow field magnitude. **(d)** Overview of nodule extraction. Images credit: Global Sea Mineral Resources (GSR)

1.1.4 Deep-sea mining concept and potential environmental impacts

The mining concept developed by Bath and Gregor (1988) and re-adapted by Oebius *et al.* (2001) is at present the most realistic approach for a full industrial mining operation (Figure 5). The system consists of:

(1) A mining platform: Directly on the vessel or as a platform located at the sea surface to separate the nodules from the sediment. The processed water will be directed back into the sea, preferably at a depth of the collector.

(2) Riser system: consist of a hydraulic transport for the nodules recovery using a rigid pipe. The nodule will be lifted using a buffer pump system and multistage pumps throughout the riser, which will assure sufficient water flow rate.

(3) A mining collector system: described in section 1.1.3.

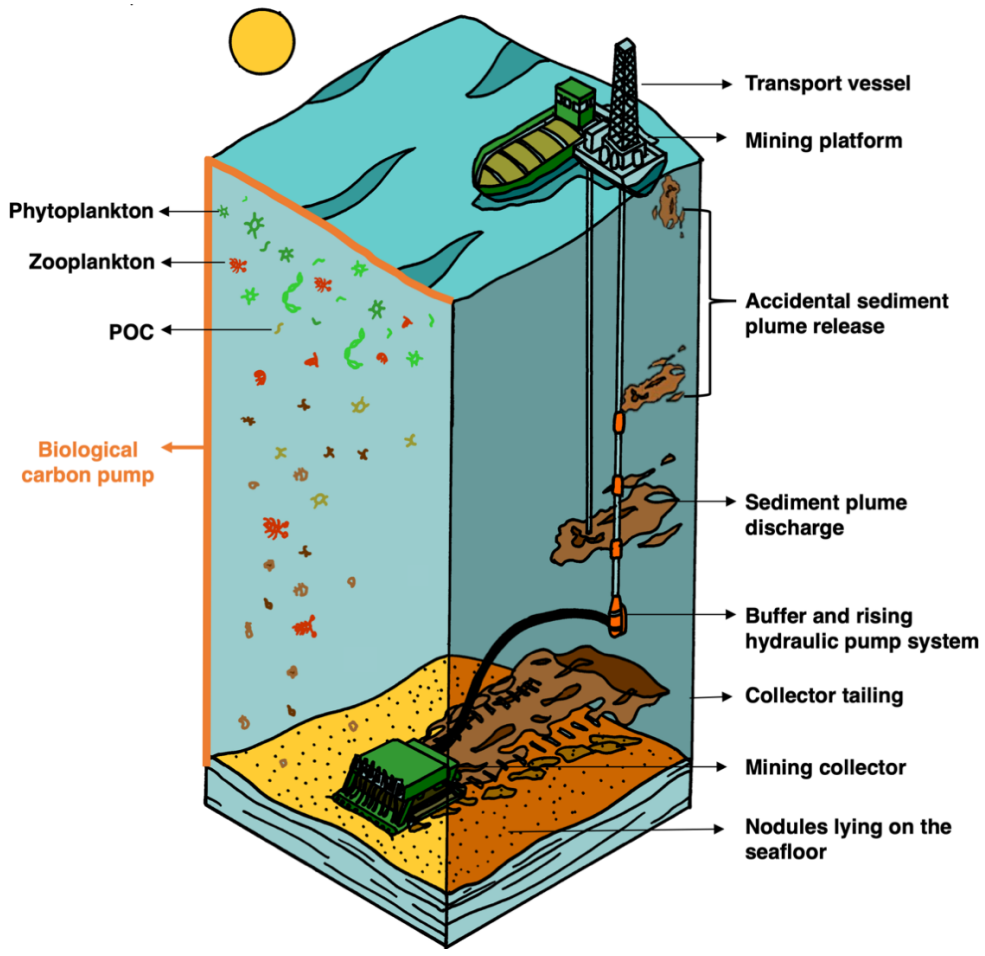

Figure 5. Schematic drawing of a manganese nodule mining concept. Courtesy Dr. Autun Purser

The most significant impact from mining activity is expected to arise from the collector on the seafloor and its interaction with the sediment (removal and compaction). The predicted impact includes habitat destruction, the destruction of sessile fauna depending on nodules (corals, sponges and associated mobile fauna) and disruption of redox zonation in surface sediments with alteration of microbial processes. The sediment discharge (sediment plume) and tailing effect from the collector will result in both a local "close field" and a more spread "far field" impact by the settling of resuspended material to the abyssal seafloor (blanketing effect). The sediment plume settling and resulting blanketing are predicted to potentially release toxic metals from the sediment pore water, bury benthic organisms, clog the respiratory surfaces of filter feeders and pollute the food supply for most benthic organisms (Gollner et al., 2017; Jones et al., 2017; Ramirez-Llodra et al., 2011; Vanreusel et al., 2016).

As the history of offshore activity has proven (e.g., 2010 Deepwater Horizon oil spill, 1989 Exxon Valdez oil spill), accidents and waste spills into the water column might occur at any time and have to be considered. For example: It cannot be ruled out that the mining platform may release increased concentrations of inorganic nutrients and trace metals into the euphotic zone that may interfere with natural particle fluxes and disrupt the biological carbon pump and microbial loop. Additionally, the riser system may fail or burst, releasing raw material or waste water at any depth, which will affect the benthic-pelagic coupling. Potential water-column impacts are e.g.: reduction of phytoplankton productivity due to the shading effect by the plume in the photic zone, change in zooplanktonic composition due to altered phytoplankton productivity and particle concentration in the upper water column, and trace metal bioaccumulation (Sharma, 2015).

Investigations of environmental impact of seabed disturbance was initiated during OMI mining trial from the Deep Ocean Mining Environmental Study project (DOMES) in 1978 (Jones *et al.*, 2017). After 26 years, the impacted sites were revisited within the framework of the JPI Oceans project Ecological Aspects of Deep-Sea Mining. Overall, fauna communities had gradually recovered but not to the baseline or control conditions from a reference site with a negative biological effect on the seafloor of the mined areas. A multidisciplinary impact assessment was made by the Coral Risk Assessment Monitoring and Modelling project (CORAMM), which investigated the impact of high suspended sediment loads and drill cuttings on cold water coral communities and settling marine snow (Pabortsava et al., 2011). Coldwater corals exposed to a lower dose of sediment

plumes (including drill cutting) caused behavioral changes of the polyps over several days after the plume impact. The combination of environmental monitoring and lab-scale experiments have resulted in recommendations for governments and industries on mining vehicle design and exhaust configurations to minimize ecological impact from mining activities (Thomsen et al., 2008).

1.2 Particle in the marine ecosystem

1.2.1 Organic matter in the ocean

1.2.1.1 Physical and biological carbon pump

The ocean constitutes the second largest carbon sinks on earth (Figure 6; Finkel, 2014; Le Quéré *et al.*, 2018). Exchange of carbon dioxide (CO_2) between the atmosphere and the ocean occurs continuously and is driven by a difference in partial pressure between the air and the water. This phenomenon is called the physical carbon pump and represents the ocean most substantial (≈ 97 %; Falkowski *et al.*, 2000) carbon pool, known as dissolved organic carbon (DIC). Only three percent of this annual carbon pool will be further transformed into biomass and transferred from the ocean surface to the deep-sea, a process known as the biological carbon pump (Figure 7; De La Rocha and Passow, 2007; Finkel, 2014).

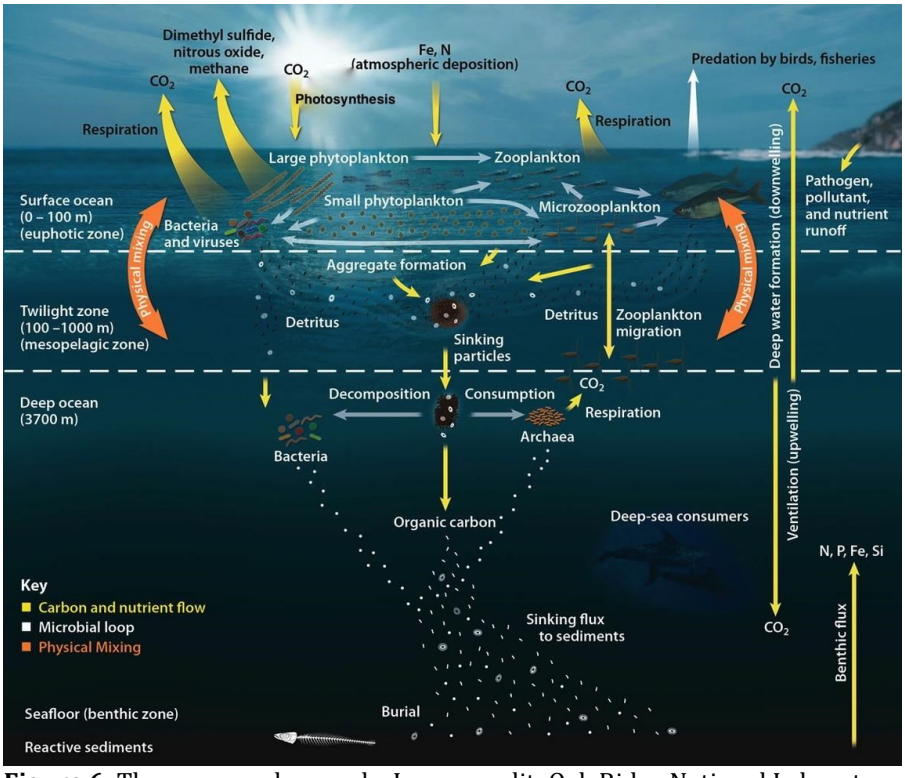

Figure 6. The ocean carbon cycle. Image credit: Oak Ridge National Laboratory

The biological carbon pump is the ocean carbon pathway in which dissolved inorganic carbon (DIC) is converted into particulate organic carbon (POC) and dissolved organic carbon (DOC) during photosynthesis by the phytoplankton (Turner, 2015). This generated biomass is then cycled in the upper ocean within the marine food web through interrelated processes including but not limited to: cells death, grazing from the zooplankton and microbial respiration.

Finally, this reconverted mix of biomass and leaving cells will form dissolve organic matter (DOM) and particulate organic matter (POM) such as aggregates (e.g., marine snow and fecal pellets) that sink out of the euphotic zone to the deep ocean, and thereby, export carbon from the surface. In the upper ocean, carbon flux attenuation seems to be controlled by zooplankton grazing (Iversen and Ploug, 2010, Iversen et al., 2010) while attenuation in the deep ocean is dominated by microbial degradation (Stemmann et al., 2004, Iversen et al., 2010). Bacterial degradation occurs through the entire water column and does continue once the particles have settled into the sediment. At this point, the organic matter is further degraded and becomes increasingly refractory until it is not available for leaving organisms and stored for thousands of years. The biological carbon pump accounts for 70 % (Passow and Carlson, 2012) of the carbon export to the deep-sea environment but is extremely inefficient with only 1 – 3 % of the surface ocean production reaching the seafloor (Ducklow, Steinberg and Buesseler, 2001; Figure 7). Overall, the export of POC to the deep-sea environment is driven by the phytoplanktonic surface composition, intensity of the net primary productivity and the efficiency of the biological carbon pump (Lutz et al., 2002). In the CCZ study area, POC flux decreases West-Northward toward the North Pacific gyre system (Figure 7).

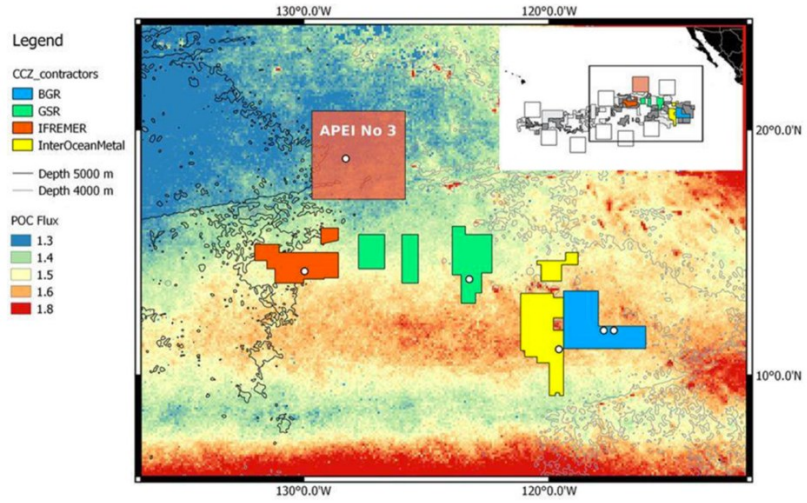

Figure 7. POC flux to the deep-sea in the Clarion Clipperton Zone.
(Vanreusel et al., 2016 ; POC raw data from Lutz et al. 2007)

1.2.1.2 Theory of aggregate formation

In the marine ecosystem, particle interactions and transformations (aggregation, disaggregation) occur continuously. Aggregate are made of primary suspended particles that must collide by physical prosses and stick together upon collision (Kiørboe, 2001). Aggregation rates are mainly controlled by their surrounding environment (turbulence) but also by their own random movement (Brownian motion) and the differences between particle sizes and settling velocities (differential settling) (McCave, 1984). Three processes are driving aggregate formation (Thomsen and McCave, 2000): (i) particles must be brought into close proximity, a process called "encounter", (ii) these particles must be brought into direct contiguity by the flow fields surrounding them, a process called "contact", (iii) the particles must "stick together". The encounter rate is a function of particle size, concentration, settling velocity and turbulence, whereas contact and stickiness are related to the relative particle size and physicochemical properties of the particles.

1.2.1.3 Deep-sea sediment

The deep-sea environments account for 65 % of the earth surface and 95 % of the global biosphere (Herrin, 2001; Thistle, 2003). It is the least known biome in the world, with only 0.001 % that has been sampled and described in terms of biodiversity (Danovaro, Snelgrove and Tyler, 2014). The epifaunal investigation is relatively young but has shown a high species diversity (e.g., Hydrozoa, Anthozoa, Echinodermata, and Porifera) with a low individual's density in nodule areas of the CCZ (e.g., 14 – 30 individuals·100m^{-2}; Vanreusel et al., 2016). Hidden inside the sediment, 0.6% of Earth's total living biomass is represented by microbes with at least 2.9 x 10^{29} cells (Whitmann, Coleman and Wiebe, 1998; Kallmeyer *et al.*, 2012). They are key organisms for organic matter re-mineralization, nutrient cycling, and energy transfer to sustain higher benthic trophic levels (Nealson, 1997). In comparison to the water column, sediment and nodule bacterial assemblages appear to be very distinct from each other (Figure 8a, Lindh et al., 2017). In the sediment, their distribution and community's composition changes according to the electron acceptor availability and redox stratification (Figure 8b, Sorensen *et al.*, 2004; Durbin and Teske, 2011).

In the CCZ, oxygen penetration depth in the sediment is between 1 – 4.5 m (Kuhn, 2015), which suggests that there is high POC degradation in the surface sediment due to the aerobic conditions. Generally anoxic sediments (e.g., continental margin) have 10 – 100 times lower degradation than oxic condition (Aller, 1994). Surprisingly, even under those oxic, clod (1.5°C) and high-pressure conditions, the sediment microbial community is known to change and fluctuate within one week when exposed to phytodetritus (Kanzog et al., 2009). Often benthic remineralization of POC is dominated by microbes while metazoan and macrofauna only play a minor role (Sweetman et al., 2019).

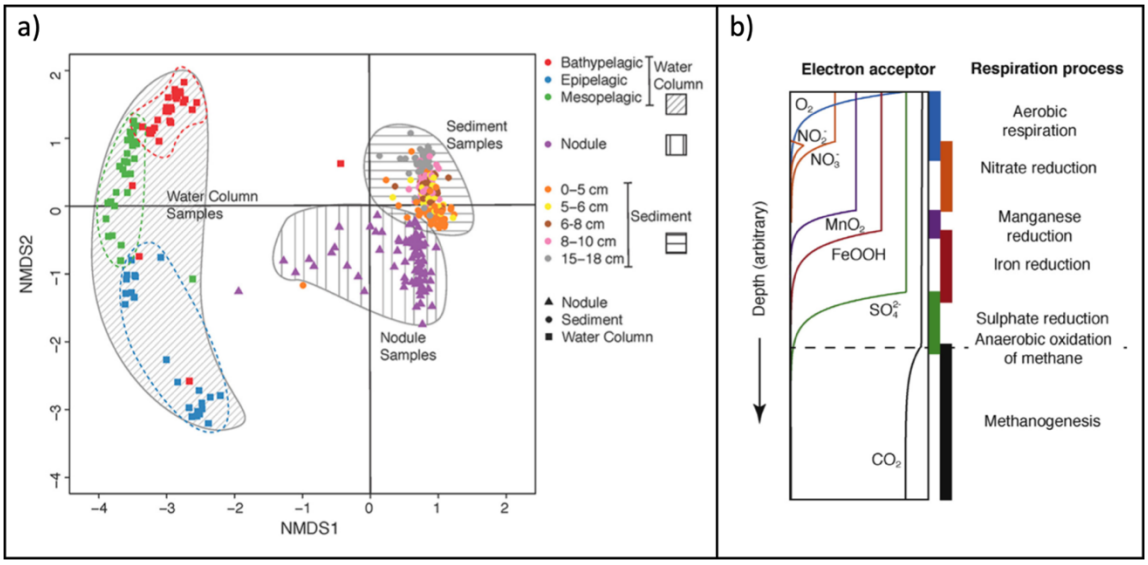

Figure 8. (a): Microbial community dissimilarities (Lindh et al., 2017). **(b)** Redox paradigm (Robert,2015)

1.3 Aim and outline of the thesis

1.3.1 General objective

The impact of deep-sea mining activities is expected to drastically affect pelagic and benthic ecosystems. However, the impact from deep-sea mining is still largely unknown. As part of an interdisciplinary research approach, the general aim of this PhD thesis is to characterize particle fluxes and the impact of sediment plume transport from mining activity in an oligotrophic area of the Pacific (Clarion Clipperton fracture zone). Very little is known about the sediment and generated plumes concentrations of biologically available heavy metals and the abundance of bacterial heavy metal resistance at micro-scale. Our results will help to predict the long-term impact of nodule mining on export flux to the deep sea by improving monitoring techniques and sediment plume model reliability.

1.4 Scientific questions

(1) What is the oceanographic setting of the area?
Manuscript I

(2) How is particulate matter distributed in the water column and what it is the fate of the organic matter in terms of aggregate distribution, transport and turnover processes?
Manuscript I

(3) What is the size-distribution of the sediment and how do different hydrodynamics regimes affect the formation of sediment plumes?
Manuscript II

(4) What is the maximum sediment plume concentration that can be released due to mining activity under different hydrological conditions in order to minimize the environmental (biological) impacts?
Manuscript II

(5) Can deep-sea bacteria be isolated from the CCZ sediments and cultivated and characterized for laboratory studies?
Manuscript III

(6) Are sediment bacteria from CCZ heavy metal resistant and what mechanisms confer such a resistance?
Manuscript III

1.5 Hypothesis

1. Vertical profiles of particulate matter distribution using a camera system will highlight short term particles transformations that may explain mechanisms for carbon flux attenuation and the low organic matter sedimentation to the seafloor at CCZ.

2. The use of site-specific sediment particle behavior under different plume concentrations and current regimes will help to determine an optimum sediment plume release from mining activity that will limit the impacted area in the CCZ.

3. Heavy-metal-resistant and -sensitive bacterial strains can be isolation and characterization from CCZ abyssal sediments. These isolations will help to establish experimental in vitro systems to study the dispersal of microorganisms within sediment plumes released during mining activity under different biotic and abiotic environmental conditions.

Reference

Aller, R. C. (1994). Bioturbation and remineralization of sedimentary organic matter: effects of redox oscillation. *Chem. Geol.* 114, 331–345. doi:10.1016/0009-2541(94)90062-0.

Berger, W. H. (1976). Biogenous deep sea sediments: production, preservation and interpretation. *Chem. Oceanogr.* 5, 266–387.

Beyond mining (2011). *Nat. Geosci.* 4, 653–653. doi:10.1038/ngeo1291.

Boschen, R. E., Rowden, A. A., Clark, M. R., and Gardner, J. P. A. (2013). Mining of deep-sea seafloor massive sulfides: A review of the deposits, their benthic communities, impacts from mining, regulatory frameworks and management strategies. *Ocean Coast. Manag.* 84, 54–67. doi:10.1016/j.ocecoaman.2013.07.005.

Danovaro, R., Snelgrove, P. V. R., and Tyler, P. (2014). Challenging the paradigms of deep-sea ecology. *Trends Ecol. Evol.* 29, 465–475. doi:10.1016/j.tree.2014.06.002.

De La Rocha, C. L., and Passow, U. (2007). Factors influencing the sinking of POC and the efficiency of the biological carbon pump. *Deep. Res. Part II Top. Stud. Oceanogr.* 54, 639–658. doi:10.1016/j.dsr2.2007.01.004.

Ducklow, H., Steinberg, D., and Buesseler, K. (2001). Upper Ocean Carbon Export and the Biological Pump. *Oceanography* 14, 50–58. doi:10.5670/oceanog.2001.06.

Durbin, A. M., and Teske, A. (2011). Microbial diversity and stratification of South Pacific abyssal marine sediments. *Environ. Microbiol.* 13, 3219–3234. doi:10.1111/j.1462-2920.2011.02544.x.

Falkowski, P. G., Scholes, R. J., Canadell, J., Canfield, D., Elster, J., Gruber, N., et al. (2000). The Global Carbon Cycle: A Test of Our Knowledge of Earth as a System. *Science (80-.).* 290, 291–296. doi:10.1126/science.290.5490.291.

Finkel, Z. V. (2014). "Marine Net Primary Production," in *Global Environmental Change*, ed. B. Freedman (Springer), 118–124. doi:10.1007/978-94-007-5784-4.

Gollner, S., Kaiser, S., Menzel, L., Jones, D. O. B., Brown, A., Mestre, N. C., et al. (2017). Resilience of benthic deep-sea fauna to mining activities. *Mar. Environ. Res.* 129, 76–101. doi:10.1016/j.marenvres.2017.04.010.

Hein, J. R., and Koschinsky, A. (2013). "Deep-Ocean Ferromanganese Crusts and Nodules," in *Treatise on Geochemistry: Second Edition* (Published by Elsevier Inc.), 273–291. doi:10.1016/B978-0-08-095975-7.01111-6.

Hein, J. R., and Koschinsky, A. (2014). Deep-Ocean Ferromanganese Crusts and Nodules. *Treatise on Geochemistry*, 273–291. doi:10.1016/B978-0-08-095975-7.01111-6.

Hein, J. R., Mizell, K., Koschinsky, A., and Conrad, T. A. (2013). Deep-ocean mineral deposits as a source of critical metals for high- and green-technology applications: Comparison with land-based resources. *Ore Geol. Rev.* 51, 1–14. doi:10.1016/j.oregeorev.2012.12.001.

Herrin, P. (2001). "The dee-sea dimension," in *The biology of the deep ocean* (Oxford University Press).

ISA (2010). A GEOLOGICAL MODEL OF POLYMETALLIC NODULE DEPOSITS IN THE CLARION-CLIPPERTON FRACTURE ZONE; technical study no.6. Kingston, Jamaica Available at: http://www.isa.org.jm.

Iversen, M. H., and Ploug, H. (2010). Ballast minerals and the sinking carbon flux in the ocean: Carbon-specific respiration rates and sinking velocity of marine snow aggregates. *Biogeosciences* 7, 2613–2624. doi:10.5194/bg-7-2613-2010.

Jones, D. O. B., Kaiser, S., Sweetman, A. K., Smith, C. R., Menot, L., Vink, A., et al. (2017). Biological responses to disturbance from simulated deep-sea polymetallic nodule mining. *PLoS One* 12. doi:10.1371/journal.pone.0171750.

Kallmeyer, J., Pockalny, R., Adhikari, R. R., Smith, D. C., and D'Hondt, S. (2012). Global distribution of microbial abundance and biomass in subseafloor sediment. *Proc. Natl. Acad. Sci.* 109, 16213–16216. doi:10.1073/pnas.1203849109.

Kanzog, C., Ramette, A., Quéric, N. V., and Klages, M. (2009). Response of benthic microbial communities to chitin enrichment: An in situ study in the deep Arctic Ocean. *Polar Biol.* 32, 105–112. doi:10.1007/s00300-008-0510-4.

Kiørboe, T. (2001). Formation and Fate of Marine Snow 57. 65, 57–71. Available at: https://moodle.cornwall.ac.uk/pluginfile.php/306155/mod_resource/content/0/marine snow 2001.pdf.

Koschinsky, A., Winkler, A., and Fritsche, U. (2003). Importance of different types of marine particles for the scavenging of heavy metals in the deep-sea bottom water. *Appl. Geochemistry* 18, 693–710. doi:10.1016/S0883-2927(02)00161-0.

Kuhn, T. (2015). Low- temperature fluid circulation at seamounts and hydrothermal pits: heat flow regime, impact on biogeochemical processes and its potential influence on the occurence and composition of manganese nodules in the NE Pacific. SO240 / FLUM Cruise Report. doi:10.2312/cr_so240.

Kuhn, T., Wegorzewski, A., and Vink, A. (2017). "Composition, Formation, and Occurrence of Polymetallic Nodules," in *Deep-Sea Mining: Resource Potential, Technical and Environmental Considerations*, 1–535. doi:10.1007/978-3-319-52557-0.

Le Quéré, C., Andrew, R., Friedlingstein, P., Sitch, S., Hauck, J., Pongratz, J., et al. (2018). Global Carbon Budget 2018. *Earth Syst. Sci. Data* 10, 2141–2194. doi:10.5194/essd-10-2141-2018.

Lindh, M. V., Maillot, B. M., Shulse, C. N., Gooday, A. J., Amon, D. J., Smith, C. R., et al. (2017). From the surface to the deep-sea: Bacterial distributions across polymetallic nodule fields in the clarion-clipperton zone of the Pacific Ocean. *Front. Microbiol.* 8, 1–12. doi:10.3389/fmicb.2017.01696.

Lutz, M., Dunbar, R., and Caldeira, K. (2002). Regional variability in the vertical flux of particulate organic carbon in the ocean interior. *Global Biogeochem. Cycles* 16, 11-1-11–18. doi:10.1029/2000gb001383.

McCave, I. N. (1984). Size spectra and aggregation os suspended particles in the deep ocean. *Deep Sea Res.* 31, 329–352.

Mewes, K., Mogollón, J. M., Picard, A., Rühlemann, C., Eisenhauer, A., Kuhn, T., et al. (2016). Diffusive transfer of oxygen from seamount basaltic crust into overlying sediments: An example from the Clarion-Clipperton Fracture Zone. *Earth Planet. Sci. Lett.* 433, 215–225. doi:10.1016/j.epsl.2015.10.028.

Miller, K. A., Thompson, K. F., Johnston, P., and Santillo, D. (2018). An Overview of Seabed Mining Including the Current State of Development, Environmental Impacts, and Knowledge Gaps. *Front. Mar. Sci.* 4. doi:10.3389/fmars.2017.00418.

Nealson, K. H. (1997). SEDIMENT BACTERIA: Who's There, What Are They Doing, and What's New? *Annu. Rev. Earth …* 25, 403–434. Available at: https://www.whoi.edu/cms/files/nealsonAnnRevEarthPlanSci1997_52473.pdf.

Oebius, H. U., Becker, H. J., Rolinski, S., and Jankowski, J. A. (2001). Parametrization and evaluation of marine environmental impacts produced by deep-sea manganese nodule mining. *Deep. Res. Part II Top. Stud. Oceanogr.* 48, 3453–3467. doi:10.1016/S0967-0645(01)00052-2.

Ozturgut, E., Lavelle, J. W., and Burns, R. E. (1981). Chapter 15 Impacts of Manganese Nodule Mining on the Environment: Results from Pilot-Scale Mining Tests in the North Equatorial Pacific. *Elsevier Oceanogr. Ser.* 27, 437–474. doi:10.1016/S0422-9894(08)71420-X.

Pabortsava, K., Purser, A., Wagner, H., and Thomsen, L. (2011). The influence of drill

cuttings on physical characteristics of phytodetritus. *Mar. Pollut. Bull.* 62, 2170–2180. doi:10.1016/j.marpolbul.2011.07.002.
Passow, U., and Carlson, C. A. (2012). The biological pump in a high CO2 world. *Mar. Ecol. Prog. Ser.* 470, 249–271. doi:10.3354/meps09985.
Ramirez-Llodra, E., Tyler, P. A., Baker, M. C., Bergstad, O. A., Clark, M. R., Escobar, E., et al. (2011). Man and the last great wilderness: Human impact on the deep sea. *PLoS One* 6. doi:10.1371/journal.pone.0022588.
Sharma, R. (2015). Environmental issues of Deep-sea mining. *procedia Earth Planet. Sci.* 11, 204–211. doi:10.1016/j.proeps.2015.06.026.
SORENSEN, K. B., LAUER, A., and TESKE, A. (2004). Archaeal phylotypes in a metal-rich and low-activity deep subsurface sediment of the Peru Basin, ODP Leg 201, Site 1231. *Geobiology* 2, 151–161. doi:10.1111/j.1472-4677.2004.00028.x.
Stemmann, L., Jackson, G. A., and Ianson, D. (2004). A vertical model of particle size distributions and fluxes in the midwater column that includes biological and physical processes - Part I: Model formulation. *Deep. Res. Part I Oceanogr. Res. Pap.* 51, 865–884. doi:10.1016/j.dsr.2004.03.001.
Sweetman, A. K., Smith, C. R., Shulse, C. N., Maillot, B., Lindh, M., Church, M. J., et al. (2019). Key role of bacteria in the short-term cycling of carbon at the abyssal seafloor in a low particulate organic carbon flux region of the eastern Pacific Ocean. *Limnol. Oceanogr.* 64, 694–713. doi:10.1002/lno.11069.
Thistle, D. (2003). "The Deep-sea floor: An overview," in *Ecosystems of the Deep Oceans*, ed. P. A. Tyler (Elsevier).
Thomsen, L. A., and McCave, I. N. (2000). Aggregation processes in the benthic boundary layer at the Celtic Sea continental margin. *Deep. Res. Part I Oceanogr. Res. Pap.* 47, 1389–1404. doi:10.1016/S0967-0637(99)00110-7.
Thomsen, L., Abed, R., Allers, E., Bergmann, M., de Beer, D., Johnsen, S., et al. (2008). The CORAMM (Coral Risk Assessment, Monitoring and Modelling) Project. in *4th International Symposium on Deep-Sea Corals* (Wellington, New Zealand). Available at: https://epic.awi.de/id/eprint/19506/.
Turner, J. T. (2015). Zooplankton fecal pellets, marine snow, phytodetritus and the ocean's biological pump. *Prog. Oceanogr.* 130, 205–248. doi:10.1016/j.pocean.2014.08.005.
Vanreusel, A., Hilario, A., Ribeiro, P. A., Menot, L., and Arbizu, P. M. (2016). Threatened by mining, polymetallic nodules are required to preserve abyssal epifauna. *Sci. Rep.* 6, 1–6. doi:10.1038/srep26808.
Verlaan, P. A., Cronan, D. S., and Morgan, C. L. (2004). A comparative analysis of compositional variations in and between marine ferromanganese nodules and crusts in the South Pacific and their environmental controls. *Prog. Oceanogr.* 63, 125–158. doi:10.1016/j.pocean.2004.11.001.
Volz, J. B., Mogollón, J. M., Geibert, W., Arbizu, P. M., Koschinsky, A., and Kasten, S. (2018). Natural spatial variability of depositional conditions, biogeochemical processes and element fluxes in sediments of the eastern Clarion-Clipperton Zone, Pacific Ocean. *Deep Sea Res. Part I Oceanogr. Res. Pap.* doi:10.1016/j.dsr.2018.08.006.
Von Stackelberg, U. (2000). "Manganese nodules of the Peru basin," in *Handbook of Marine Mineral Deposits (Marine Science)*, ed. D. S. Cronan (CRC Press), 197–238.
Whitmann, W. B., Coleman, D. C., and Wiebe, W. J. (1998). Prokaryotes: The unseen majority. *Proc. Natl. Acad. Sci.* 95, 6578–6583. doi:10.1016/0006-8993(80)90730-1.

2 MANUSCRIPTS

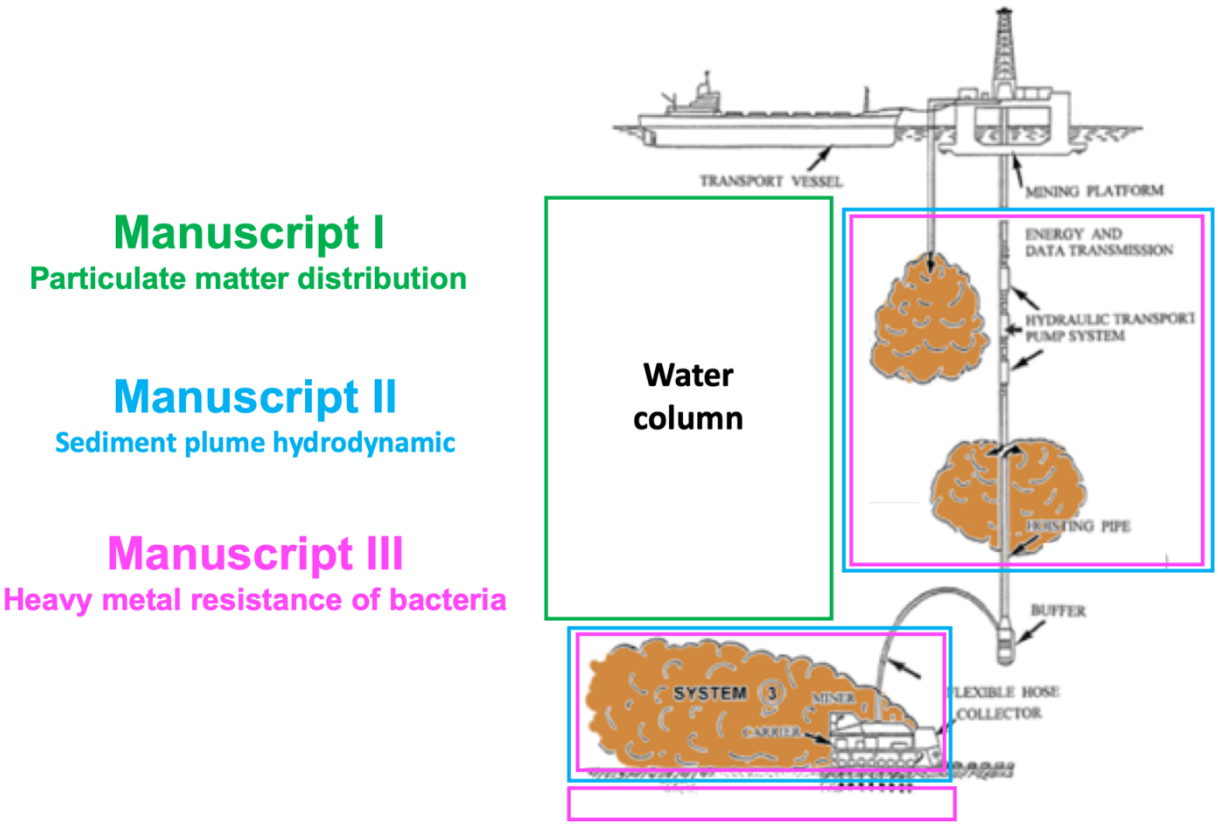

Figure 9. Summarize of research topics.
Figure adapted from Oebius (2001).

2.1 Manuscript I: From the surface to the seafloor: vertical profile of particulate matter in the Clarion Clipperton Fracture Zone (eastern-central Pacific)

Benjamin Gillard [1, 2, *], Robert Harbour [3], Nicolas Nowald [1], Laurenz Thomsen [2], Morten H. Iversen [1, 4]

[1] MARUM - Center for Marine Environmental Sciences, University of Bremen, Bremen, Germany

[2] The OceanLab, Jacobs University, Bremen, Germany

[3] The Lyell Centre for Earth and Marine Science and Technology, Heriot-Watt University, Edinburgh, UK

[4] Alfred Wegener Institute for Polar and Marine Research, Bremerhaven, Germany

* b.gillard@jacobs-university.de

In preparation for submission to Progress in Oceanography

2.1.1 Abstract

Research on the impact from mining of deep-sea polymetallic nodules in the Clarion Clipperton Zone (CCZ) has largely focused on the effect of mining activity on the benthic environment. However, release of plume sediment into the water column might have large implications for the pelagic community and the distribution and export of organic matter. We therefore need to study the impact from discharged sediment on the pelagic environment in order to be able to understand and model the impacts from deep-sea mining on both pelagic and benthic environments. Particle size-distribution and abundance was measured as vertical profiles with an *in-situ* camera system from the surface to the abyssal seafloor at 4000 m. The median particle size in the upper ocean (0 – 400 m) was 96 ± 12 µm and decreased to 67 ± 20 µm at depths between 400 and 4000 m. The maximum particle abundance in the upper 400 m (595 part·l^{-1}) was correlated with the maximum chlorophyll peak (± 65 m). We observed a decrease in both particle abundance and chlorophyll at the beginning of the oxygen minimum zone (OMZ). At depths below 400 m larger aggregates (> 300 µm) were rare. The study region (the German licence area in the CCZ) showed relatively constant productivity estimates from satellite images throughout the year (295.9 ± 36.8 mg·C·m^{-2}·day^{-1}). During the winter, we observed the formation of a sharp chlorophyll transition zone, suggesting that our study region is a productive transitional zone toward a more oligotrophic ocean gyre system. Vertical changes in particle size-distribution and abundance suggested that the OMZ had an impact on transport and alteration of the aggregates, this effect seemed more pronounced at night. We suggest that the combination of small, slow-sinking aggregates, bottom currents and slow seafloor consolidation may explain the extremely low sedimentation rates in the CCZ.

2.1.2 Introduction

Phytoplankton living in the photic zone fix carbon dioxide to produce particulate organic carbon through the process of photosynthesis. More than 50% of this organic carbon is grazed by zooplankton and remineralised by bacteria within the upper few hundred metres of water (Martin et al. 1987). However, a fraction of the organic carbon fixed in surface waters sinks through the water column as faecal pellets, decaying organisms or amorphous aggregates called ‘marine snow’ (particles > 0.5 mm). The transformation of dissolved inorganic carbon (DIC) to particulate organic carbon (POC),

the subsequent processes of remineralisation and aggregation, and downward transport to the deep sea is known as the biological carbon pump, and it serves as an important part of the global CO_2 cycle (Fowler and Knauer 1986). Due to zooplankton grazing and microbial degradation during sinking, only ~1% of organic carbon reaches the deep seafloor on a global scale (Lutz et al. 2002).

Particle camera systems (Honjo et al. 1984; Asper 1987; Ratmeyer and Wefer 1996; Gorsky et al. 2000) have significantly improved during the past three decades (Shen and Maa 2016). It is now possible to develop camera systems with higher resolution capable of imaging smaller aggregates than previously possible (Picheral et al. 2010). The advantage of particle cameras lies in their non-destructive nature acquiring particle size and abundance *in-situ*. Camera systems can capture both short- and long-term dynamics from individual vertical profiles and moored deployments. Previous studies have combined sediment trap fluxes with particle camera data to obtain high-resolution fluxes (Iversen et al. 2010; Nowald et al. 2015). Sediment traps collect settling particles sinking from depths above the trap and by relating the trap opening area and opening time, they provide flux to a particular depth over time. Traps can be deployed from day(s) to year(s) and provide long-term time series of export fluxes. While traps only collect sinking particles, camera systems image both suspended and settling particles throughout the water column. When traps and camera data are combined, they provide data on the export history and particle distribution at different depths with a high data resolution (Picheral et al. 2010).

The Clarion Clipperton Zone (CCZ, Figure 1) is located approximately 2500 km off the coast of Mexico within the eastern German licence area allocated for deep-sea mining exploration (~ 56,000 km^2). The CCZ is characterised by vast deposits of polymetallic nodules that lie on the abyssal seafloor. Polymetallic nodules may form between 4000 and 6000 m where the water is well oxygenated, and sedimentation is less than less than 10 $mm \cdot kyr^{-1}$ (Gollner et al. 2017); in the CCZ they occur in the greatest concentration found anywhere on earth (ISA 2010). The nodules are enriched with metals such as manganese, copper, nickel and cobalt, as well as rare earth elements (Wegorzewski and Kuhn 2014), and have been considered as potential mining targets since the 1970s. A growing demand for the use of these materials in electronics has accelerated research and development of viable deep-sea mining technologies in recent decades (Miller et al. 2018). However, deep-sea mining activities have been recognised for their potential to drastically impact marine ecosystems (Jones et al. 2017). Besides the direct impact of the mining crawler

and sediment plume on the seafloor (Gillard et al. 2019), uncontrolled discharge of waste products such as sediment and nodules into the pelagic environment needs to be taken into account (Oebius et al. 2001).

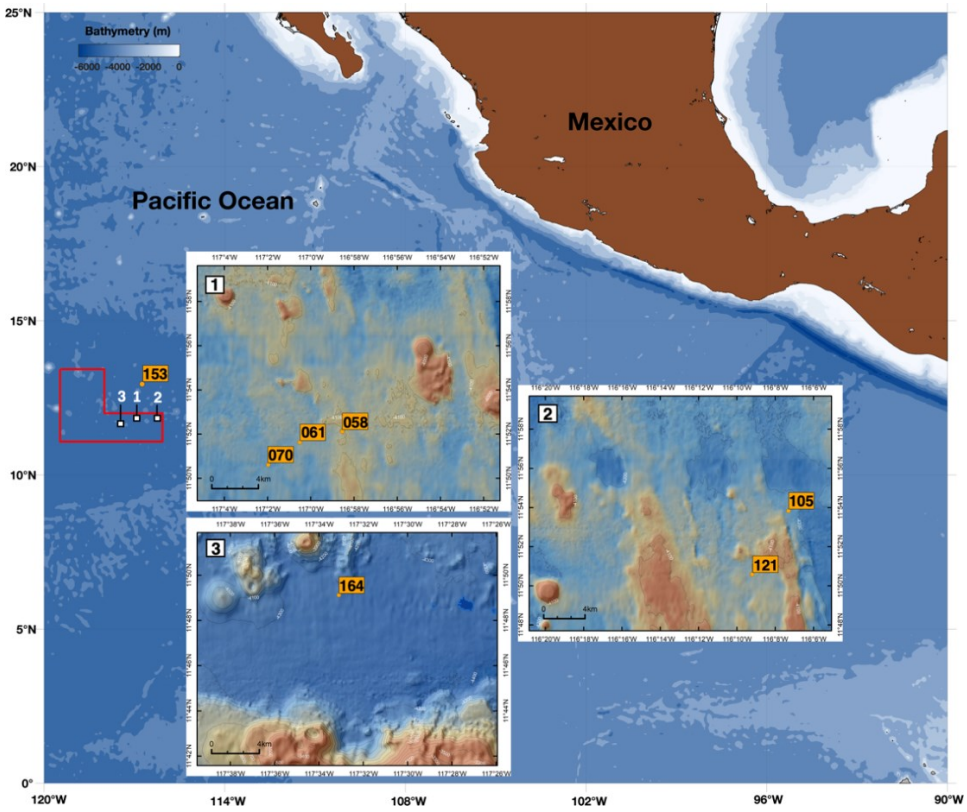

Figure 1. Map showing camera deployment stations in relation to the bathymetry of the study area. The three study sites (WA 1-3) are located within the eastern German manganese nodule license area (red polygon), north-eastern Pacific. Camera profiling stations are indicated by the yellow boxes. Bathymetry of the WA area based on EM 120 measurements (Wiedicke-Hombach, 2009). Contours are 100 m; resolution of each data point is 120 m by 120 m.

To date, the magnitude of the impact generated by mining activity on the pelagic environment is still unpredictable, as a full-scale mining test has not yet been performed (Christiansen et al. 2019). It is suggested that a sediment plume released in the epipelagic layer will increase turbidity and decrease light penetration, resulting in a net decrease of primary productivity (Chan and Anderson 1981). After release and dilution of mining plumes, increased inorganic nutrients and trace metal concentrations in the surface water might result in a shift in the planktonic community (e.g. diatoms) and affect the entire food web structure (Taylor et al. 1998). Furthermore, incorporation of lithogenic material, e.g. from mining plumes, during aggregate formation will cause an increase in settling velocity (e.g., drill cutting exposure; Pabortsava et al. 2011) and potentially enhance carbon export to a greater depth (Hamm 2002; Iversen and Robert 2015; van der Jagt et al. 2018).

So far, most studies in the CCZ have focused on benthic environments, with little attention given to the wider benthic–pelagic coupling influences such as phytoplankton composition, water column particle distribution, particle transport processes and carbon flux from the surface to the deep sea. Such data are essential for an understanding of how mining operations may impact the ecosystem in the CCZ.

In the present study, we used a high-resolution profiling camera system to study short-term vertical particle dynamics from the surface down to the seafloor in the German licence area for nodule exploration within the CCZ. The aims of this study are to: (***i***) give a general overview of the oceanographic background of the German license area in the CCZ, (***ii***) describe how particulate matter is distributed in the water column and (***iii***) identify the transport processes and pathways that affect particle distribution in the water column.

2.1.3 Materials and methods

2.1.3.1 Field sampling

A vertically profiling still-image camera system was deployed at seven locations to acquire the vertical abundance and size distribution of aggregates through the water column. The camera system was deployed during the RV *Sonne* cruise SO-262 in April/May 2018 in the north-eastern Pacific Ocean (Figure 1 and Table 1). The camera system was deployed in depths down to 400m and ≅ 4000m in the three working areas (WA 1–3).

Table 1. Station list description.

Station # **(SO262)**	WA	Date **(2018)**	Position		Depths (m)		Day	Night
			Latitude (N)	**Longitude (W)**	**Water**	**Profile**		
058CTD	1	22.04	11°52.114’	116°58.546’	4136	400	X	
061CTD	1	23.04	11°51.627’	117°00.511’	4115	4096		X
070CTD	1	25.04	11°50.608’	117°01.970’	4129	400		X
105CTD	2	02.05	11°53.833’	116°07.310’	4172	400	X	
121CTD	2	03.05	11°50.589’	116°09.206’	4157	4150	X	
153CTD	UKSLR	08.05	12°37.316’	116°29.741’	4236	400	X	
164CTD	3	10.05	11°47.876	117°30.580’	4327	3071		X

2.1.3.2 Hydrography

Oceanographic data were collected during all deployments using the onboard CTD-Rosette sampler. The CTD (SBE 19plus V2 SeaCAT) was equipped with additional sensors such as oxygen (Sea-Bird SBE 43), chlorophyll (Wet Labs ECO) and PAR/irradiance sensors (Biospherical QCP2300), and a Seapoint turbidity meter facing externally to the CTD. Seasoft (version 2.4.0) was used for data processing, and downcast profile was binned in 1 m intervals.

2.1.3.3 Camera system description

The underwater profiling particle system (PPS; Figure 2) was developed based on the improved version of the ParCa system (Nowald et al. 2006). The PPS was designed for deployments down to 6000 m and is fully autonomous. The system is composed of two separate pressure housings, one containing the camera and one containing the flash.

The PPS was equipped with a Canon EOS 760D SLR with a resolution of 24.2 megapixels and a Canon EF-S 60 mm f 2.8 macro lens. The use of a macro lens allows the image to be taken closer to the lens and provides a higher resolution, more detail and a better even illumination of the sample volume. A collimated light source (Yongnuo YN-468 II Speedlite strobe) was mounted perpendicularly at a distance of 20 cm to the camera. A short flash duration of (1/200 s) allows the acquisition of sharp images without motion blur effects. At maximal zoom factor, the field of view was 1.53 × 0.96 × 0.2 cm (width × height × depth), resulting in a sample volume of 2.94×10^{-4} l. The minimum particle size that can be detected with this optical setup is 0.03 mm with a pixel resolution of 0.01 mm.

The system was mounted inside the lower section of the RV *Sonne* CTD-Rosette carousel next to the CTD sensor (Figure 2). The position inside the carousel's frame was best suited for imaging particles without larger disturbances. The mounting position also provided protection of the camera system itself in case the CTD-Rosette accidently hit the ship's hull.

Prior to deployment, the system was programmed using mission planner software to trigger the camera at given time intervals (10 s) by a microcontroller. The deployments were done at a winch speed of 1 $m \cdot s^{-1}$, which translated into trigger depth intervals of 10 m. All images were stored internally and uploaded using an external USB port after each deployment.

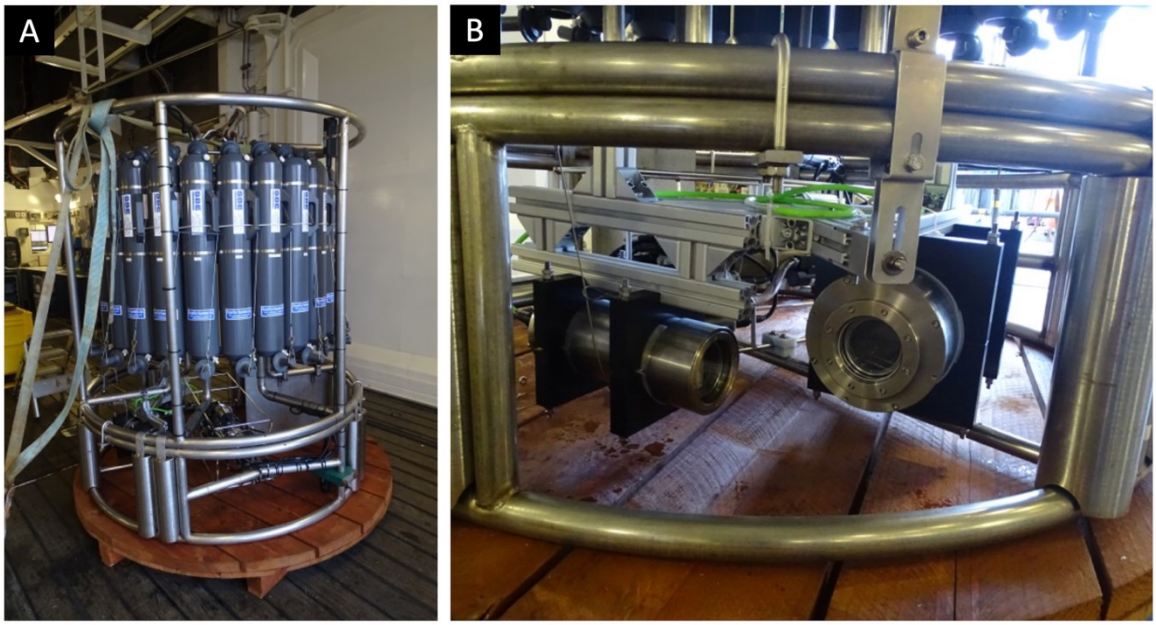

Figure2. (**a**) CTD-Rosette in the hangar of RV SONNE. (**b**) The PPS installed in the lower section of the CTD-Rosette next to the CTD.

2.1.3.4 Image analysis

We used the MATLAB (R2016a) software package 'Image Processing toolbox' as described by Iversen et al. (2010) and the architecture code of Markussen (2016) to remove the image background and extract the size of the particles in each image. Only downcast profiles were used for image analysis, to avoid any water disturbance from the CTD-Rosette. Background illumination was corrected using a rolling set of three pictures to accurately estimate the illumination inconsistency through the entire profile. The median value of each pixel was assumed to be the background intensity and was subtracted from that set of pictures. Thresholding value was manually determined on randomly chosen pictures and applied for the entire set of profiles. The area of each particle was converted to equivalent spherical diameter (ESD) and equivalent spherical volume (ESV). Zooplankton were manually removed from the images and excluded from the measurements. All particles from one image were binned into 20 predetermined size classes (Supplementary Table S1).

In order to illustrate the change of particle size with depth, the number of particles per size bin was converted into their frequency as a percentage. This conversion was made due to the broad range of particle abundance s and sizes captured by the camera system (Nowald et al. 2006). This approach allowed a better display of changes in abundance and size with depth compared to using absolute particle numbers.

2.1.3.5 Satellite imagery-derived parameters

The moderate resolution imaging spectroradiometer (MODIS) satellite datasets used were downloaded from the Ocean Biology Processing Group at NASA's Goddard Space Flight Center (oceancolor.gsfc.nasa.gov). Monthly (January 2018 – December 2018) chlorophyll a (Chla), sea surface temperature (SST, 11 µ night-time) and POC were used. Ocean net primary production (NPP) data were retrieved from the vertically generalised production model (VGPM; Behrenfeld and Falkowski 1997a, 1997b) estimated from the Ocean Productivity website (science.oregonstate.edu/ocean.productivity). The average value of each parameter was extracted from the area corresponding to the German licence area (Figure 1, red polygon) using SeaWiFS Data Analysis System software (SeaDAS version 7.5-1; O'Reilly et al. 1998). Monthly mean climatology (2002–2018) datasets (MODIS) were used as reference values for comparison with 2018 datasets.

2.1.3.6 Statistical analysis

We used MATLAB (R2016a) software for statistical analysis of the datasets. For every deployment, Spearman correlation coefficient (significance threshold using a P value < 0.001) was applied to determine the interdependence between two parameters from the camera system (median diameter (D_{50}), abundance) and the CTD (turbidity, fluorescence and chlorophyll).

2.1.4 Results

2.1.4.1 Oceanographic conditions

A hydrographic summary of the eastern German licence area is shown in Figure 3. The sea surface water parameters derived from monthly satellite imagery analysis (Figure 3a) indicated a pronounced seasonal signal as shown by the variation of SST (amplitude of 1.6 °C). The highest SST was observed during June (28.5 ± 0.4 °C) and declined at the start of the hurricane season to reach a colder period from November till March (27 ± 0.1 °C). Primary production (as indicated by changes in Chla) followed an inverse trend in comparison to SST, with maximum productivity (0.17 ± 0.03 $mg \cdot m^{-3}$ equivalent to net primary productivity of 379 ± 26.2 $mg \cdot C \cdot m^{-2} \cdot day^{-1}$) at the end of the colder period of the year during March. In contrast with the monthly climatology (2002–2018; dotted lines in Figure 3a), 2018 exhibited a net increase of 45% in productivity,

reaching up to 0.21 ± 0.03 mg·m^{-3} at the end of the hurricane season (October – November).

CTD casts obtained from the 22nd April till the 10th of May through the entire water column are presented in Figure 3b. The temperature profiles indicated the presence of a shallow mixed layer down to 40 m depth followed by a sharp temperature gradient (maximum thermocline strength = 0.6 °C·m^{-1}) down to 94 ± 10 m depth. Salinity increased steeply from the surface (33.74 ± 0.08 PSU) to reach a maximum value of 34.8 ± 0.01 PSU at around 134 ± 5 m depth. The combination of a strong halocline/thermocline (located at 67 ± 3 m depth) resulted in strengthening of the sub-pycnocline which separated the epipelagic layer from the deeper stable layer. The deeper layer was characterised by a slowly decreasing temperature (average Δ of 0.3 °C·100m^{-1}) and nearly uniform salinity (average Δ of 0.002 PSU·100m^{-1}). Surface water was well oxygenated in the mixed layer and reached 187.35 ± 25.9 µmol·l^{-1}, equivalent to 93 ± 13% oxygen saturation. The oxygen concentration started to decrease at a depth which coincided with the thermocline. The oxygen minimum zone (OMZ; Figure 3b) was well established and characterised by an upper (94 ± 9 m) and a lower oxycline (474 ± 8 m) in which the water mass oxygen concentration dropped below 10 µmol·l^{-1}(< 4% saturation). Inside the OMZ, the suboxic water mass was on top of an anoxic layer depleted of oxygen (< 4.5 µmol·l^{-1}; 0.1% saturation). At the lower oxycline, oxygen concentration started to increase gradually with depth. Four distinctive water mass signatures were identified and are presented in Table 2.

Table 2. Water mass structure of the eastern German License area.

Water mass	Abbr.	Min depth (m)	Max depth (m)
Tropical surface water	TSW	0	46 ± 13
North Pacific Intermediate Water	NPIW	474 ± 8	1501 ± 13
North Pacific Deep Water	NPDW	2031 ± 65	3711 ± 29
Lower Circumpolar Water	LCPW	3711 ± 29	Bottom

Based on a larger oceanic context, the German licence area is located in the transition zone (10° N) between the North Equatorial Current (NEC) and the North Equatorial Counter Current (NECC). Satellite images (Figure 3c and Supplementary Figure S1) indicated that surface productivity was influenced by enriching water transported westward from the coast of southwest Mexico and Guatemala through the area of investigation. During the hurricane season (June – November; Neumann 1993), a clear

separation was observed between the German licence area and the Equatorial and North Pacific Gyre Systems.

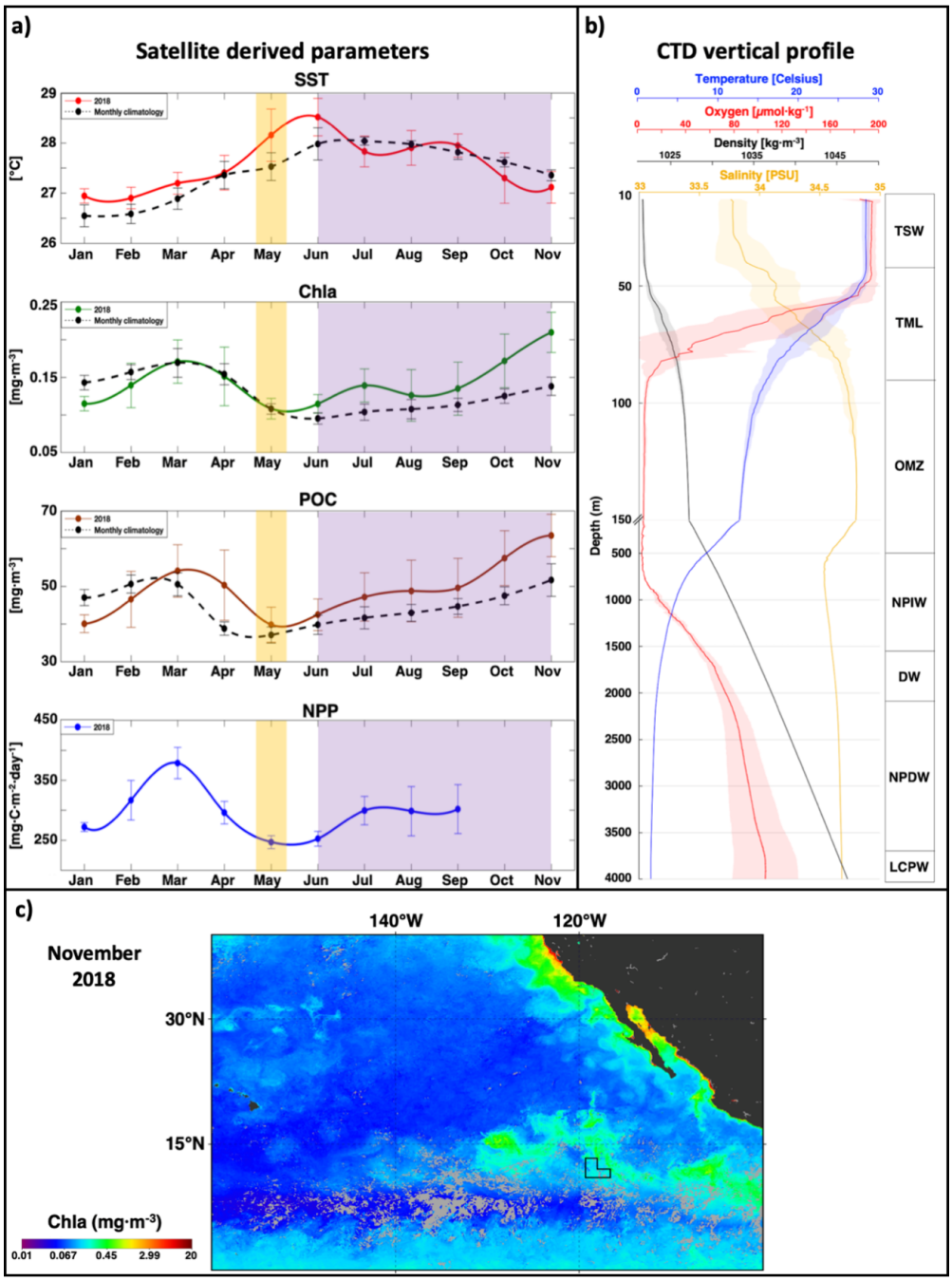

Figure 3. Oceanographic condition of the eastern German Licensed area in CCZ.
a) Surface water characteristics from 2018 and monthly climatology (2002–2018) using satellite (MODIS) derived parameters including sea surface temperature (SST), Chlorophyll a (Chla), particulate organic carbon (POC) and net primary production (NPP). Yellow shaded areas represent the time frame during which all vertical profiles were acquired, and purple shaded areas indicate the hurricane season (Neumann, 1993); **b)** Vertical water masses characteristics using CTD downcast profiles. Bold lines represent the median values and shaded areas indicate the variation from all profiles. The vertical water mass distribution is shown on the right side: tropical surface water (TSW), thermocline layer (TML), oxygen minimum zone (OMZ), north pacific intermediate water (NPIW), deep water (DW), north pacific deep Water (NPDW) and lower circumpolar water (LCPW). **c)** November 2018 surface chlorophyll distribution in the north-eastern Pacific. Light grey corresponds to cloud coverage and the eastern German Licensed area is indicated by a black polygon.

2.1.4.2 Shallow camera profiles

Analysis of all stations, from the surface water down to 400 m depth, denoted evident spatial and temporal variability, summarised in Figure 4. In the German licence area (WA-1 and 2), this tendency was also observed for satellite analysis of surface Chla (8 rolling days; Supplementary Table S2) which also depicted temporal variability. An increase of surface chlorophyll concentration until mid-May was followed by a general decrease over time and space. Opposite to that, surface chlorophyll remained constant for station 153 (UKSLR) and decreased for station 164 (WA-3) over time. A positive linear correlation ($R^2 = 0.86 \pm 0.06$) between turbidity and fluorescence was found at all stations (Figure 4a and b; Supplementary Table S3). On average, particle abundance (Figure 4c) in the upper water column varied between stations (WA-1: 29 part·l^{-1}; WA-2: 119 part·l^{-1}; UKSLR: 149 part·l^{-1}; WA-3: 179 part·l^{-1}), but followed a general increase over the sampling period. Median particle size express (Figure 4d) was relatively constant (96 ± 12 µm) with the exception of stations 061 and 070, which showed a smaller median particle size of 30 µm. No aggregate larger than 700 µm was found for any station.

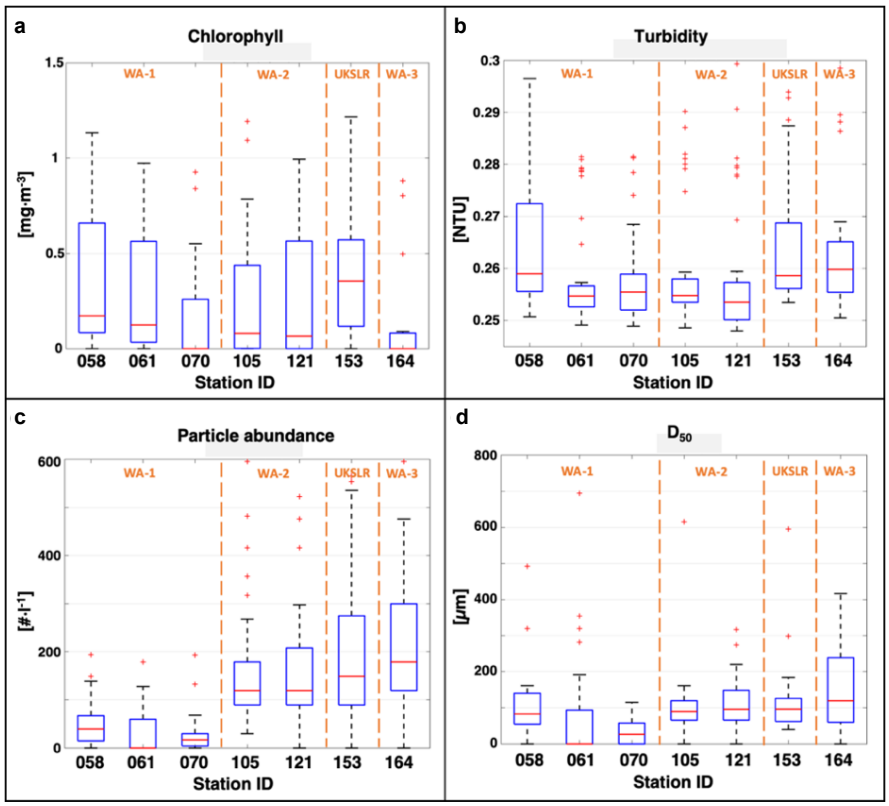

Figure 4. Box plots of all CTD and camera data from the shallow stations
(a) Chlorophyll and **(b)** turbidity data were measured with the CTD. **(c)** Particle abundance and **(d)** median diameter values were extracted from the camera pictures. Upper and lower boxplot whiskers represent the maximum and minimum values of the dataset. Interquartile range is shown as the blue box (50% of the dataset). Red line indicates the median value and red "+" are outliers. Working areas are shown in orange.

Here, we focus on station 105 because it reflects the particle properties seen in the majority of the camera profiles (Figure 5). Results from other deployments are provided in supplementary Figures S2 to S7. Camera data from station 105 were characterised by a large variation of the particle distribution in the upper 150 m in comparison to the deeper section (Figure 5a). The maximum particle abundance was found at a depth of 65 m where particle abundance reached 595 part·l^{-1} and particle size distribution varied the most, ranging between 34 and 694 µm (Figure 5b). A subsurface particle abundance maximum was found at 125 m depth (upper section of the OMZ), reaching an abundance of 417 part·l^{-1}. Below the subsurface particle maximum (145 m), size spectra shifted toward increasing particle size up to 354 µm, corresponding to 50% of the total size distribution in terms of abundance. Below 200 m depth, the particle abundance fluctuated less, with the average being 113 ± 53 part·l^{-1} and 70% of the particles being smaller than 66 µm.

Overall, the size–frequency distribution indicates that smaller particles (≤ 66 µm) were dominant and provided the majority of the size spectra in terms of abundance, with an average of 59 ± 27% throughout the water column. Medium-sized particles (66 to 295 µm) contributed to 36 ± 25% of the size spectra in terms of abundance while particles larger than 300 µm in diameter were rarely found (4 ± 11%).

A significant linear correlation (R^2 = 0.7 ± 0.1; P < 0.001; Supplementary Table S3) was found between CTD (turbidity, fluorescence) and camera data (particle abundance). This relation was more pronounced at the pycnocline and oxycline depth (≈ 65 m) where the chlorophyll (1.19 mg·m^{-3}), particle abundance (595 part·l^{-1}) and turbidity (0.3 NTU) reached their maximum values (Figure 5).

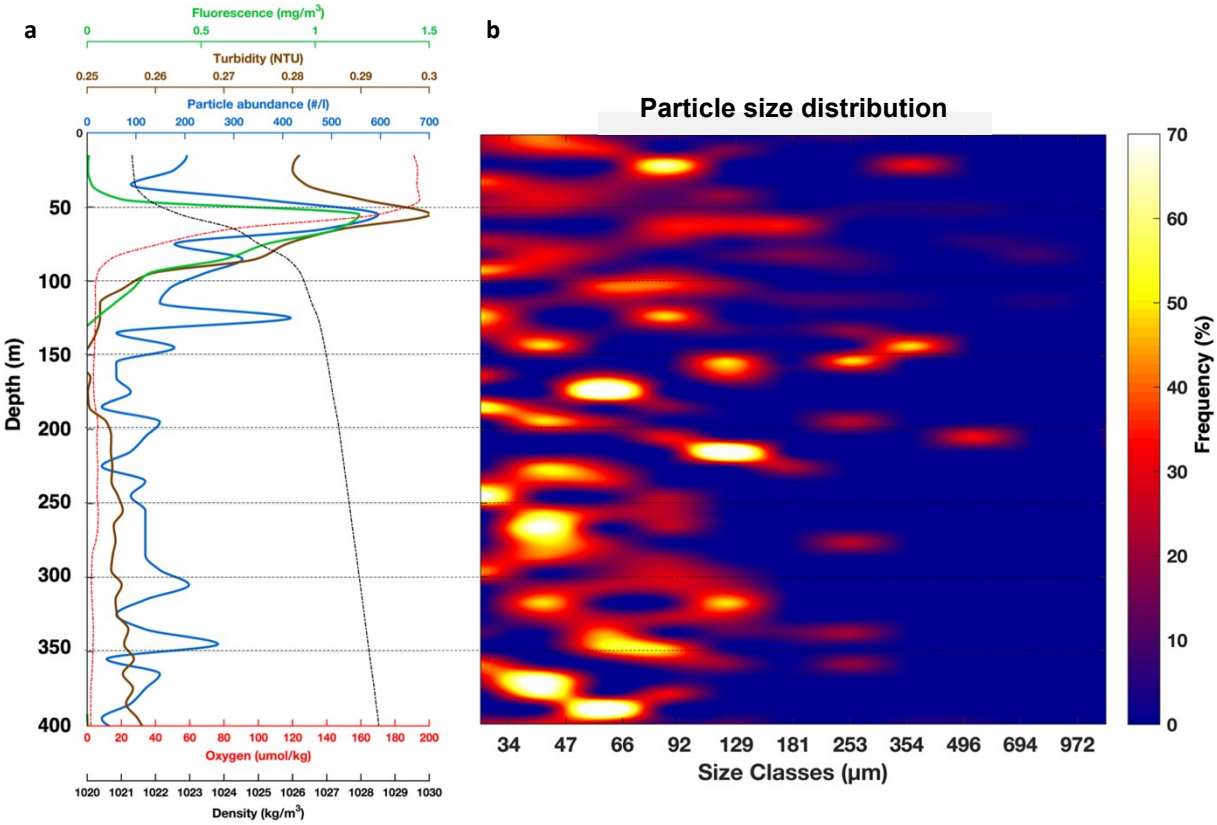

Figure 5. Particle abundance, size distribution and oceanographic parameters from station 105
(a) Vertical cross section from CTD data (fluorescence, turbidity, oxygen, density) and particle abundance versus depth. **(b)** Particle size distribution expressed in percent frequency versus depth.

2.1.4.3 Deep water camera profiles

Four stations (numbers 061, 070, 121 and 164) were located in the German licence area from the ocean surface down to 4000 m depth. Results are shown in the boxplot of Figure 6. Particle properties (turbidity, abundance, median particle size (D_{50})) of the deeper water column (400–4000 m) depicted less temporal and spatial variability in comparison to the shallow camera profile (0–400 m). Turbidity was relatively constant between stations, with a value of 0.273 ± 0.002 NTU. Low particle abundances measured in working area 1 (WA-1; stations 061 and 070; Figure 6b), remained similar to those in the surface water layer (Figure 4c) with 40 ± 20 part·l^{-1} (D_{50} = 48 ± 5 µm). A three-fold decrease in particle abundance was observed for WA-2 (station 121; D_{50} = 79 µm) and WA-3 (station 164; D_{50} = 94 µm), down to 40 and 60 part·l^{-1}, respectively. No significant correlation was found between any of the parameters.

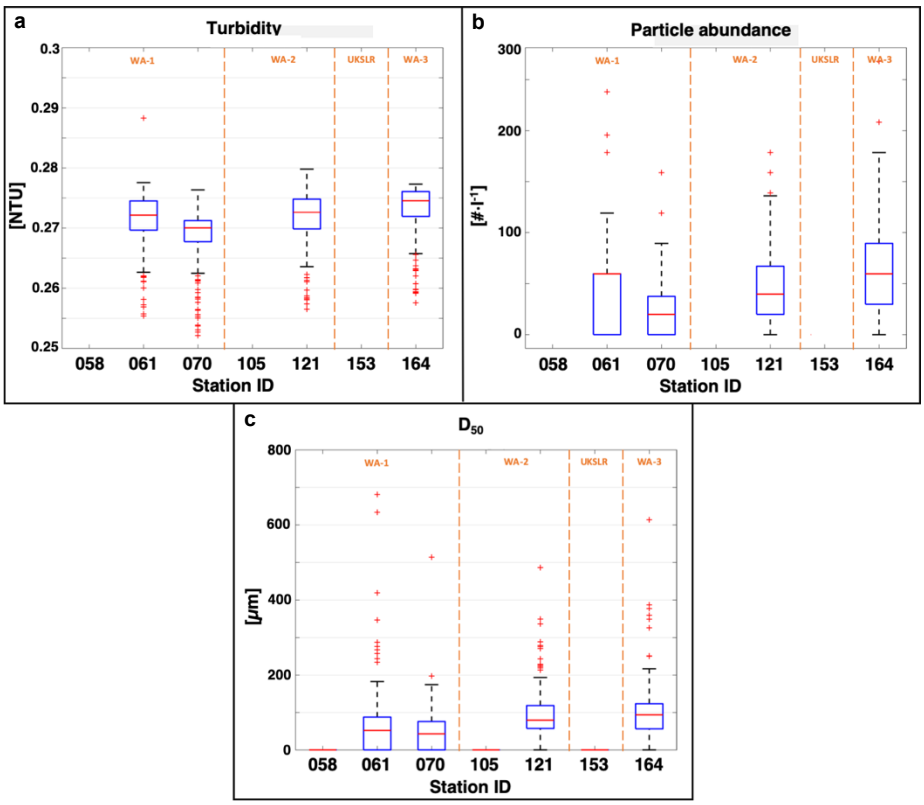

Figure 6. Box plots of all CTD and camera data from the whole water column versus sampling stations.

Turbidity data were measured with the CTD. Particle abundance and median diameter values derived from the profiling camera pictures. Upper and lower boxplot whiskers represent the maximum and minimum values of the dataset. Interquartile range is shown as the blue box (50% of the dataset). Red line indicates the median value and red "+" are outliers. Working areas are shown in orange.

Description of the particle abundance and size distribution for deeper water profiles will focus on profile 121, presented in Figure 7. Table 3 summarises the general trend of particle characteristics for every water mass. Profiles from other deployments are provided in Supplementary Figures S8 to S10. The maximum particle abundance was observed in the surface water masses (thermocline layer: 523 ± 266 part·l^{-1} and tropical surface water (TSW): 351 ± 178 part·l^{-1}) followed by a net decrease, which reached a minimum particle abundance in the deep water layer (DW; 38 ± 72 part·l^{-1}) and a slight increase in the lower circumpolar water mass (LCPW; 61 ± 73 part·l^{-1}). The same trend was observed for total particle volume which ranged from 10 ± 20.8 ppm in the TSW down to 0.8 ± 7.7 ppm in the LCPW. Overall, median particle size (D_{50}) was rather constant, with particle sizes ranging from 71 to 113 µm. The small-sized particles (≤ 66 µm) were the most dominant (65 ± 4%) through all water masses, followed by medium-sized particles (67–295 µm; 34 ± 6%) and larger particles (> 295 µm; 5 ± 3%).

Table 3. Station 121 particles related parameters summary from each water masses

Water masses	Depth range (m)		Abundance (#/L)	Total Volume (ppm)	D_{50} (µm)	Size ≤ 66µm (%[1])	Size 66 > x ≤ 295µm (%[1])	Size > 295µm (%[1])
TSW	0	43	351 ± 178	10.0 ± 20.8	79 ± 54	67.7 ± 19.4	22.8 ± 18.6	9.6 ± 0.0
TML	43	87	523 ± 266	6.7 ± 14.1	71 ± 47	61.5 ± 23.0	31.2 ± 4.6	7.3 ± 18.7
OMZ	87	483	148 ± 114	1.8 ± 5.4	113 ± 154	64.6 ± 2.0	28.1 ± 3.7	7.3 ± 6.3
NPIW	483	1509	71 ± 80	0.5 ± 3.4	93 ± 85	69.5 ± 1.3	25.5 ± 2.4	5.0 ± 5.1
DW	1509	2011	38 ± 72	0.1 ± 0.3	97 ± 69	60.6 ±4.1	39.4 ± 3.9	0.0
NPDW	2011	3762	41 ± 73	0.3 ± 2.4	95 ± 82	61.5 ±1.3	34.8 ± 1.4	3.8 ± 4.4
LCPW	3762	4160	61 ± 73	0.8 ± 7.7	96 ± 101	67.7 ±4.7	31.2 ± 4.0	1.1 ± 17.1

[1] Results are express in % of the total abundance. Tropical surface water (**TSW**), thermocline layer (**TML**), Oxygen minimum zone (**OMZ**), north Pacific intermediate water (**NPIW**), deep water (**DW**), North Pacific deep water (**NPDW**) and lower circumpolar water (**LCPW**).

Particle size distribution (Figure 7) was most variable in the top 50 m where all size classes were found (34 to 972 µm). Particles larger than 300 µm were rarely found throughout the entire water column. Total volume profile (Supplementary Figure S11) clearly showed the formation of seven maxima, all related to increased median particle size. Even though smaller particles (≤ 66 µm) were numerically the dominant particle fraction in terms of abundance at all depths (Table 3), larger particles contributed to 98 ± 4% of the maxima total volume. The depth range at which those volume maxima occurred was closely related to the transition zone between water masses.

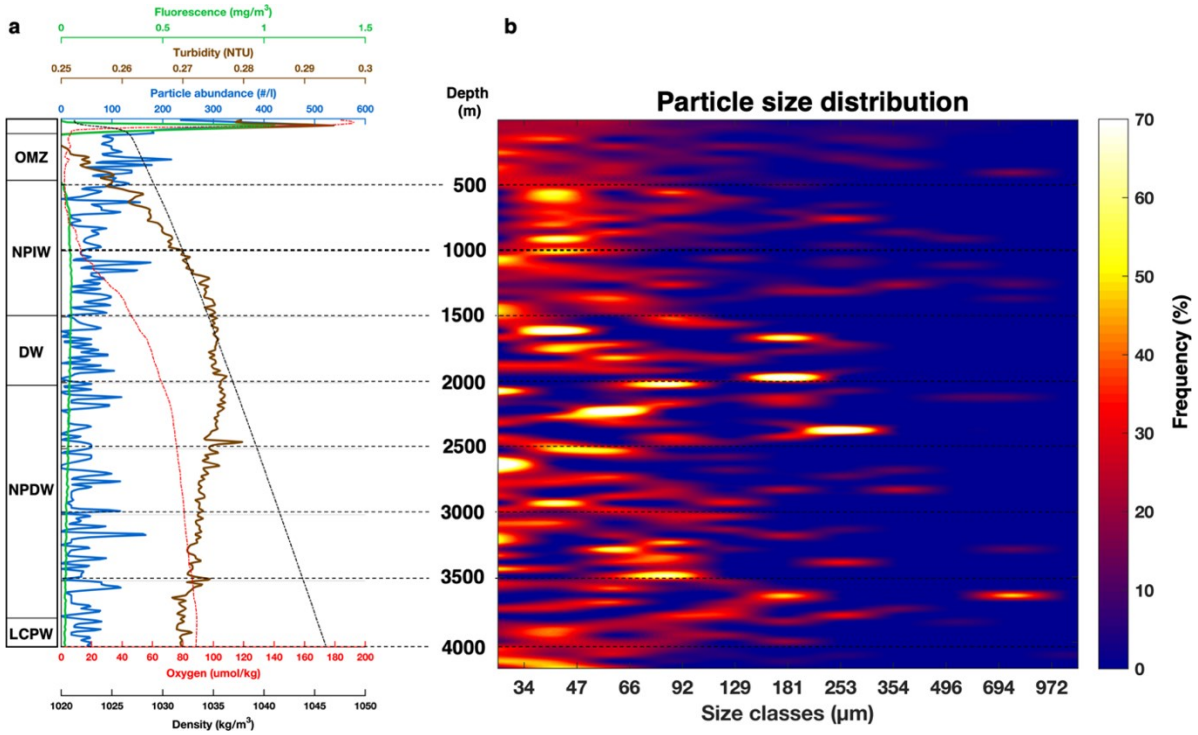

Figure 5. Particle abundance, size distribution and oceanographic parameters from station 121 **(a)** Vertical cross section from CTD data (fluorescence, turbidity, oxygen, density) and particles abundance versus depth. **(b)** Particles size distribution expressed in percent frequency versus depth. Oxygen minimum zone (**OMZ**), north Pacific intermediate water (**NPIW**), deep water (**DW**), North Pacific deep water (**NPDW**) and lower circumpolar water (**LCPW**).

2.1.5 Discussion

The CCZ is currently targeted by countries and industries for its mineral resources (polymetallic nodules), which are ecologically and economically relevant (Hein and Koschinsky 2013). Over the last decade, the scientific community has mainly focused on the response of the benthic ecosystem to the anticipated anthropogenic impact from deep-sea mining. However, very little attention has been given to describing benthic–pelagic coupling mechanisms. This study aimed to provide a general oceanographic overview of the eastern German licence area of the CCZ, to investigate vertical particulate matter distributions and to identify possible transport and transformation mechanisms in the water column.

The use of profiling cameras over recent decades has given a broader overview of particulate matter structure in the water column (e.g., UVP system; Gorsky et al. 2000). We agree that the use of a particle camera only gives a glimpse of particulate matter distribution at a specific time and depth and does not provide any information about aggregate chemical composition. It should be considered as a complementary research method allowing the capture *in situ* of aggregates properties (e.g. size, abundance, shape, type, etc.) without any disturbance to short- and long-term time series investigation.

2.1.5.1 Oceanographic conditions and productivity

Surface water analysis of the German licence area in the CCZ (Figure 2) depicted a clear seasonal signal; this was observed especially for Chla concentration. Seasonality in the CCZ was directly coupled to meridional migration of the intertropical convergence zone (ITCZ), which extended to 10° N from August to September and was near the Equator during March (Amador et al. 2006). Analysis of a similar concentration range of annual surface Chla (Figure 8) has shown a distinct oceanic distribution pattern of these transitional zones located between productive upwelling areas and more oligotrophic subtropical gyres (Figure 8b).

In comparison to the North Pacific Subtropical Gyre, the eastern German licence area seems to maintain relatively constant productivity (295.9 ± 36.8 $mg{\cdot}C{\cdot}m^{-2}{\cdot}day^{-1}$; Figure 3) over the year. During the winter season, we observed the formation of a sharp transition zone chlorophyll front (TZCF; Supplementary Figure 8c) similar to the one reported in the North Pacific by Ayers and Lozier (2010). Satellite imagery

(Supplementary Figure S1) revealed an apparent influence of water masses from the south-eastern coast of Mexico, suggesting that lateral advection of nutrient-rich water sustained the year-round primary productivity in the area. Surface currents have been described as a combination of northward Ekman transport generated from the easterly trade wind system, seasonal wind jet episodes from the Gulf of Tehuantepec, Papagayo and Panama, and a geostrophic current balance (Chelton et al. 2002; Kessler 2006; Willett et al. 2006). Overall, nutrient-rich water upwelled in the Costa Rica Dome is the main nutrient source to the CCZ via lateral advection (Fiedler and Talley 2006) and seem to explain the constant productivity throughout all seasons.

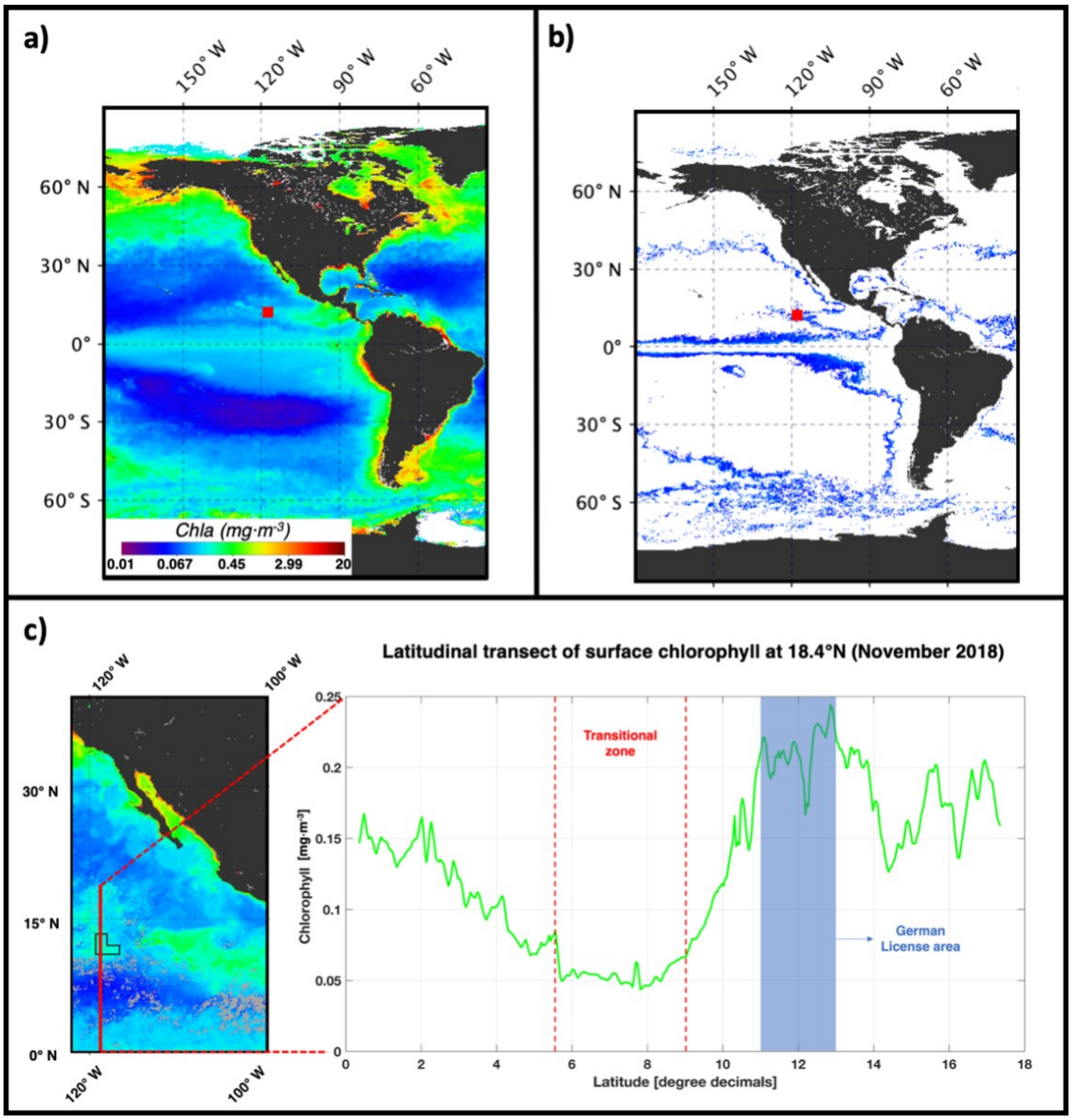

Figure 8. Worldwide 2018 chlorophyll-a distribution pattern.
(a) 2018 annual chlorophyll-a (mg·m^{-3}) global distribution from SeaWiFS. German licensed nodule area location is indicated by a red square. **(b)** Coloured area showing distribution patterns where the annual chlorophyll-a concentration is equal to the German licensed area. **(c)**Latitudinal transect of surface chlorophyll at 18.4°N from November 2018 showing the transitional zone between the equator toward the German license area.

2.1.5.2 Particle alteration in the upper ocean

The efficiency of the biological carbon pump is mainly driven by the formation and settling of aggregates in the ocean, which rely on surface primary production (species composition, size structure, transfer efficiency), trophic coupling (grazer dynamics) and the remineralisation of exported material with depth (Guidi et al. 2009; Iversen et al. 2010; Henson et al. 2015; Mouw et al. 2016). Surface chlorophyll measurements in the euphotic zone showed variations throughout the sampling period (Figure 4a). This was related to the particle abundance and significantly correlated to four out of the seven stations analysed for vertical particle abundance (Supplementary Table S3). The particle abundance was highest at depths corresponding to the maximum Chla concentration. A strong linear correlation between Chla and turbidity measurements (R^2 = 0.86 ± 0.06) indicated that those particles contained a large proportion of phytoplanktonic material. This might be explained by the remineralisation of organic matter, which is at its highest in the surface water, reaching up to 50% (Martin et al. 1987). Higher remineralisation rates in the area studied could only be explained by assuming a low settling velocity (3 to 5 $m \cdot day^{-1}$; Karakaş et al. 2009; Iversen et al. 2010), a relatively high temperature, increasing microbial degradation (Bendtsen et al. 2015) and a close coupling between production and zooplankton grazing. Similar trends have also been reported in the upwelling system of Cape Blanc (Nowald et al. 2006; Iversen et al. 2010). Furthermore, in low latitude regions where the seasonality signal is weaker, phytoplankton composition is dominated by smaller cells (Fryxell et al. 1979). Even if all particles of that size class acquired by the camera could not be attributed to a phytoplanktonic cell, at all stations analysed, particle composition indicated that smaller particles constituted up to 59%.

It is possible to identify the mechanisms responsible for export and attenuation of particles by comparing vertical changes in median particle size, particle abundance and total volume of aggregates (Marcussen et al. submitted). Five processes were defined: i) filter feeding by zooplankton (Frost 1972), ii) microbial degradation (Iversen and Ploug 2010), iii) flux feeding from waiting organisms (Jackson 1993), iv) aggregation (Burd and Jackson 2009) and v) disaggregation (Jackson 1998, 1995). To avoid any misinterpretation due to the mixing of previous and recent particles settling at greater depth and strong horizontal advection, only surface profiles (0 to 400 m) were considered when we investigated the particle dynamic mechanisms (Figure 9).

Inside the thermocline layer, where particle abundance and Chla reached their maximum, flux feeding from organisms seemed to represent the major degradation mechanism of settling aggregates. These water masses have been reported to possess the highest biomass and abundance of zooplankton (Longhurst 1985; Saltzman and Wishner 1997). Significant contrasts appeared between daytime and night-time deployments. We observed an increase in aggregation/disaggregation processes taking place at night inside the OMZ, for all profiles. The presence of a thick OMZ layer represents a key environmental feature affecting all trophic levels in the Pacific Ocean (Fernández-Álamo and Färber-Lorda 2006; Seibel 2010). Night-time diel migration of zooplankton and nekton through more oxic layers in the OMZ has also been reported (Kimmel et al. 2010; Wischner et al. 2013) and might explain the high particle turnover that we observed in the profiles made at night compared to the daytime profiles.

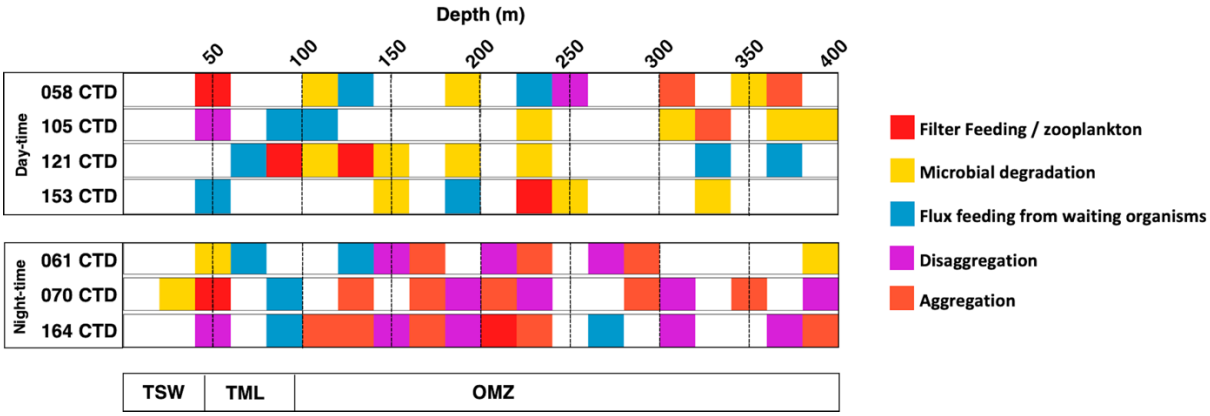

Figure 9. Particle alteration interpretation of the upper section of the water column from the surface down to 400 m depth.

All profiling stations were split in a day and night period for visual facility of interpretation. The water masses distribution is showing on the bottom: tropical surface water (TSW), thermocline layer (TML), oxygen minimum zone (OMZ).

At depths below the thermocline and OMZ, a decrease in Chla concentration and increase in turbidity suggested the presence of small inorganic particles. Since the aggregates within the thermocline layer and the OMZ were of biological origin, it seems likely that the deep particles were not directly related to the surface layer. A similar observation was found from vertical camera profiles off Cape Blanc (Karakaş et al. 2006; Nowald et al. 2006; Iversen et al. 2010), suggesting that lateral advection of aggregates and particles from the shelf region that was hundreds of kilometres away. It is possible that our study region has a similar lateral advection of particles at depths below the OMZ.

2.1.5.3 Export of particulate matter to the seafloor

The formation of polymetallic nodules is still under debate, but it occurs in all major oceans at a depth between 4000 and 6000 m (Hein and Koschinsky 2013) where the sedimentation rate is extremely low (CCZ: 0.2 to 1.15 cm·kyr^{-1}; Volz et al. 2018). The high abundance of polymetallic nodules in the eastern German license area of the CCZ suggest that this region has an extremely low sedimentation rate. However, this region has a stable rate of photosynthetic carbon fixation throughout all seasons and is described as a productivity transition zone with relative high export out of the surface ocean compared to other regions in the CCZ (Jeek Kim et al. 2012). Our vertical profiles of particle size-distribution and abundance provided some evidence supporting low sedimentation. We found that the aggregate size spectra were mainly centered around smaller particles (≤ 77 µm) and that large aggregates (> 300 µm) were very scarce. It was not possible to measure particle settling velocity *in situ* using our equipment. However, based on previous size-specific sinking velocity measurements of similar aggregate types (Iversen and Ploug 2010), we assume settling velocities ranging from 3 to 15 m·day^{-1} for aggregates of sizes ranging from 30 to 70 µm. Such low sinking velocities result in long residence times of the aggregates in the water column. This allows a long time for microbial degradation, zooplankton grazing and horizontal transportation, resulting in a low export efficiency (Henson et al. 2012) and hence the low sedimentation in the German licence area in the CCZ. Finally, once an aggregate is deposited on the seafloor it might be easily resuspended by increased bottom current velocity (eddies) or even benthic storms (Thomsen and Gust 2000; Aleynik et al. 2017). Furthermore, Becker et al. (2001) demonstrated that consolidation of surface sediments might take up to 20 years in the deep-sea environment.

2.1.6 Conclusion

The eastern German licence area is of particular interest and was identified as a productive transitional zone toward a more depleted ocean gyre system. Nine verticals in situ camera and CTD profiles indicated that despite a constant primary productivity in the surface ocean, only very little material reaches the seafloor due to a dominance of small, slow-sinking aggregates. We found that the combination of small aggregate size, bottom currents and slow seafloor consolidation explained the extremely low sedimentation rate

in the CCZ. Possible near-future mining of the seafloor will impact not only the benthic ecosystem but also the entire pelagic environment. We believe that our finding will improve full water-depth modelling and help make more precise predictions regarding the potential impact of mining activities on deep-sea benthic and pelagic ecosystems.

2.1.7 Acknowledgments

The authors would like to thank BGR Hannover for the invitation to participate in the SO262 cruise. We would like also to thank the shipboard team and scientist staff of the RV SONNE cruise.

2.1.8 Funding information

We acknowledged BGR Hannover for co-financing this study. B.G. is supported by JPI Oceans2 project "EcoMining-DEU – Ecological Aspects of Deep-Sea Mining". This publication is supported by the HGF Young Investigator Group SeaPump "Seasonal and regional food web interactions with the biological pump": VH-NG-1000 and by the OceanLab of Jacobs University. I.M.H. was supported by the Helmholtz Association, the Alfred Wegener Institute Helmholtz Centre for Polar and Marine Research and the DFG-Research Center/Cluster of Excellence "The Ocean in the Earth System" at MARUM.

2.1.9 References

Aleynik, D., Inall, M.E., Dale, A., Vink, A., 2017. Impact of remotely generated eddies on plume dispersion at abyssal mining sites in the Pacific. Sci. Rep. 7, 1–14. https://doi.org/10.1038/s41598-017-16912-2

Amador, J.A., Alfaro, E.J., Lizano, O.G., Magaña, V.O., 2006. Atmospheric forcing of the eastern tropical Pacific: A review. Prog. Oceanogr. 69, 101–142. https://doi.org/10.1016/j.pocean.2006.03.007

Ayers, J.M., Lozier, M.S., 2010. Physical controls on the seasonal migration of the North Pacific transition zone chlorophyll front. J. Geophys. Res. Ocean. 115, 1–11. https://doi.org/10.1029/2009JC005596

Becker, H.J., Grupe, B., Oebius, H.U., Liu, F., 2001. The behaviour of deep-sea sediments under the impact of nodule mining processes. Deep. Res. Part II Top. Stud. Oceanogr. 48, 3609–3627. https://doi.org/10.1016/S0967-0645(01)00059-5

Behrenfeld, M.J., Falkowski, P.G., 1997a. Photosynthetic rates derived from satellite-based chlorophyll concentration. Limnol. Oceanogr. 42, 1–20.

Behrenfeld, M.J., Falkowski, P.G., 1997b. 1997 Behrenfeld a consumer's guide to phyto primary productivity models 42.

Bendtsen, J., Hilligsøe, K.M., Hansen, J.L.S., Richardson, K., 2015. Analysis of

remineralisation, lability, temperature sensitivity and structural composition of organic matter from the upper ocean. Prog. Oceanogr. 130, 125–145. https://doi.org/10.1016/j.pocean.2014.10.009

Burd, A.B., Jackson, G.A., 2009. ParticleAggregation. Ann. Rev. Mar. Sci. 1, 65–90. https://doi.org/10.1146/annurev.marine.010908.163904

Chan, A.T., Anderson, G.C., 1981. Environmental investigation of the effect of deep-sea mining on marine phytoplankton and primary productivity in the tropical eastern north Pacific ocean. Mar. Min. 3, 121–149.

Chelton, D.B., Freilich, M.H., Esbensen, S.K., 2002. Satellite Observations of the Wind Jets off the Pacific Coast of Central America. Part II: Regional Relationships and Dynamical Considerations. Mon. Weather Rev. 128, 2019–2043. https://doi.org/10.1175/1520-0493(2000)128<2019:sootwj>2.0.co;2

Christiansen, B., Denda, A., Christiansen, S., 2019. Potential effects of deep seabed mining on pelagic and benthopelagic biota. Mar. Policy 0–1. https://doi.org/10.1016/j.marpol.2019.02.014

Fernández-Álamo, M.A., Färber-Lorda, J., 2006. Zooplankton and the oceanography of the eastern tropical Pacific: A review. Prog. Oceanogr. 69, 318–359. https://doi.org/10.1016/j.pocean.2006.03.003

Fiedler, P.C., Talley, L.D., 2006. Hydrography of the eastern tropical Pacific: A review. Prog. Oceanogr. 69, 143–180. https://doi.org/10.1016/j.pocean.2006.03.008

Fowler, S.W., Knauer, G.A., 1986. Role of large particles in the transport of elements and organic compounds through the oceanic water column. Prog. Oceanogr. 16, 147–194. https://doi.org/10.1016/0079-6611(86)90032-7

Frost, B.W., 1972. Effects of Size and Concentration of Food Particles on the Feeding Behavior of the Marine Planktonic Copepod Calanus Pacificus. Limnol. Oceanogr. 17, 805–815. https://doi.org/10.4319/lo.1972.17.6.0805

Fryxell, G.A., Taguchi, S., El-Sayed, S.Z., 1979. Vertical distribution of diverse phytoplankton communities in the central Pacific, in: Piper, by J.L.B. and D.Z. (Ed.), Marine Geology and Oceanography of the Pacific Manganese Nodule Province. Plenum Publishing Corporation, pp. 203–239. https://doi.org/https://doi.org/10.1007/978-1-4684-3518-4_6

Gillard, B., Purkiani, K., Chatzievangelou, D., Vink, A., Iversen, M.H., Thomsen, L., 2019. Physical and hydrodynamic properties of deep sea mining-generated , abyssal sediment plumes in the Clarion Clipperton Fracture Zone (eastern-central Pacific). Elem. Sci. Anthr. https://doi.org/https://doi.org/10.1525/elementa.343

Gorsky, G., Picheral, M., Stemmann, L., 2000. Use of the underwater video profiler for the study of aggregate dynamics in the North Mediterranean. Estuar. Coast. Shelf Sci. 50, 121–128. https://doi.org/10.1006/ecss.1999.0539

Guidi, L., Stemmann, L., Jackson, G.A., Ibanez, F., Claustre, H., Legendre, L., Picheral, M., Gorsky, G., 2009. Effects of phytoplankton community on production, size, and export of large aggregates: A world-ocean analysis. Limnol. Oceanogr. 54, 1951–1963. https://doi.org/10.4319/lo.2009.54.6.1951

Hamm, C.E., 2002. Interactive aggregation and sedimentation of diatoms and clay-sized lithogenic material. Limnol. Oceanogr. 47, 1790–1795. https://doi.org/10.4319/lo.2002.47.6.1790

Hein, J.R., Koschinsky, A., 2013. Deep-Ocean Ferromanganese Crusts and Nodules, in: Treatise on Geochemistry: Second Edition. Published by Elsevier Inc., pp. 273–291. https://doi.org/10.1016/B978-0-08-095975-7.01111-6

Henson, S.A., Sanders, R., Madsen, E., 2012. Global patterns in efficiency of particulate organic carbon export and transfer to the deep ocean. Global Biogeochem. Cycles 26,

1–14. https://doi.org/10.1029/2011GB004099
Henson, S.A., Yool, A., Sanders, R., 2015. Variability in efficiency of particulate organic carbon export: A model study. Global Biogeochem. Cycles 33–45. https://doi.org/10.1002/2014GB004965
Iversen, M.H., Nowald, N., Ploug, H., Jackson, G.A., Fischer, G., 2010. High resolution profiles of vertical particulate organic matter export off Cape Blanc, Mauritania: Degradation processes and ballasting effects. Deep. Res. Part I Oceanogr. Res. Pap. 57, 771–784. https://doi.org/10.1016/j.dsr.2010.03.007
Iversen, M.H., Ploug, H., 2010. Ballast minerals and the sinking carbon flux in the ocean: Carbon-specific respiration rates and sinking velocity of marine snow aggregates. Biogeosciences 7, 2613–2624. https://doi.org/10.5194/bg-7-2613-2010
Jackson, G.A., 1998. Using fractal scaling and two-dimensional particle size spectra to calculate coagulation rates for heterogeneous systems. J. Colloid Interface Sci. 202, 20–29. https://doi.org/10.1006/jcis.1998.5435
Jackson, G.A., 1995. Comparing observed changes in particle size spectra with those predicted using coagulation theory. Deep. Res. Part II 42, 159–184. https://doi.org/10.1016/0967-0645(95)00010-N
Jackson, G.A., 1993. Flux feeding as a mechanism for zooplankton grazing and its implications for vertical particulate flux. Limnol. Oceanogr. 38, 1328–1331. https://doi.org/10.4319/lo.1993.38.6.1328
Jones, D.O.B., Kaiser, S., Sweetman, A.K., Smith, C.R., Menot, L., Vink, A., Trueblood, D., Greinert, J., Billett, D.S.M., Arbizu, P.M., Radziejewska, T., Singh, R., Ingole, B., Stratmann, T., Simon-Lledó, E., Durden, J.M., Clark, M.R., 2017. Biological responses to disturbance from simulated deep-sea polymetallic nodule mining. PLoSOne 12. https://doi.org/10.1371/journal.pone.0171750
Karakaş, G., Nowald, N., Blaas, M., Marchesiello, P., Frickenhaus, S., Schlitzer, R., 2006. High-resolution modeling of sediment erosion and particle transport across the northwest African shelf. J. Geophys. Res. Ocean. 111, 1–13. https://doi.org/10.1029/2005JC003296
Karakaş, G., Nowald, N., Schäfer-Neth, C., Iversen, M., Barkmann, W., Fischer, G., Marchesiello, P., Schlitzer, R., 2009. Impact of particle aggregation on vertical fluxes of organic matter. Prog. Oceanogr. 83, 331–341. https://doi.org/10.1016/j.pocean.2009.07.047
Kessler, W.S., 2006. The circulation of the eastern tropical Pacific: A review. Prog. Oceanogr. 69, 181–217. https://doi.org/10.1016/j.pocean.2006.03.009
Kim, H.J., Hyeong, K., Yoo, C.M., Khim, B.K., Kim, K.H., Son, J.W., Kug, J.S., Park, J.Y., Kim, D., 2012. Impact of strong El Niño events (1997/98 and 2009/10) on sinking particle fluxes in the 10°N thermocline ridge area of the northeastern equatorial Pacific. Deep. Res. Part I Oceanogr. Res. Pap. 67, 111–120. https://doi.org/10.1016/j.dsr.2012.05.008
Kimmel, D.G., Boicourt, W.C., Pierson, J.J., Roman, M.R., Zhang, X., 2010. The vertical distribution and diel variability of mesozooplankton biomass, abundance and size in response to hypoxia in the northern Gulf of Mexico USA. J. Plankton Res. 32, 1185–1202. https://doi.org/10.1093/plankt/fbp136
Longhurst, A.R., 1985. Relationship between diversity and the vertical structure of the upper ocean. Deep Sea Res. Part A, Oceanogr. Res. Pap. 32, 1535–1570. https://doi.org/10.1016/0198-0149(85)90102-5
Lutz, M., Dunbar, R., Caldeira, K., 2002. Regional variability in the vertical flux of particulate organic carbon in the ocean interior. Global Biogeochem. Cycles 16, 11-1-11–18. https://doi.org/10.1029/2000gb001383

Markussen, T.N., 2016. Parchar – Characterization of Suspended Particles Through Image Processing in Matlab. J. Open Res. Softw. 4, 1–7. https://doi.org/10.5334/jors.114

Martin, J.H., Knauer, G.A., Karl, D.M., Broenkow, W.W., 1987. VERTEX: carbon cycling in the northeast Pacific. Deep. Res. 34, 267–285. https://doi.org/10.7591/9781501723667

Miller, K.A., Thompson, K.F., Johnston, P., Santillo, D., 2018. An Overview of Seabed Mining Including the Current State of Development, Environmental Impacts, and Knowledge Gaps. Front. Mar. Sci. 4. https://doi.org/10.3389/fmars.2017.00418

Mouw, C.B., Barnett, A., Mckinley, G.A., Gloege, L., Pilcher, D., 2016. Phytoplankton size impact on export flux in the global ocean. Global Biogeochem. Cycles 1542–1562. https://doi.org/10.1002/2015GB005355

Nowald, N., Iversen, M.H., Fischer, G., Ratmeyer, V., Wefer, G., 2015. Time series of in-situ particle properties and sediment trap fluxes in the coastal upwelling filament off Cape Blanc, Mauritania. Prog. Oceanogr. 137, 1–11. https://doi.org/10.1016/j.pocean.2014.12.015

Nowald, N., Karakas, G., Ratmeyer, V., Fischer, G., Schlitzer, R., Davenport, R.A., Wefer, G., 2006. Distribution and transport processes of marine particulate matter off Cape Blanc (NW-Africa): results from vertical camera profiles. Ocean Sci. Discuss. 3, 903–938. https://doi.org/10.5194/osd-3-903-2006

O'Reilly, J.E., Maritorena, S., Mitchell, B.G., Siegel, D.A., Carder, K.L., Garver, S.A., Kahru, M., Mcclain, C., 1998. Ocean color chlorophyll algorithms for SeaWiFS. J. Geophys. Res. 103, 24937–24953.

Oebius, H.U., Becker, H.J., Rolinski, S., Jankowski, J.A., 2001. Parametrization and evaluation of marine environmental impacts produced by deep-sea manganese nodule mining. Deep. Res. Part II Top. Stud. Oceanogr. 48, 3453–3467. https://doi.org/10.1016/S0967-0645(01)00052-2

Pabortsava, K., Purser, A., Wagner, H., Thomsen, L., 2011. The influence of drill cuttings on physical characteristics of phytodetritus. Mar. Pollut. Bull. 62, 2170–2180. https://doi.org/10.1016/j.marpolbul.2011.07.002

Picheral, M., Guidi, L., Stemmann, L., Karl, D.M., Iddaoud, G., Gorsky, G., 2010. The underwater vision profiler 5: An advanced instrument for high spatial resolution studies of particle size spectra and zooplankton. Limnol. Oceanogr. Methods 8, 462–473. https://doi.org/10.4319/lom.2010.8.462

Ratmeyer, V., Wefer, G., 1996. A high resolution camera system (ParCa) for imaging particles in the ocean: System design and results from profiles and a three month deployment. J. Mar. Res. 54, 589–603.

Reddy, C.M., Arey, J.S., Seewald, J.S., Sylva, S.P., Lemkau, K.L., Nelson, R.K., Carmichael, C.A., McIntyre, C.P., Fenwick, J., Ventura, G.T., Van Mooy, B.A.S., Camilli, R., 2012. Composition and fate of gas and oil released to the water column during the Deepwater Horizon oil spill. Proc. Natl. Acad. Sci. 109, 20229–20234. https://doi.org/10.1073/pnas.1101242108

Saltzman, J., Wishner, K.F., 1997. Zooplankton ecology in the eastern tropical pacific oxygen minimum zone above a seamount: 1. General trends. Deep. Res. Part I Oceanogr. Res. Pap. 44, 907–930. https://doi.org/10.1016/S0967-0637(97)00007-1

Seibel, B.A., 2010. Critical oxygen levels and metabolic suppression in oceanic oxygen minimum zones. J. Exp. Biol. 214, 326–336. https://doi.org/10.1242/jeb.049171

Taylor, P., Hyun, J.H., Kim, K.H., Jung, H.S., Kim, K., Jung, H., Lee, K., 1998. Marine Georesources& Geotechnology Potential environmental impact of deep seabed manganese nodule mining on the synechococcus(cyanobacteria) in the northeast

equatorial pacific : Effect of bottom water - sediment slurry Potential Environmental Impact 37–41.

Thomsen, L., Gust, G., 2000. Sediment erosion thresholds and characteristics of resuspended aggregates on the western European continental margin. Deep. Res. Part I Oceanogr. Res. Pap. 47, 1881–1897. https://doi.org/10.1016/S0967-0637(00)00003-0

Volz, J.B., Mogollón, J.M., Geibert, W., Arbizu, P.M., Koschinsky, A., Kasten, S., 2018. Natural spatial variability of depositional conditions, biogeochemical processes and element fluxes in sediments of the eastern Clarion-Clipperton Zone, Pacific Ocean. Deep. Res. Part I Oceanogr. Res. Pap. 140, 159–172. https://doi.org/10.1016/j.dsr.2018.08.006

Wegorzewski, A. V., Kuhn, T., 2014. The influence of suboxic diagenesis on the formation of manganese nodules in the Clarion Clipperton nodule belt of the Pacific Ocean. Mar. Geol. 357, 123–138. https://doi.org/10.1016/j.margeo.2014.07.004

Wiedicke-Hombach, 2009. Cruise Report "MANGAN 2008" with R/V Kilo Moana. Hannover.

Willett, C.S., Leben, R.R., Lavín, M.F., 2006. Eddies and Tropical Instability Waves in the eastern tropical Pacific: A review. Prog. Oceanogr. 69, 218–238. https://doi.org/10.1016/j.pocean.2006.03.010

Wischner, K.F., Outram, D.M., Seibel, B.A., Daly, K.L., Williams, R.L., 2013. Zooplankton in the eastern tropical north Pacific: Boundary effects of oxygen minimum zone expansion. Deep Sea Res. Part I Oceanogr. Res. Pap. 122–140. https://doi.org/10.1016/j.dsr.2013.05.012

2.1.10 Supplementary materials

Table S1. Particle size classification

Size classes		1	2	3	4	5	6	7	8	9	10	11
Lower limit	**(µm)**	28	39	55	77	108	151	211	295	413	579	810
Upper limit	**(µm)**	39	55	77	108	151	211	295	413	579	810	1134
Median	**(µm)**	34	47	66	92	129	181	253	354	496	694	972

Table S2. MODIS Chlorophyll a concentration (mg/m^3) over 8 days period interval.

Station #	Period Interval (2018)							
	30.03 07.04	07.04 15.04	15.04 23.04	23.04 01.05	01.05 09.05	09.05 17.05	17.05 25.05	25.05 02.06
058	0.112	-	-	-	-	0.142	-	0.093
061	0.110	-	-	-	-	0.144	-	0.097
070	0.110	-	-	-	-	0.144	-	0.097
105	0.125	-	-	0.142	-	-	0.115	0.098
121	0.125	-	-	0.142	-	-	0.115	0.098
153	0.109	0.113	-	-	-	0.104	-	0.112
164	0.211	-	-	-	-	0.137	-	0.104

(-) indicate cloud coverage

Table S3. Spearman correlation coefficients for selected parameters of all stations from the surface till 400 m depth.

Station #	Parameters	D50	Abundance	Turbidity	Fluorescence	Total Volume
58	**D50**	1	**0.66408**	0.34086	0.31038	**0.94138**
	Abundance	**0.66408**	1	0.4302	0.33197	**0.78071**
	Turbidity	0.34086	0.4302	1	**0.93096**	0.39669
	Fluorescence	0.31038	0.33197	**0.93096**	1	0.36085
	Total Volume	**0.94138**	**0.78071**	0.39669	0.36085	1
61	**D50**	1	**0.82402**	**0.56765**	**0.52258**	**0.98234**
	Abundance	**0.82402**	1	**0.68368**	**0.62912**	**0.85295**
	Turbidity	**0.56765**	**0.68368**	1	**0.93996**	**0.59844**
	Fluorescence	**0.52258**	**0.62912**	**0.93996**	1	0.53251
	Total Volume	**0.98234**	**0.85295**	**0.59844**	0.53251	1
70	**D50**	1	-0.28861	0.15719	-0.027717	**0.91907**
	Abundance	-0.28861	1	0.29311	0.081457	-0.17322
	Turbidity	0.15719	0.29311	1	**0.7758**	0.3347
	Fluorescence	0.027717	0.081457	**0.7758**	1	0.13677
	Total Volume	**0.91907**	**-0.17322**	0.3347	0.13677	1
105	**D50**	1	0.12773	-0.23875	-0.087054	**0.7551**
	Abundance	0.12773	1	0.42083	**0.59855**	0.35474
	Turbidity	-0.23875	0.42083	1	**0.7961**	-0.087719
	Fluorescence	0.087054	**0.59855**	**0.7961**	1	0.080398
	Total Volume	**0.7551**	0.35474	-0.087719	0.080398	1
121	**D50**	1	0.40314	-0.0093813	0.030395	**0.88596**
	Abundance	0.40314	1	**0.60756**	**0.55846**	**0.66136**
	Turbidity	0.009381	**0.60756**	1	**0.84803**	0.29234
	Fluorescence	0.030395	**0.55846**	**0.84803**	1	0.34412
	Total Volume	0.88596	0.66136	0.29234	0.34412	1

Table S3. Continued

Station #	Parameters	D50	Abundance	Turbidity	Fluorescence	Total Volume
153	**D50**	1	0.21896	0.14833	0.22814	**0.83002**
	Abundance	0.21896	1	**0.69279**	**0.62303**	0.53292
	Turbidity	0.14833	**0.69279**	1	**0.86049**	0.29534
	Fluorescence	0.22814	**0.62303**	**0.86049**	1	0.34053
	Total Volume	**0.83002**	0.53292	0.29534	0.34053	1
164	**D50**	1	**0.95331**	0.025722	0.071165	**0.74662**
	Abundance	**0.95331**	1	0.071144	0.18094	**0.71806**
	Turbidity	0.025722	0.071144	1	**0.89362**	0.034088
	Fluorescence	0.071165	0.18094	**0.89362**	1	0.1094
	Total Volume	**0.74662**	**0.71806**	0.034088	0.1094	1

Number in **bold** show significant correlations (p< 0.001)

Table S4. Spearman correlation coefficients for selected parameters of all stations from 400 m till 4000 m depth.

Station #	Parameters	D50	Abundance	Turbidity	Total Volume
61	**D50**	1	**0.52747**	-0.22057	-0.22974
	Abundance	**0.52747**	1	-0.0407	-0.01611
	Turbidity	-0.22057	**-0.040699**	1	**0.85343**
	Total Volume	-0.22974	-0.01611	0.85343	1
70	**D50**	1	0.14893	**-0.24411**	-0.18755
	Abundance	0.14893	1	0.078858	0.09079
	Turbidity	**-0.24411**	0.078858	1	**0.78701**
	Total Volume	-0.18755	0.09079	**0.78701**	1
121	**D50**	1	**0.51208**	0.006751	-0.03688
	Abundance	**0.51208**	1	**-0.26631**	-0.10742
	Turbidity	0.006751	-0.26631	1	**0.37093**
	Total Volume	-0.03688	-0.10742	**0.37093**	1
164	**D50**	1	**0.63657**	0.068701	0.042851
	Abundance	**0.63657**	1	-0.03618	-0.048677
	Turbidity	0.068701	-0.03618	1	**0.43908**
	Total Volume	0.042851	-0.048677	**0.43908**	1

Number in **bold** show significant correlations (p< 0.001)

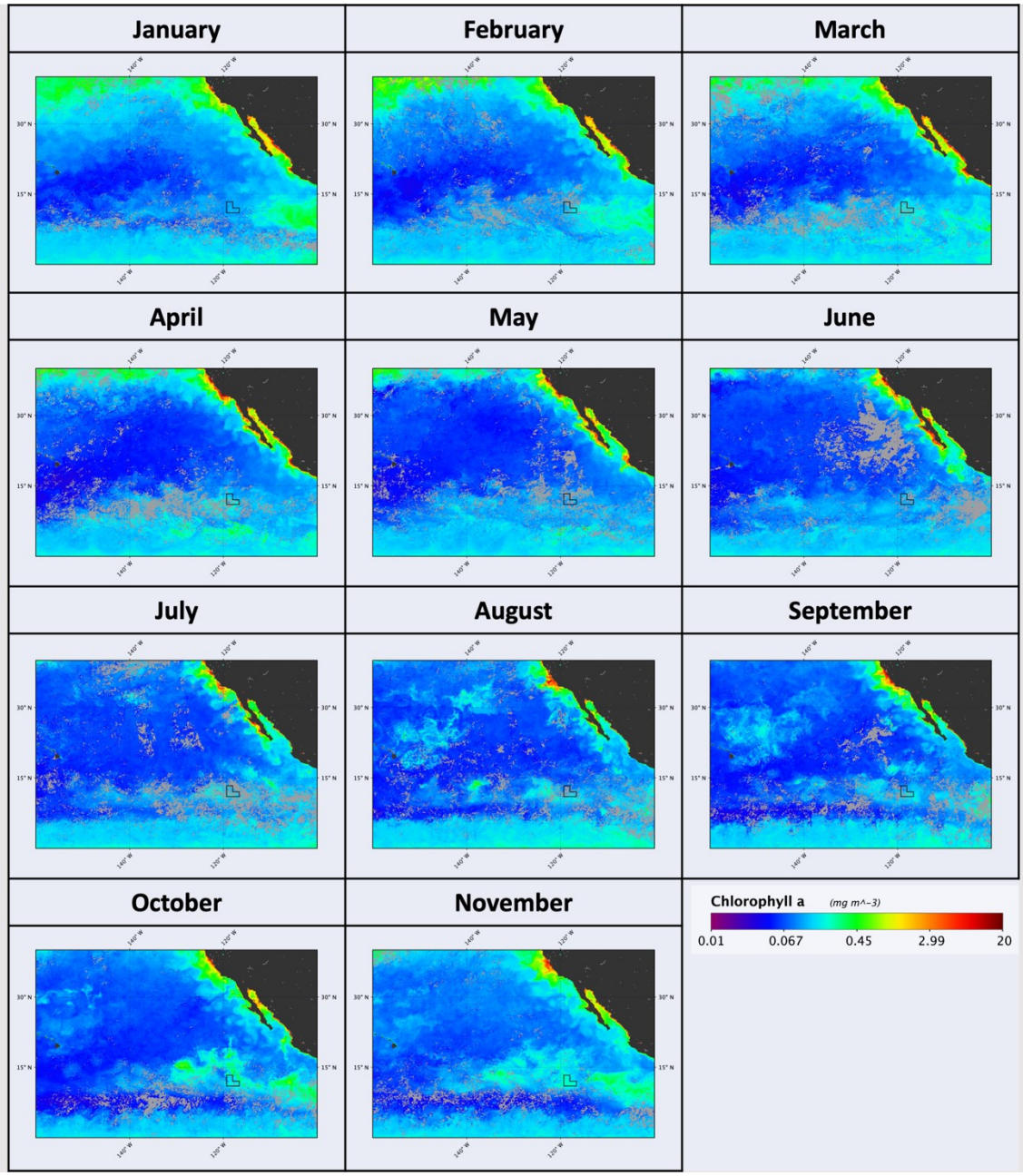

Figure S1. Monthly 2018 surface chlorophyll distribution in the north-eastern Pacific
Light gray corresponds to cloud coverage and the Mexican coast is represented in dark color. Eastern German Licensed area is indicated by a black polygon.

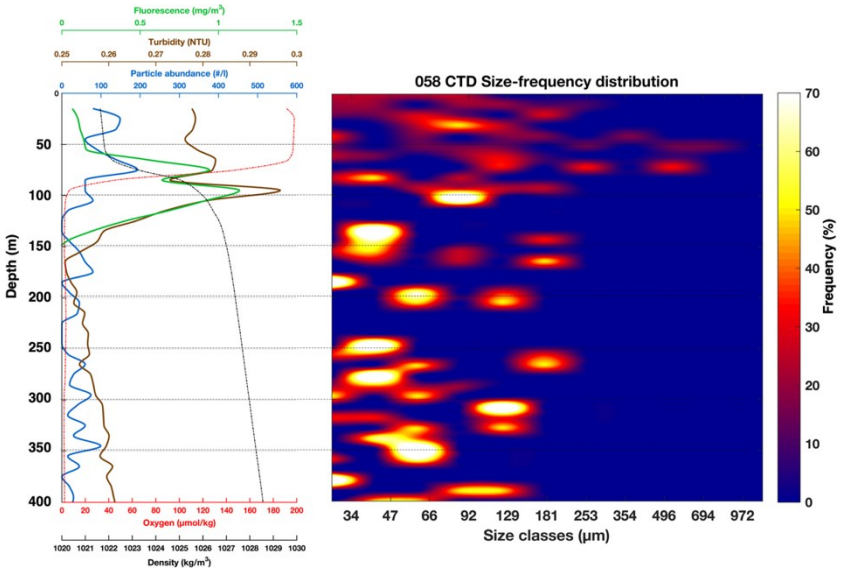

Figure S2. Concentration and size distribution of profile 058CTD from the surface down to 400m.

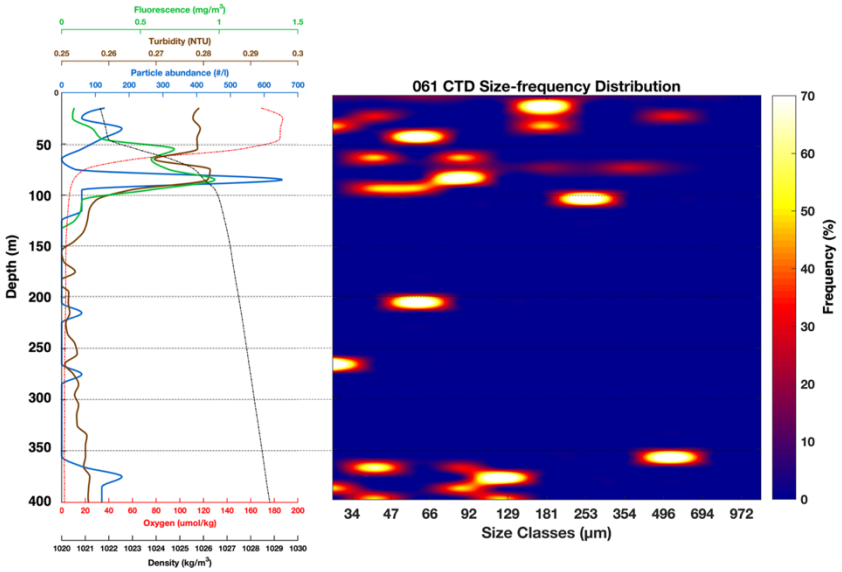

Figure S3. Concentration and size distribution of profile 061CTD from the surface down to 400m.

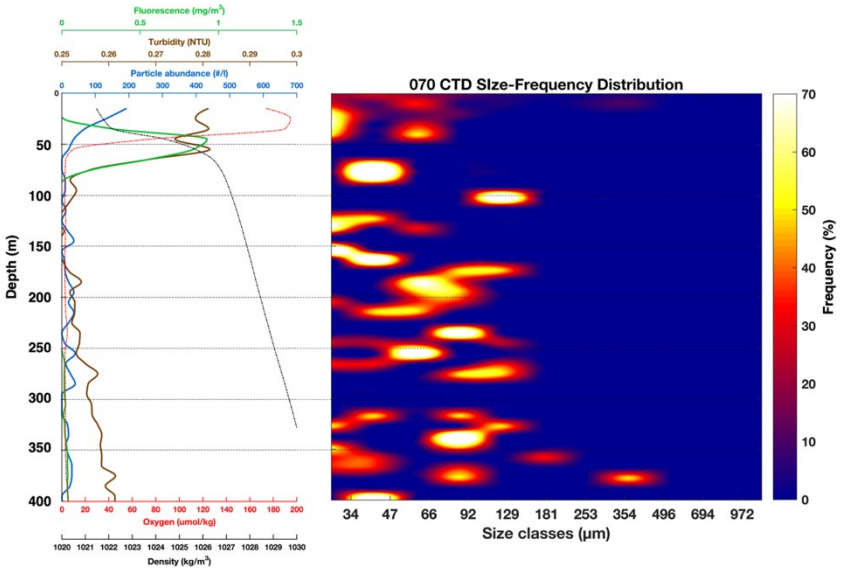

Figure S4. Concentration and size distribution of profile 070CTD from the surface down to 400m.

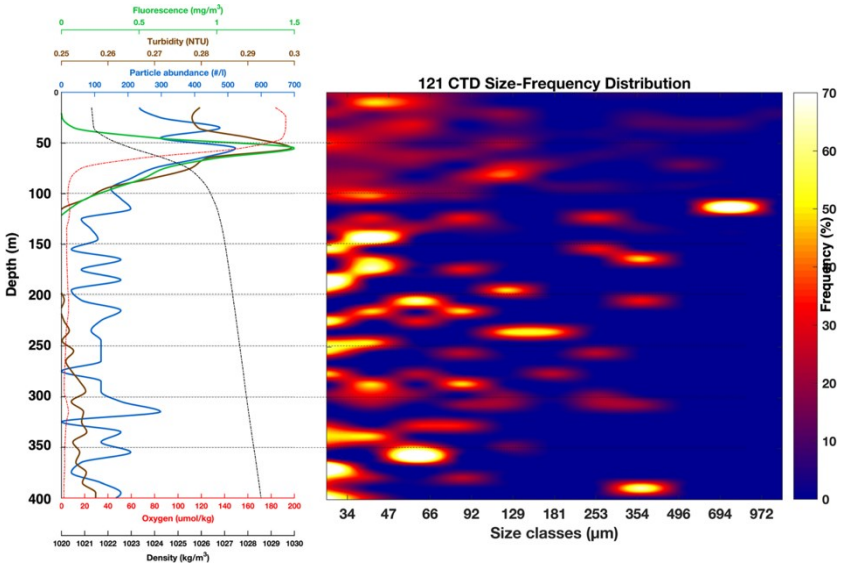

Figure S5. Concentration and size distribution of profile 121CTD from the surface down to 400m.

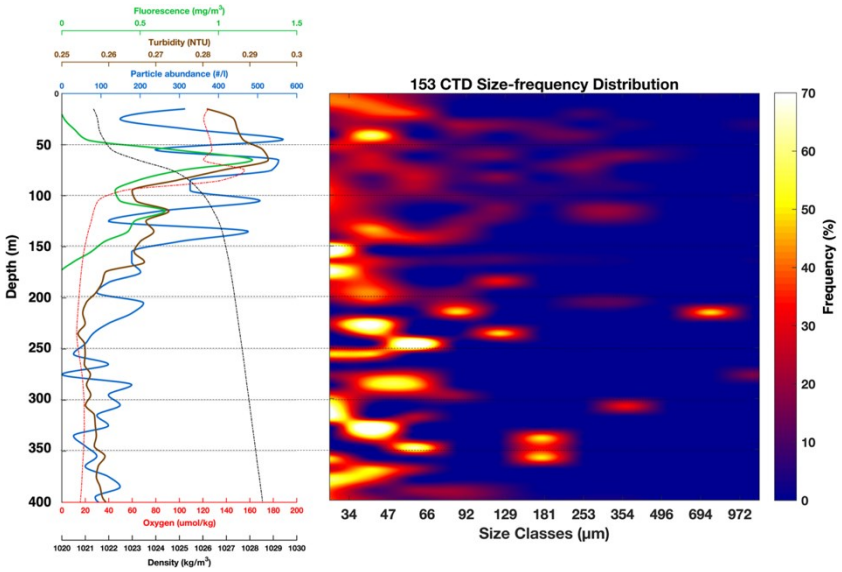

Figure S6. Concentration and size distribution of profile 153CTD from the surface down to 400m.

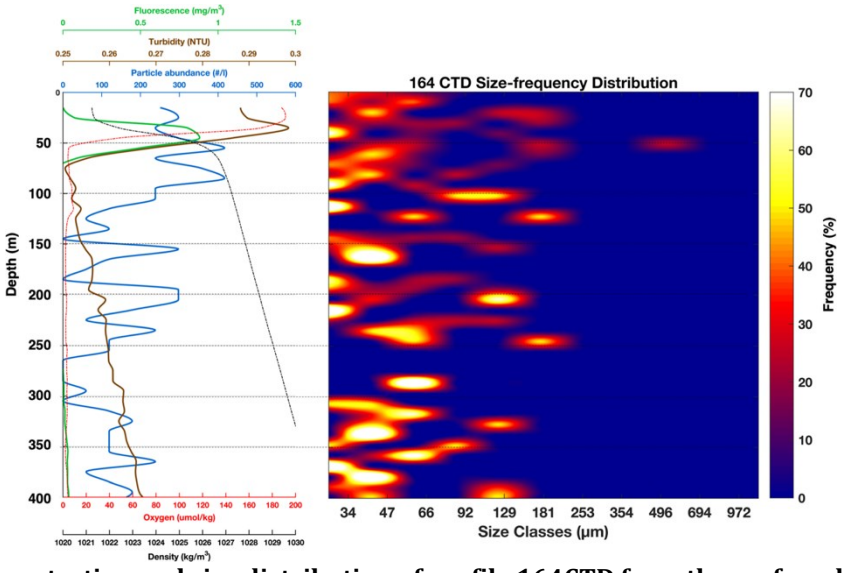

Figure S7. Concentration and size distribution of profile 164CTD from the surface down to 400m.

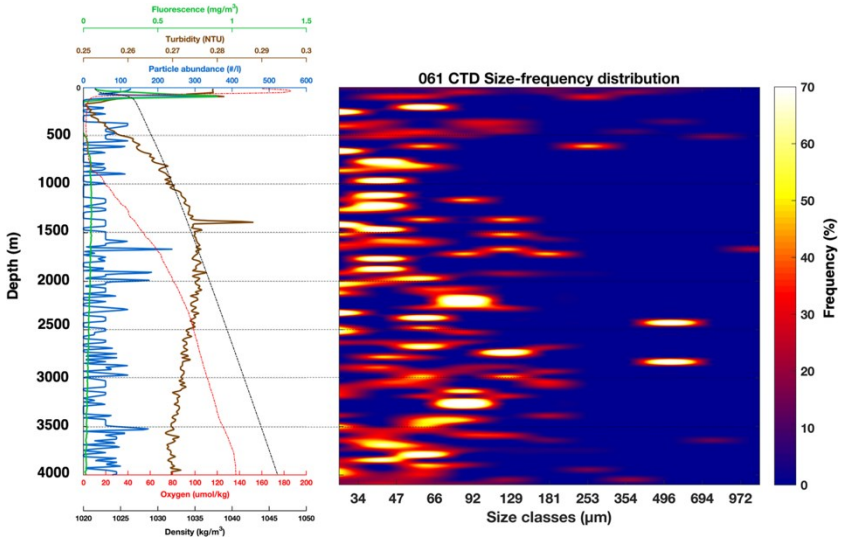

Figure S8. Concentration and size distribution of profile 061CTD from the surface down to 4000m.

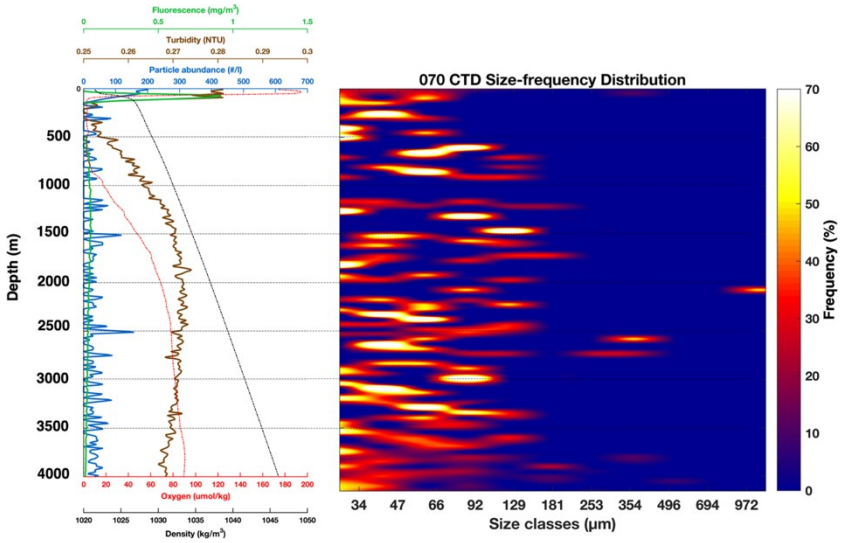

Figure S9. Concentration and size distribution of profile 070CTD from the surface down to 4000m.

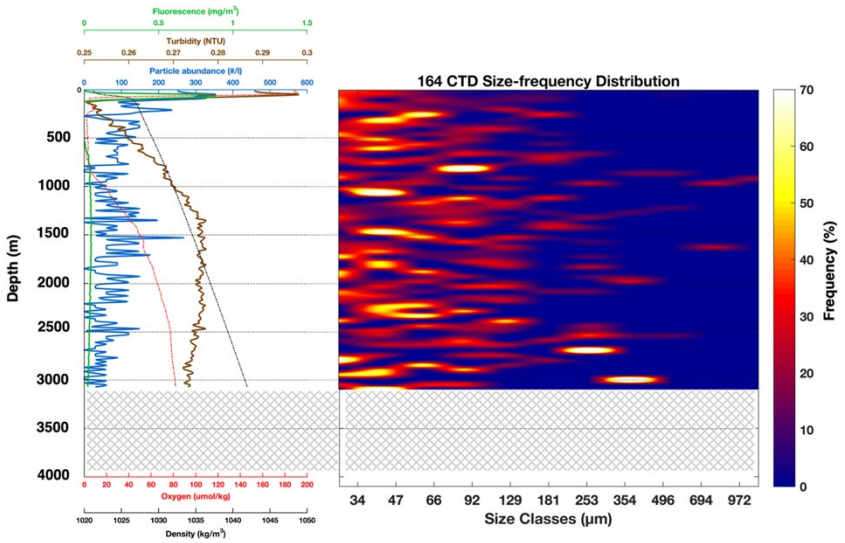

Figure S10. Concentration and size distribution of profile 164CTD from the surface down to 4000m.

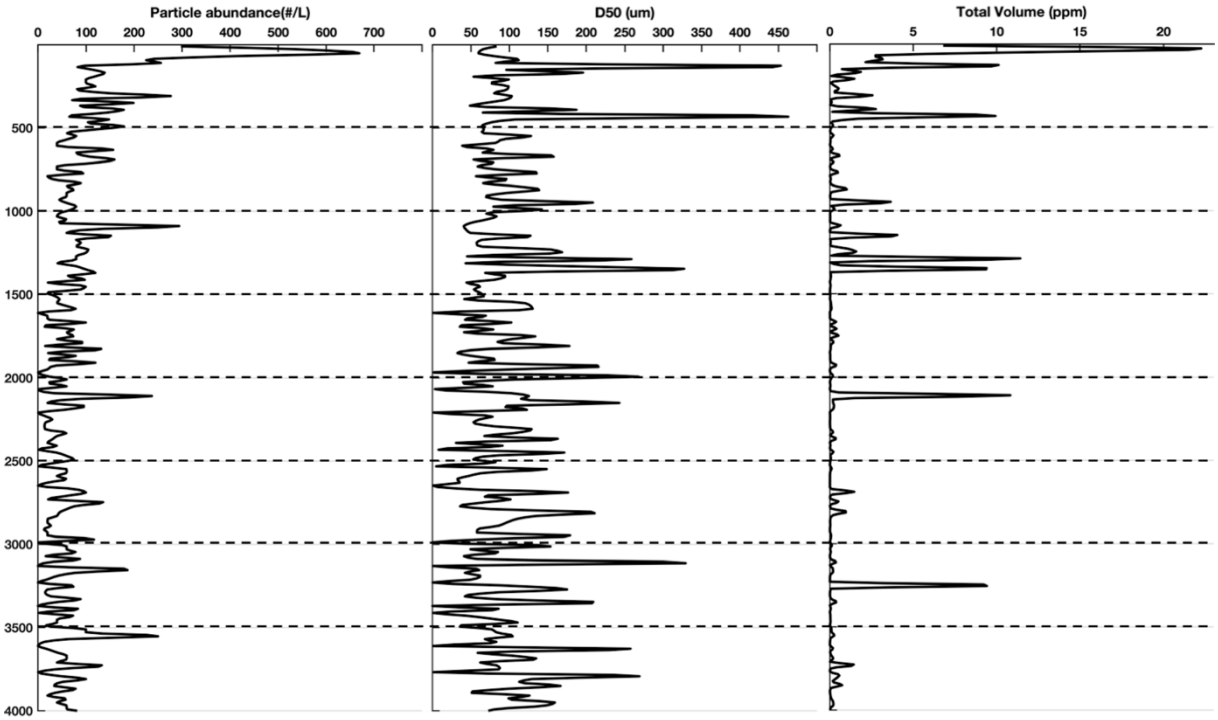

Figure S11. Profile 121 particles related parameters captured by the camera system.

2.2 Manuscript II: Physical and hydrodynamic properties of deep sea mining-generated, abyssal sediment plumes in the Clarion Clipperton fracture zone (eastern-central Pacific)

Benjamin Gillard[1, 2, *], Kaveh Purkiani [1], Damianos Chatzievangelou [2], Annemiek Vink [3], Morten H. Iversen [1], Laurenz Thomsen [2]

[1] MARUM - Center for Marine Environmental Sciences, University of Bremen, Bremen, Germany

[2] Jacobs University, Bremen, Germany

[3] BGR, Bundesanstalt für Geowissenschaften und Rohstoffe, Hannover, Germany

* b.gillard@jacobs-university.de / bgillard@marum.de

Published in Elementa Science of the Anthropocene, DOI: 10.1525/elementa.343

2.2.1 Abstract

The anthropogenic impact from polymetallic nodule harvesting in the Clarion Clipperton Fracture Zone is expected to strongly affect the benthic ecosystem. To predict the long-term, industrial-scale impact of nodule mining on the deep sea, the characteristics of deep-sea particles have to be provided to improve sediment plume model reliability. Discharge simulations of mining-related fine ($d_{50} \approx 20$ μm) sediment plumes with a concentration of 35 -500 mg L^{-1} indicate a rapid flocculation propensity within 10 to 135 minutes, resulting in the formation of large aggregates that are up to 1100 μm in size. A clear deviation between the range of analyzed settling velocities (7 - 355 m d^{-1}) of large plume aggregates (>100 μm) and from model-based calculations (e.g. Stokes) was observed. Our findings indicate that the discharge of elevated plume concentrations (500 mg L^{-1}) under elevated shear rate ($G \geq 2.4$ s^{-1}) would result in an improved sediment flocculation efficiency. Furthermore, our model results suggest that even under typical deep-sea flow conditions a relatively fast deposition of particles can be expected and, thereby, restrict the blanketing to a relatively small fall-out area near the source.

2.2.2 Introduction

Over the past decade, increasing global consumption and rising market prices of metals, together with technological improvements, have driven several countries and industries to prospect the deep-sea environment for mineral resources, including polymetallic nodules (Hein and Koschinsky, 2013).

Polymetallic nodules that are rich in metals and rare earth elements lie on the surface of the abyssal sediment. The Clarion Clipperton Fracture Zone (CCZ), located in the north-eastern equatorial Pacific (Fig. 1), contains the most extensive nodule deposition known (Halbach and Fellerer, 1980) and is of high economic interest (Wedding et al., 2015). However, nodule fields are also essential habitats for benthic communities (Kaiser et al., 2017) and more than half of the megafauna discovered in the CCZ rely on the nodules as hard substrate (Amon et al., 2016).

The potential future use of mining equipment on the ocean floor and the subsequent return of mining products (e.g. sediment, water, abraded nodule debris) to the benthic boundary layer (BBL) will create an operational and discharge plume of fine

particulate material (Oebius et al., 2001). Sediment re-deposition and bottom blanketing in the vicinity of the mining site ("near field") will potentially bury benthic organisms, clog the respiratory surfaces of filter feeders and pollute the food supply for most benthic organisms. Potential long-range, lateral and vertical dispersion of plume particles will have a lower local impact but is expected to spread over several hundreds of kilometers from the disturbance location ("far field"). Both processes will affect deep-sea ecosystem structure and functioning to a certain, although presently, unknown extent (Ramirez-Llodra et al., 2011).

To date, very few studies have focused on analyzing the hydrodynamic behavior of original plume particles and modeling the scale of the impact at different temporal and spatial scales (Aleynik et al., 2017; Jones et al., 2017). Multiple local and regional factors such as the physical and chemical properties of the bottom sediments, the hydrodynamic regime (near and far field), bottom topography and the type of mining equipment, must to be considered simultaneously.

Transport modeling of two small-scale benthic impact experiments carried out in the nineties (discharge of ca. 10 kg s^{-1} along predefined tracks) showed that 90 % of the suspended particles created by artificial disturbance of the seafloor settled within a radius of 2 km from the disturbance area (Fukushima, 1995; Nakata et al., 1997).

Recent modeling of an industrial-scale, near-bottom sediment plume in a case study area in the CCZ with a discharge rate of 280 kg s^{-1} has shown that more than 50 % of the suspended particles settled within several kilometers of the source region within ten days. The remaining particles were transported outside the model boundary (Aleynik et al., 2017). However, the cohesive properties, aggregation potential, and different settling processes of the fine-grained deep-sea sediments were not considered, although they have an important effect on (rapid) plume sediment deposition. We believe that the use of site-specific particle behavior under different plume concentrations, in combination with high-resolution bathymetric and oceanographic data, will greatly aid in the initialization and calibration of existing sediment transport models for the nodule fields of the CCZ.

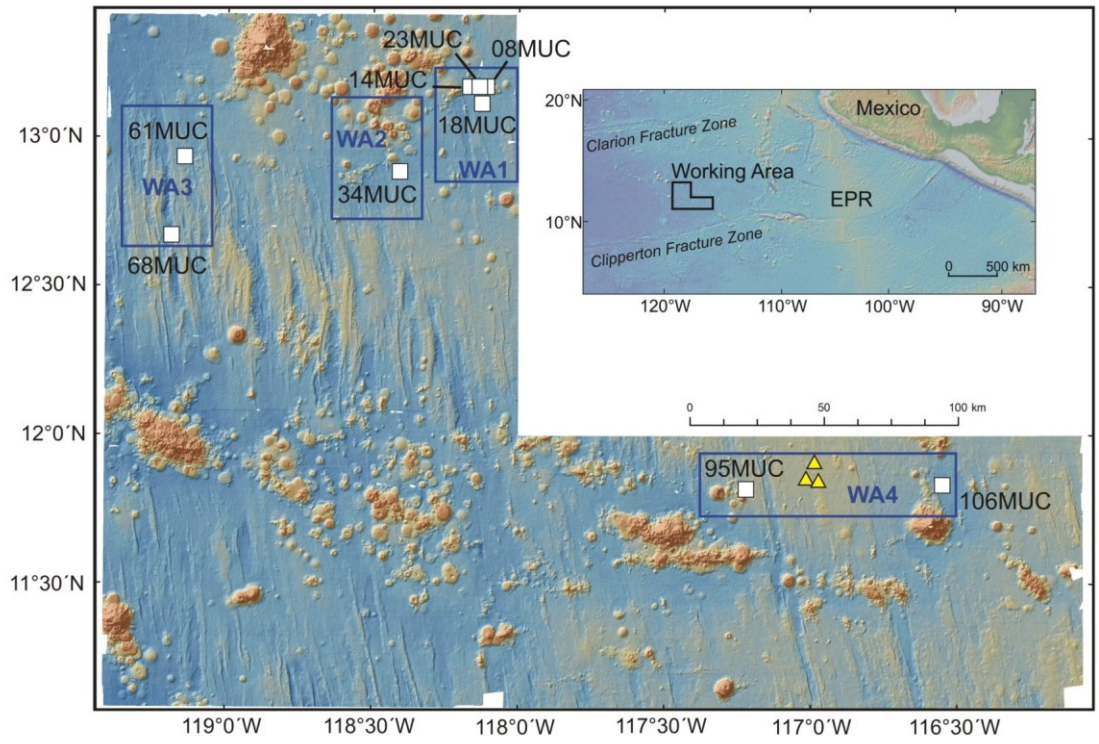

Figure 1. Study areas and locations of sediment samples in relation to the topography.

The area is located in the eastern German manganese nodule license area, north-eastern Pacific Ocean and characterized by numerous seamounts, NW-SE ridge systems and flat abyssal plains. ◘ Represent the working areas WA1 to WA4 of cruise SO-240 (Kuhn, 2015). ◘ Sediment core sampling Locations.△ Positions of three acoustic current meters that recorded current speeds and directions close to the seafloor throughout three consecutive years. Inset: view of the license area in relation to the East Pacific Rise (EPR) and the Clarion and Clipperton Fracture Zones.

To provide more insight into the likely behavior of the sediment plume produced by an industrial-scale mining operation, our research aims were to: (**1**) produce a complete set of sedimentological parameters that are crucial for model reliability and accuracy, and (**2**) recommend optimal discharge release conditions that will result in a low impact on the environment. For these purposes, laboratory experiments and particle transport modeling have been carried out using abyssal sediments from and simulating the *in-situ* conditions encountered at the CCZ area.

2.2.3 Materials and methods

2.2.3.1 Sampling site and oceanographic data acquisition

Surface sediment samples were obtained with a multicorer from 9 different locations within the eastern German license area for the exploration of polymetallic nodules in the CCZ (RV Sonne Cruise SO-240 (Kuhn, 2015); see Fig. 1 and Supplemental Table S1 for details on exact locations). The eastern license area with a total size of 56,000 km^2 is located approximately 2,500 km westward of Mexico. The predominantly fine-grained sediments derive from different topographic environments at water depths of 4300 m, including flat abyssal plains, NW-SE trending ridge systems and the feet of seamounts.

The top 10 centimeters of sediment from one multicore per location were sampled at 1 cm intervals for detailed sedimentological analysis. Long-term data on current speed and direction, as well as background turbidity close to the seafloor were obtained from three moorings deployed in the eastern part of the license area (yellow triangles in Fig. 1) throughout three consecutive years, from April 2013 to May 2016. The upward-looking 600 kHz ADCPs measured in hourly intervals during the first year and then in 45 min intervals during the next two years. High-quality data were retrieved for the water mass 15 - 20 m above the seafloor (Kuhn, 2015).

2.2.3.2 Experimental conditions

All experiments were conducted in triplicates, to account for random experimental error and to facilitate the posterior statistical treatment. In-situ temperature and salinity (1.5 °C and 34.68 PSU) were reproduced in refrigerate chamber under control temperature (± 0.3 °C) and using filtered (0.2 μm) artificial seawater.

2.2.3.3 Sediment particle size distribution

Particle size-distribution of suspended sediment was measured using a combined approach of a high-resolution Digital Floc Camera (DFC) and a LISST-100X type C (Mikkelsen et al., 2005; Hill et al., 2011). Detection of particles by the floc camera was inspired by Sternberg *et al.* (Sternberg et al., 1996). The choice of applying those technics was made in the purpose of: (1) using a non-disturbing measurements technic on

untreated suspended sediments, and (2) applying both in-situ and ex-situ technologies to allow a realistic comparison of impact assessment from future mining activities.

The suspension was first analyzed with the LISST-100X (60 measurements at 1 Hz) and then transferred into the viewing chamber of the floc camera for images analysis. The resulting particle volume distributions from both instruments were compared in their overlapping detection range (10 size classes ranging from 66.9 to 381 μm). A correction was applied based on the linear relationship between the volume concentrations detected by the two instruments. The subsequent merging procedure resulted in a size distribution ranging from 1.9 μm to couples of millimeters. As in Mikkelsen et al. (2005), the correction only served for scaling between instruments, without affecting the shape of the size distribution. Instruments details, linear coefficients and experimental protocols are provided in the Supplemental Figure S1, Tables S2-S3 and Text S1.

2.2.3.4 The deep-sea sediment aggregation process

2.2.3.4.1 Aggregation due to differential settling

The propensity of deep-sea sediment (inorganic and organic materials) in suspension to form aggregates over time under differential settling conditions was assessed using roller tank incubation (Lick et al., 1993; Iversen et al., 2010). The vessel consists of a 1.15 L Plexiglas cylinder that is rotated on his side at fix angular speed to reach solid body rotation providing a continuous settling environment. The hydrodynamics of the system have been characterized by Jackson (Jackson, 2015). Four sediment concentrations (35, 105, 175 and 500 mg L^{-1}) were prepared from a stock solution of 5 g L^{-1}. The suspension was first analyzed with the LISST-100X (60 measurements at 1 Hz), then introduced into the roller tank and rotated at a fixed rate of 3 rpm. The formation of aggregates was followed with camera over time. For every measurement, a horizontal particle camera transect from the center to the outer rim of the roller tank was performed to ensure a complete view inside the cylinder. The experiment was stopped when the first aggregates reached the bottom of the rotating roller tank to prevent disproportionate aggregation due to the re-circulation of settled aggregates in the vessel. After a couple of minutes, when all the aggregates had settled to the bottom, the supernatant was re-analyzed with the LISST-100X.

2.2.3.4.2 Aggregation due to turbulent shear

The effect of shear rate on the aggregation behavior of plume particles (inorganic and organic materials) was investigated in a horizontal Couette reactor (Drapeau et al., 1994). The chamber consists of a fix inner cylinder and an outer rotating cylinder. Depending on the angular velocity of the outer cylinder, variable shear flow regime can be produced. A detailed description of the chamber is provided in Supplemental Figure S2. The calculation of the mean shear rate G (s^{-1}) produced in the chamber was provided by Van Duuren (Van Duuren, 1968). The use of a Couette-flow reactor compared to other mixing devices, such as an oscillating grid or paddle mixer, was based the uniformity of the produced turbulent shear flow and the none presence of mixing mechanisms which avoid aggregates breakup during mixing (Serra and Casamitjana, 1998; Coufort et al., 2005; Zhu et al., 2016). Three sediment plume concentrations (105, 175 and 500 mg L^{-1}) were prepared from the stock solution. The suspension was first analyzed with the LISST-100X (60 measurements at 1 Hz), then introduced into the Couette reactor and rotated under three different fixed shear rates (2.4, 5.7 and 10.4 s^{-1}). Floc detection was followed with camera over time. As for the differential settling aggregation, the experiment was stopped when the first aggregates reached the bottom of the chamber. After a couple of minutes, when all the aggregates had settled to the bottom, the supernatant was re-analyzed with the LISST-100X.

2.2.3.5 Settling velocity

To assess the sinking velocities of aggregates produced under differential settling and turbulent flow vs. particle size, a custom-made sedimentation column was built. The conceptual design was inspired by a combination of the settling column of the LISST-STX (Agrawal and Pottsmith, 2000) and a square cross-section cylinder shape (Thomsen and Gust, 2000) used for camera analysis. A detailed description of the settling column and preparation are given in Supplemental Figure S3 and Text S1.

Aggregates from the flocculation chambers were carefully transferred into a settling tube via settling/sliding along the walls of the flocculation chambers into the next experimental chamber. This approach is similar to the process occurring inside in-situ particle cameras or water column simulators (Sternberg et al., 1999; Porter et al., 2004). Aim was to characterize the general size/settling relationship (Lick et al., 1993; Manning

and Dyer, 1999) and erosion behavior of these aggregates (Thomsen and Gust, 2000; Thomsen et al., 2002) for subsequent numerical modeling of varying particle size classes.

Particle sinking velocities were measured with the camera at the lower end of the column, allowing the aggregates to reach their terminal settling velocities before video-analyses (Nowald et al., 2009).

2.2.3.6 Bedload transport and critical shear velocity (U_{*cri})

Bedload transport and critical shear velocity (u^*_{cri}) were determined in a 20 cm diameter Gust erosion chamber, with controlled bottom shear stress (Thomsen and Gust, 2000). Aggregates were carefully transferred from the flocculation reactor to the erosion chamber (see method described above for settling velocity). $U*$ was increased in increments of 0.1 cm s^{-1} every 5 min until u_{*cri} was attained and aggregates were resuspended (Pabortsava et al., 2011).

2.2.3.7 Modeling of sediment plume dispersion

A three-dimensional numerical ocean model has been developed to assess the realistic application of our experimental results and predict the sediment transport in the deep ocean. The numerical simulations were carried out using the Massachusetts Institute of Technology general circulation model (MIT-gcm; Marshall et al., 1997). No-slip conditions at lateral and bottom boundaries were applied. The initial values of horizontal and vertical diffusivity of every tracer were set to 0.1 and 10^{-4} m^2 s^{-1}. However, the model uses the parameterization method of Klymak and Legg (2010) to obtain the suitable content of eddy viscosity and turbulence dissipation values.

A multiple one-way nesting approach was applied. The coarsest model (3600 m horizontal resolution) is laterally forced by the seawater properties. The zonal and meridional current velocities were extracted from the Hybrid Coordinate Ocean Model (HYCOM). For the following higher resolution configuration (1000 m, 300 m), the lateral boundary conditions were supplied by the previous coarser model to a final horizontal resolution of 150 m and a vertical resolution of 5 m.

The model domain is located in the CCZ German license area (Fig. 1), where a collector vehicle trial is being planned for early 2019. A flat ocean bottom with a depth of 4200 m was assumed for simplicity. Sediment transport was simulated by solving the

passive tracer equation with an additional settling velocity and sediment source for each sediment class. The sediment transport equation (1) is written as:

$$\frac{\partial c}{\partial t} + u\frac{\partial c}{\partial x} + v\frac{\partial c}{\partial y} + w\frac{\partial c}{\partial z} + \frac{\partial (w_s c)}{\partial z} = \frac{\partial}{\partial x}\left(\nu_x \frac{\partial c}{\partial x}\right) + \frac{\partial}{\partial y}\left(\nu_y \frac{\partial c}{\partial y}\right) + \frac{\partial}{\partial z}\left(\nu_z \frac{\partial c}{\partial z}\right) + q_s \qquad (1)$$

where c was the sediment concentration, the velocity field was shown as (u, v, w), settling velocity was represented as w_s, the horizontal diffusivity coefficients were shown as (ν_x, ν_y, ν_z) respectively, and the source term which was indicated as q_s. The settling velocities of sediment particles were directly employed from the results of the experimental analysis considering the natural condition of the seawater, sediment properties and flocculation process. Based on data provided by the manufacturer of the collector vehicle, sediment discharge was set at a rate of 60 t h^{-1} for a period of 4 days at 5 m above the seafloor, with the collector moving at a constant velocity of 0.5 m s^{-1} in an area with the size of 300 m by 300 m. Our current model grid resolution is not enough to simulate a water swirl exerted by a moving the collector underwater though it also might be computationally much more expensive. Therefore, induced turbulence by the mining collector and the effect of initial momentum of collector's exhaust on the movement of sediment particles have been mimicked by a relatively higher shear rate (G=2.4) which is at least one order of magnitude higher than the shear rate of the ambient flow in deep-ocean from this area.

The responses of sediment deposition to deep ocean hydrodynamic conditions were investigated under two different benthic flow scenarios: (1) a collector discharge concentration of 500 mg dw l^{-1} under typical average flow conditions of 3.8 cm s^{-1} and a predominantly eastward current flow (aggregates dataset G = 0); (2) a collector discharge concentration of 500 mg dw l^{-1}, followed by a remaining plume concentration of 105 mg dw l^{-1} of a simulated passage of an “eddy” under a north-easterly flow of 10 cm s^{-1} (aggregates dataset G = 2.4).

2.2.3.8 Image treatment analysis

Values of particle size, shape descriptor factors (i.e. circularity, roundness and solidity) and settling velocities were obtained using the FIJI software (v.1.51n), adapting the processing steps of raw images described by Shen (Shen, 2016). The BIOVOXXEL toolbox macro was used to evaluate the sensitivity of the thresholding technique,

resulting in the automatic "Intermode" thresholding algorithm being selected as the most accurate for our dataset. Out of focus particles were removed manually. Particle settling velocities were determined using the FIJI plugin TrackMate. A stack of pictures was first pre-processed, and the plugin ran with binary images. Every track was visually evaluated and a minimum of 3-time points per track was required to validate it. The average settling speed was converted to m d^{-1} velocity.

2.2.3.9 Statistical analysis

Statistical analysis was performed in R (R Core Team 2016). The particle size and settling velocity datasets were first cleaned of extreme outliers (i.e. values higher / lower than 1.5 interquartile ranges above / below the 0.75 / 0.25 quartiles, respectively) and grouped by sediment concentration (i.e. 105, 175 and 500 mg L^{-1}) and by shear rate (i.e. 0, 2.4, 5.7 and 10.4 s^{-1}). Since particle sizes differed among the different groups, the measured velocities were normalized to the median particle size. Kruskal-Wallis rank sum tests, followed by pairwise Dunn's tests with Bonferroni correction, were performed to the normalized settling velocities.

2.2.3.10 Modeling of settling velocities

A non-linear (logistic-sigmoidal) curve was fitted to model settling velocity against particle size for each concentration-shear rate combination, and 95 % confidence and prediction intervals were calculated based on each model. The curves followed Eq. 2:

$$y = \frac{a_1}{1+e^{\frac{a_2-x}{a_3}}} \quad (2)$$

where a_1 was the upper asymptotic limit of the curve, a_2 was the inflection point of the curve and a_3 a scaling factor for the size axis. All model coefficients and significance levels were provided in detail in Supplemental Table S4.

2.2.4 Results

2.2.4.1 Analysis of sediment particle size distribution

Nine sediment cores from the German polymetallic nodule license area in the CCZ (Fig. 1) were analyzed for their particle size distribution and showed two regional

variations (i.e. abyssal plain vs. local seamounts / ridges) within the four working areas investigated (Fig. 2).

Sediment size distributions from abyssal plain environments (i.e. Multiple Corer (MUC) samples 14, 18, 23, 34 and 61; d_{50} = 20.0 ± 3.1 μm) were characterized by finer grain sizes, with 28 %, 57 % and 15 % by volume of the cumulative frequency corresponding to size ranges < 10 μm, 10 - 63 μm and > 64 μm, respectively. All samples exhibited a multimodal distribution, with the 90 % inter-percentile range spreading between 3 μm to 139 μm, a dominant mode in the coarse silts around 20 μm and three weaker ones located at 6 μm, 56 μm and 252 μm.

On the contrary, sediments in the vicinity of local seamounts and ridges (i.e. samples 08, 68, 95 and 106 MUC; d_{50} = 32.8 ± 13 μm) showed a shift toward coarser size fractions, with an average cumulative frequency of 46 % by volume in the size range > 63 μm. The same multimodal distribution was observed as for abyssal plain samples, except with a broader inter-percentile range (4 μm to 273 μm), with modes rising at 56 μm and 252 μm. The sand fraction was investigated using a binocular and identified as debris of biogenic deposits, including foraminiferal and diatom residues (Supplemental Figure S4). The descriptive statistical analysis of sediment particle size distribution is provided in Supplemental Table S5.

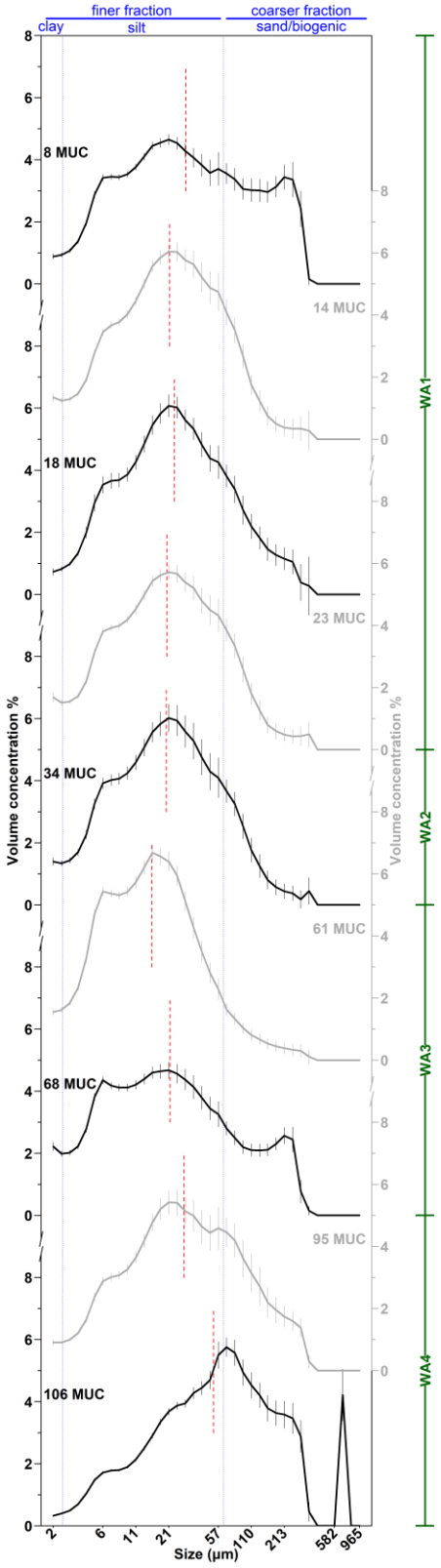

Figure 2. Particle size distribution of mixed top 10 cm sediment layer.
Distributions are expressed in percentage of the volume concentration obtained from the merged results of the LISST-100X and floc camera (figure inspired by McCave et al. (1995)). - Indicates the d_{50} of the sample distribution; ■ Indicates the sample location in the 4 different working areas investigated; ■ We refer to "finer fraction" for particles of size < 63 µm, including clay (< 2.5 µm) and silt (2.5 ≥ x < 63 µm). "Coarser fraction" refers to particles ≥ 63 µm and was identified as biogenic deposit. Alteration between black and gray only serves for better visual sample distinction and does not represent any grouping of the samples.

2.2.4.2 The plume aggregation process

Flocculation of plume particles under typical deep-sea flow conditions with very low shear rate (G ≈ 0 s^{-1}) took longer and resulted in a larger plume aggregates (aggregation time (T_a) = 45 - 135 min to reach a median diameter d_{50} = 850 - 1100 µm) when compared to aggregates produced under elevated shear rate (G = 2.4 – 10.4 s^{-1}; T_a = 10 - 50 min. to reach d_{50} = 250 - 550 µm) as expected during the passage of an eddy or in the wake of large mining vehicles (Fig. 3.A-E).

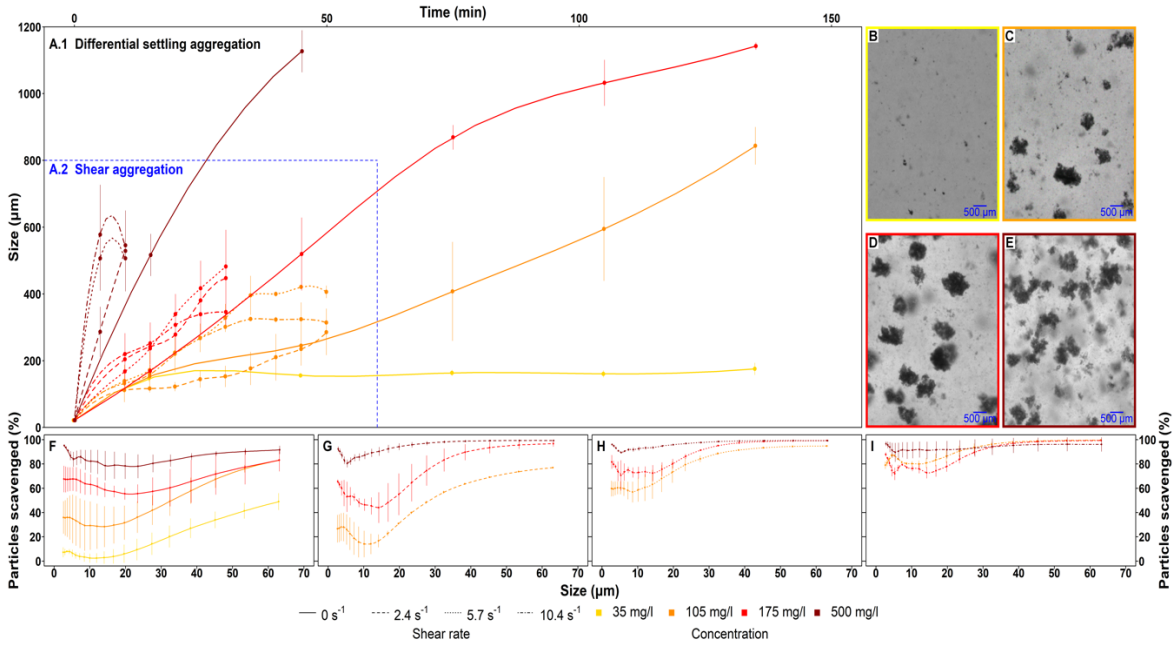

Figure 3. Aggregation propensity of deep-sea sediment.
(**A**) Evolution of median size floc produced under variable sediment plume concentrations over time. Pictures of aggregates produced under sediment plume concentration of: (**B**) **35 mg L^{-1}**; (**C**) **105 mg L^{-1}**; (**D**) **175 mg L^{-1}**; (**E**) **500 mg L^{-1}**. Particle size involvement during the aggregate formation under variable shear rate: (**F**) G = 0 s^{-1}; (**G**) G = 2.4 s^{-1}; (**H**) G = 5.7 s^{-1}; (**I**) = 10.4 s^{-1}.

In the absence of shear rate, flocculation rates increased proportionally with increasing plume concentration (linear slope factor of 0.05; Supplemental Figure S5); e.g., by doubling the initial discharge concentration aggregates doubled the size during similar aggregation time.

At a fixed plume concentration, increasing shear rate led to a 30 % higher flocculation rate (Fig. 3.A). At a shear rate of G ≈ 10 s^{-1}, which can be expected behind a fast-moving mining vehicle, the plume flocs revealed a shift towards smaller aggregate sizes, indicating disaggregation.

The scavenging of plume particles by already formed aggregates was a function of the concentration of plume particles and shear rate (Fig. 3.F-I). Hence, by either increasing

the plume concentration or the shear rate we observed faster scavenging by the formed aggregates (Fig. 3.I).

2.2.4.3 Settling velocities of aggregated plume particles

The size and settling velocities of flocculated plume particles varied from 70 - 1,357 µm and 7 - 355 m d^{-1}, respectively (Fig. 4). In general, larger aggregates settled at a higher rate than small aggregates. However, the size-specific settling velocities of the formed aggregates depended on the initial sediment plume concentration and the shear rate applied during the aggregation (Fig. 4.C-D).

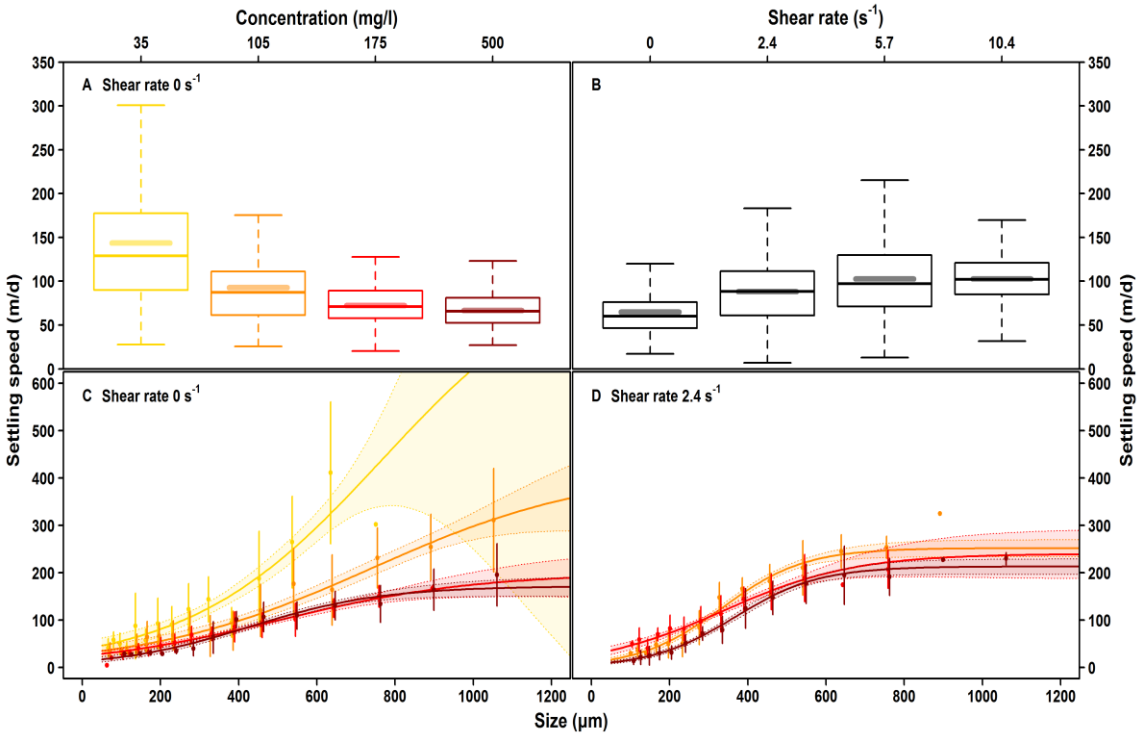

Figure 4. Settling velocity of deep-sea plume aggregates.
(**A**) Boxplots of settling velocities of aggregates produced under a shear rate of G= 0 s^{-1} per sediment plume concentration. (**B**) Boxplots of settling velocity against shear rate, for concentrations 105-500 mg L^{-1}. For comparison of treatments in A and B, settling velocities were normalized to the median particle size. (**C**) Fitted model curves (non-linear logistic-sigmoidal) of settling velocity against particle size for aggregates produced under a shear rate of G= 0 s^{-1}. (**D**) Fitted model curves (non-linear logistic-sigmoidal) of settling velocity against particle size for aggregates produced under a shear rate of G= 2.4 s^{-1}. 95 % confidence intervals are depicted for every modeled curve. For visual purpose, size data grouped in classes were plotted on the curves. The raw data can be found in the Supplemental Table S6.

Under G = 0 s^{-1} (i.e. differential settling), the size-specific settling velocities were significantly lower for aggregates formed under higher sediment concentrations of 175 mg L^{-1} (Kruskal-Wallis H = 145.3 for 3 df, $p < 0.0001$) compared to those formed at low concentrations of 35 mg L^{-1}. Average settling velocities (W_{50}) decreased from 143.5 m d^{-1}

to 66.6 m d^{-1} between the lowest and highest plume concentration (Fig. 4.A). No significant differences in settling velocities (Supplemental Table S7 for Dunn's pairwise comparisons) were observed at concentrations ≥ 175 mg L^{-1}. Morphological analysis (circularity, roundness and solidity) of the entire size spectrum, available in Supplemental Figure S6, revealed that higher plume concentrations resulted in the formation of more complex-shaped (fluffy) aggregates.

Regardless of the plume concentrations, moderate shear rate of G = 2.4 s^{-1} during aggregation resulted in elevated size-specific settling velocities (Kruskal-Wallis H = 411.5 for 3 df, $p < 0.0001$, Fig. 4.B; W50= 65 - 103 m d^{-1}). Once the shear rate exceeded 5.7 s^{-1} no significant differences for the size-specific settling velocities of the aggregates were detected (see Supplemental Table S8, for Dunn's pairwise comparisons).

To derive further conclusions on plume behavior, only 0 G and 2.4 G conditions (representing free-stream velocities of 0 and ≈ 25 cm s^{-1}) were selected as model input parameters, since they represent the full spectrum of the expected hydrodynamical *in-situ* conditions at the study site. A non-linear (logistic-sigmoidal) curve model was chosen to best fit the behavioral change of settling velocity against particle size (Fig. 4.C-D). All coefficients, significance levels and the model's sensitivities are provided in detail in Supplemental Figure S7 and Table S4.

2.2.4.4 Critical shear velocities for resuspension of aggregated plume particles

For model input, as well as for the calculation of the mass fluxes in the benthic boundary layer, critical shear velocities of the resuspension of newly settled plume aggregates were measured in a benthic erosion chamber.

The resuspension behavior of aggregates under varying plume concentrations did not differ under conditions of 0 G and 2.4 G. A critical shear velocity of u_{*cri} = 0.3 cm s^{-1} corresponding to bottom current velocity at u_{100} (1 m above seabed) of ≈ 4 - 5 cm s^{-1} was required to initiate bedload transport.

Suspended load transport was observed at u_{*cri} ≥ 0.5 cm s^{-1} (u_{100} = 7 - 8 cm s^{-1}) when plume aggregates were resuspended. Full resuspension was observed at u_{*cri} ≥ 0.7 cm s^{-1} (u_{100} = 9 – 12 cm s^{-1}).

2.2.4.5 Sediment plume dispersion modeling

The input parameters derived from our analyses were implemented in a hydrodynamic model to predict plume-dispersal and blanketing during a simulated 4 days collector trial following by one day of plume settling which is planned for the German license area in early 2019.

The amount of sediment deposition from the plume that was modeled for each of the three particle size classes d_{25}, d_{50} and d_{75} is shown in Fig. 5. Under low flow conditions a plume blanketing of > 0.1 mm extended to a maximum of 2.5 km away from the mining site (source 0;0) and thinned out to zero within a maximum distance of 4 km. Under enhanced bottom current velocities such as those associated with eddy passage, the d_{50} and d_{75} coarse fractions settled even more quickly and a plume deposition of > 0.1 mm reached a maximal distance of 3.5 km downstream from the source. However, due to the greater current speeds, the lower aggregation and subsequent settling speeds of fine particles (d_{25}), only 80 % of the plume as settled in comparison to 96 % under low flow condition (Table 1). The resulting blanketing thins out to zero 9 km away from the mining site.

Table 1. Remaining percentage of suspended particles at the end of modeling.

	Remaining suspended material (%)		
Experiment	**d_{75}**	**d_{50}**	**d_{25}**
G = 0 s^{-1}	1.43	2.59	4.02
G = 2.4 s^{-1}	2.26	2.47	19.70

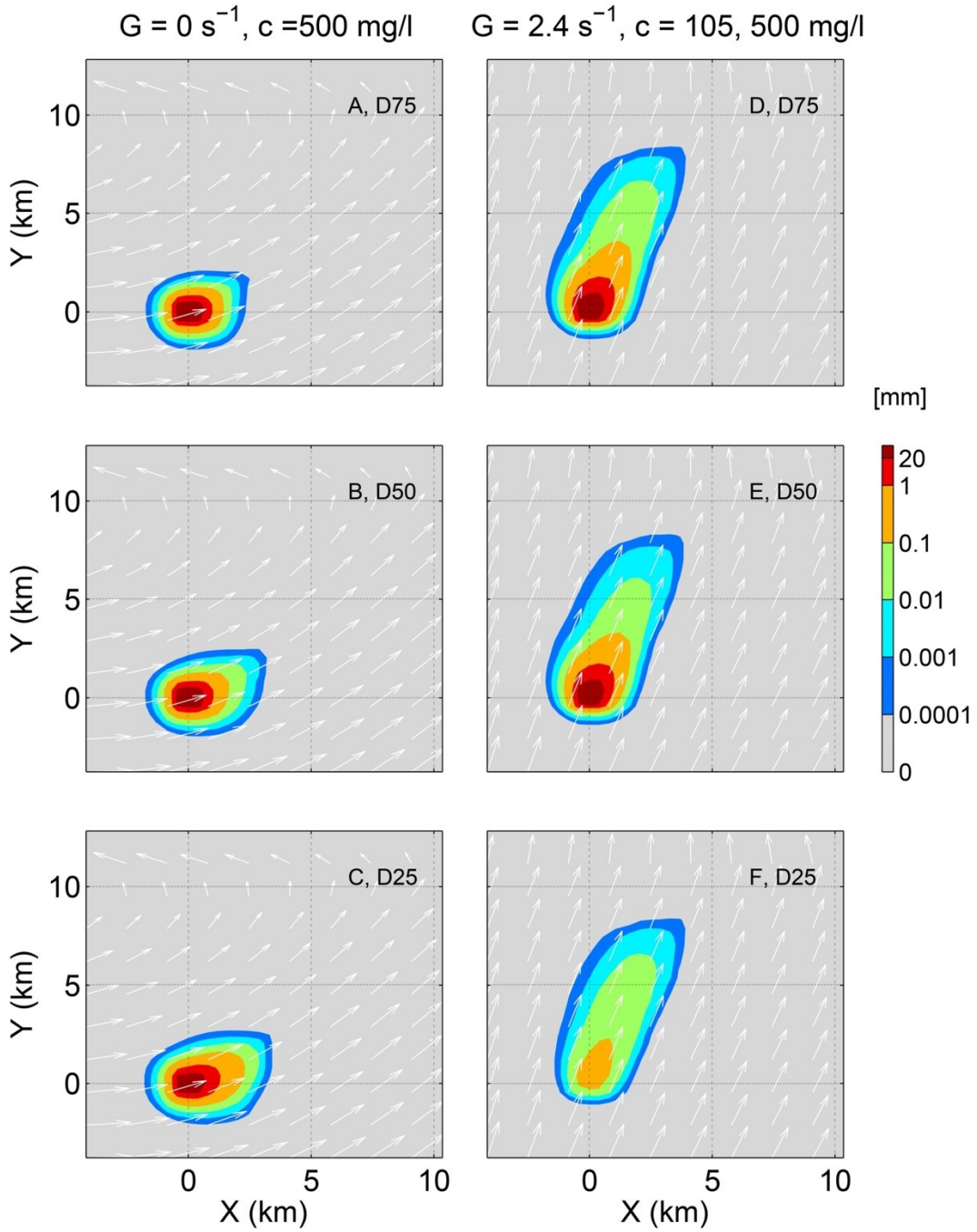

Figure 5. Sediment deposition / blanketing (mm) of plume particles on the seafloor.
Sediment deposition is shown for three particle size classes (d_{25}, d_{50}, d_{75}) after 4 days of continuous sediment discharge (60 t h^{-1}) 5 m above the seafloor (position 0;0), followed by 1 day of settling at initial discharge concentrations of 500 mg dw l^{-1}. The mean current velocity is shown as arrows which correspond to 3.8 cm s^{-1} in A-C and 10 cm s^{-1} in D-F.

2.2.5 Discussion

Deep-sea mining activities bear great economic potential, but come with a high environmental risk (Ramirez-Llodra et al., 2015), concerning more and more the general sensitized public. The main issue when addressing the potential impacts of mining activities is the presently limited knowledge of the biotic and abiotic processes occurring in the abyssal environment. To predict the long-term, industrial-scale impact of mining activity, numerical modeling techniques are applied. However, the reliability of such models depends drastically on the quality of their input parameters (Jankowski and Zielke, 1997). This study aimed at providing a reliable dataset on the behavior of deep-sea particles during mining plume discharge.

2.2.5.1 Analysis of sediment particle size distribution

Attention should be paid to the location site of the mining activity and the sediments that predominate there. Sedimentological grain sizes in the German nodule license area in the CCZ showed a multimodal size distribution pattern. Sediments from the vast abyssal plain environment generally exhibit a finer grain size (d_{50} = 20 μm), in agreement with the particle size spectrum obtained from several other deep-sea locations (McCave, 1984; Bianchi and McCave, 2000; Thomsen and Gust, 2000). Coarser sediments (d_{50} = 32 μm) were found near seamounts and ridges. Sediment size distribution in the area is controlled by the hydrodynamical regime of the respective environment following the theory of "sortable silt" (McCave et al., 1995). In a higher current velocity field, such as at the base of a seamount or ridge (White et al., 2008), sediment particle selection and sorting will result in the formation of coarser particle size distribution over time.

Sampled at the side of a large seamount, the sediment core 106 MUC depicted the highest median particle size (d_{50}= 52 μm, Fig. 2). Further, this site was dominated by biogenic sediments throughout the entire sediment core depth, suggesting that this site accumulates biologically derived material. Taking the generally low sedimentation rate of 5 mm 10^{-3} year $^{-1}$ in the CCZ (Khripounoff et al., 2006) into account, this seamount which rises to a depth of 2300 m will unlikely cause elevated biological production at the sea surface but interferes with the deep sea currents producing a wake effect (Roden, 1991; Comeau et al., 1995) . Since seamounts or ridges are considered as a hotspot for biodiversity (Samadi et al., 2006; Sautya et al., 2011), they should remain out of the dispersion path of a mining plume.

2.2.5.2 The plume aggregation process

Discharge simulations of mining-related sediment plumes indicate a rapid flocculation propensity (within 10 to 135 min), resulting in the formation of large-sized aggregates (up to 1100 μm). The analysis of aggregation under differential settling and turbulent shear aggregation showed that both sediment plume concentration and shear rate dictate the behavior of particles in suspension. Increasing either the suspended particle concentration or the shear rate up to 5.6 G (representing a free-stream velocity of ≈ 0.5 m s^{-1}) promoted aggregate growth, showing that aggregation dominated over breakup. These results corroborate observations reported for laboratory and natural systems (McCave, 1984; Lick et al., 1993; Milligan and Hill, 1998; Manning and Dyer, 1999; Winterwerp, 2002) . Flocculation efficiency was found to be rapid (within 10 min) for a sediment plume concentration of 500 mg L^{-1} and a shear rate (G) of 2 - 10 s^{-1}. Under these hydrodynamical conditions, which are expected in the wake of a mining vehicle moving with ≈ 1m s^{-1}, more than 90 % of the finer fraction was scavenged within that time. This would result in a fast clearance of the water column subsequently limiting the fallout area of the mining activity.

2.2.5.3 Settling velocities of aggregated plume particles

The residence time of the mining plume in the water column is controlled by the settling velocities of particles that compose it. Our results confirm that the size-specific settling velocities of aggregates are regulated by the hydrodynamic conditions during formation. Increasing shear rate during aggregation significantly increases aggregate size-specific settling velocities (Supplemental Table S3). A similar relationship has been reported in previous investigations for different types of sediments (Lick et al., 1993; Manning and Dyer, 1999). Under negligible shear rate, aggregates formed under low plume concentrations of 35 mg L^{-1} showed higher size-specific settling velocities than similar sized particles under higher plume concentrations. Our results indicate that the aggregate's shape which is often neglected in many modelling equations (Joshi et al., 2014) for computational reason, may be an important regulating factor causing a net decrease of the size-specific settling velocity (Fig.4A). Furthermore, our findings revealed that a clear difference between size-specific settling velocities of plume aggregates > 100 μm when compared to typical model-based calculations using either Stokes or the recalculated Ws of Ferguson & Church shown in Figure 6 (Ferguson and Church, 2004).

Very few studies have quantitatively measured deep-sea particle settling velocities, but our values appear to be in the same order of magnitude as those found for organo-mineral aggregates from the benthic boundary layer of the deep sea and comparable to dredging operation (Thomsen et al., 2002; Smith and Friedrichs, 2011).

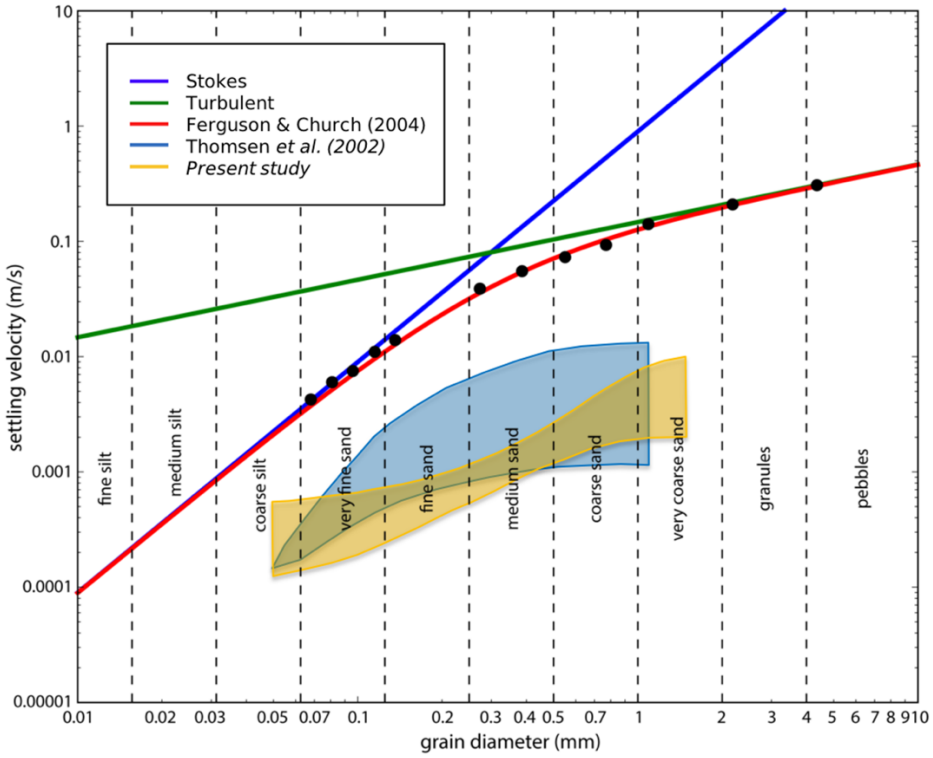

Figure 6. Comparison of measured aggregates settling velocities from predicted Stoke law and Ferguson & church relation.
Figure modified from Ferguson and Church (2004) using Python programming language (following the code of Sylvester (2013)).

2.2.5.4 Critical shear velocities for resuspension of aggregated plume particles

Resuspension critical shear velocities of aggregates produced in this study are consistent with the previously reported value of deep sea particle (Southard, 1971; Thomsen and Gust, 2000). Once the plume has settled on the seabed, similarities in aggregate resuspension behavior are observed irrespective of their flocculation history. Under a current flow velocity of 3 - 4 cm s^{-1}, which corresponds to the mean velocity flow in the investigated area (Kuhn, 2015), bedload transport will start. Aggregates are expected to passively accumulate behind the nodules. Flow velocities > 7 cm s^{-1}, which are lower than that encountered during the passage of a mesoscale eddies would potentially yield a new sediment plume of large aggregates.

2.2.5.5 Sediment plume dispersion modeling

Our 4 days mining model prediction reveals a clear variation of the area impacted. This ranged from 4 km under normal current conditions to up to 9 km conditions of an eddy passing through the study site. Near-field hyper sedimentation of > 20 mm (Fig.5) is expected to drastically impact deep sea ecosystem functioning to a varying extent (Gollner et al., 2017), which are much less adapted to such events than their counterparts at continental margins (Larsson et al., 2013). In the transitional areas with a decreasing blanketing Layer, studies of underwater disposal mining wastes (i.e. dredging, drill cutting (Trannum et al., 2010), land mining (Smith and Rule, 2001; Hughes et al., 2015)) showed that instantaneous burial of up to 1 mm does not affect macrofaunal species richness or abundance (Olsgard and Hasle, 1993). However, increasingly divergent communities were observed at a burial rate of 3 mm applied monthly over a period of 6 months (Lohrer et al., 2004). Based on a precautionary approach, we believe that an ecological blanketing threshold value around 1 mm has to be followed. Such threshold levels could thus only be reached if small-sized fallout areas of a few square-kilometers with a massive blanketing effect are accepted. These fallout areas will then expand during the passage of deep-sea eddies. However, this plume resuspension would then carry large aggregates, which do not disaggregate into smaller particles unless shear rate reaches high levels of > 5.6 G.

2.2.6 Conclusions

As industrial-scale deep-sea mining is coming closer to reality, environmental impact assessment and international policy requirements have to be formulated (Boetius and Haecke, 2018). Limiting the plume dispersal as much as possible will become a key factor to prevent an extended ecological impact on the benthic communities. Our findings suggest that the use of a high sediment discharge (500 mg L^{-1}) under turbulent shear rate ≥ 2.4 s^{-1} allowed the most rapid sediment flocculation. The modeling results also suggest that mining under “normal” flow conditions result in a relatively fast deposition of particles from the plume, thus restricting a blanketing effect to a relatively small fall-out area. Setting such requirements should therefore be considered for the design of the mining collector and exhaust pipe. Further expansion of this study should consider even higher sediment discharge concentrations and investigate the effect of hindered settling processes (sediment concentration > 2-3 g L^{-1};Winterwerp, 2002) and the gelling effect of

cohesive sediment (sediment concentration > 30 g L^{-1}; Camenen and van Bang, 2011), which is expected to influence the aggregation and the dispersion potential of the mining plume.

2.2.7 Contributions

Contributed to conception and design: BG, KP, LT
Contributed to acquisition of data: BG, KP, AV
Contributed to analysis and interpretation of data: BG, DC, MIH
Drafted and/or revised the article: BG, KP, DC, AV, MIH, LT
Approved the submitted version for publication: BG, KP, DC, AV, MIH, LT

2.2.8 Acknowledgments

The authors would like to thank the shipboard teams and the scientist staff of the RV-SONNE 240 for the collection of the samples. We are also grateful for the useful proofreading of our manuscript made by Candice Thorstenson.

2.2.9 Funding information

We acknowledged BGR Hannover for co-financing this study. I.M.H. was supported by the Helmholtz Association, the Alfred Wegener Institute Helmholtz Centre for Polar and Marine Research and the DFG-Research Center/Cluster of Excellence "The Ocean in the Earth System" at MARUM. This publication is supported by the HGF Young Investigator Group SeaPump "Seasonal and regional food web interactions with the biological pump": VH-NG-1000 and by the OceanLab of Jacobs University.

2.2.10 Competing interests

The authors have declared that no competing interests exist. Co-author Laurenz Thomsen is associate editor of Elementa.

2.2.11 Data accessibility statement

Raw data generated during this study have been archived using UC Press Dash under the title of the manuscript; https://doi.org/10.15146/R3K966

2.2.12 Supplementary material

Text S1. Supplemental materials and methods

Samples preparation and experimental conditions

An aliquot of approximately 0.5 g from every sediment core layer (i.e. 1 cm) was weighted on a fine-scale balance and dried at 105 °C to constant mass in an oven. The difference in mass before and after the drying procedure was used to determine the initial water content. Based on the wet / dry weight (d_w) calculation, a sediment stock solution with a final concentration of 5 g L^{-1} (d_w) was prepared. The suspension was stirred (1250 rpm) multiple times for 30 minutes. Total disaggregation was confirmed when particle size distribution didn't change over time using the LISST-100X.

Instrumentation use for suspended particle size detection

LISST-100 X

A LISST-100 type C (**L**aser **I**n **S**itu **S**cattering and **T**ransmissometry; Sequoia Scientific) was used for the detection of smaller particle sizes (i.e. < 500 μm). The principle of laser diffraction, use and mathematical model for data analysis are detailed in Agrawal and Pottsmith (2000). The LISST-100X provides particle volume concentration (μl l^{-1}) measured in 32 logarithmically spaced size bins ranging from 2.5 - 500 μm. A small volume flow through chamber (Sequoia Scientific) was mounted reducing the optical path length to 1 cm and extending the measurable suspended sediment limit concentration of the laser. The scattering pattern of the instrument was inverted using the random shape model (Agrawal et al., 2008).

Digital floc camera configuration

Larger particle sizes (i.e. > 70 μm) and their concentration where estimated by image analysis. Floc images were captured using a DFK 23UX174 (1920 x 1200 pixels at 54 fps; The Imaging Source) camera mounted with a TEC-M55MPW telecentric lens (Computar) and 15 mm extension tube. The resolution of the set up was calibrated with a 1 mm ruler (Thor labs A1L3S2) and the depth of field was estimated with a 45° depth of field target (Edmund Optic 54-440). The resulting field of view produced was 1.53 cm x 0.96 cm (8 μm/pixel) for a 2 mm depth of field.

The minimum number of pixels defining the smallest particle resolution may vary from 1 pixel up to a standard rule of 9 pixels (Mikkelsen et al., 2004; Maggi et al., 2007; Smith and Friedrichs, 2015). The minimum particle size used in this study was based on the ISO regulation (13322-1:2014) for image analysis with a particle made of at least of 10 pixels.

Since a high shutter speed (min 1/1000 s) was required, a strong Light source was necessary for high image quality. Thus, a square open LED bar light (OPT-LIM11222, Opto Engineering) was used, ensuring optimum illumination conditions. The set-up allows a bright 360° illumination, used as back illumination with or without a white filter for all experiments.

Sediment particle size distribution

A suspended sediment concentration of approximately 60 mg L^{-1} was prepared from the stock solution. This effective concentration allows the LISST-100X laser transmission to be ± 60 % and represent an appropriate number of particles to be visualized by the camera.

The camera was facing towards the measuring chamber, consisting of two coated glasses of 20 x 18 cm which were separated by a two 2 mm thick silicone grid, forming six isolated measuring columns. With this configuration, all the particles flowing through the measuring chamber were in the field of view of the camera. Images were captured vertically, starting from the lower part of the column to ensure that bigger particles were measured.

Volume concentrations detected between the two instruments in each of the overlapping size bins differed in orders of magnitude. Therefore, a correction formula was applied to the Digital Floc Camera values, separately for each sample. The correction factors applied, corresponded to the slope and intercept of a linear regression between the Digital Flocculation Camera and the LISST (Table S3). For each sample, the maximum number of consecutive overlapping size bins giving a significant linear relationship was used for calculations, always excluding from the bigger size bins and downwards when necessary.

Settling column description

Made of a square 4 cm cross-section and 50 cm high bore silica glass, the column can be mounted either on a LISST-100X or used separately for higher size aggregates (Figure S3). An outer 6 cm square cross-section column running with a cooling fluid (distilled water + 20 % ethanol) was maintained at fix temperature of 1.5 °C by a cooler system. This way, a drastic reduction of temperature gradient in the column is provided, avoiding the formation of convection cells.

The settling column was first filled with the same water used during the aggregation experiments and was left standing during a couple of hours. For minimizing evaporation at air-water interface, the column was closed with a lid (Johnson et al., 1996; Ploug et al., 2010).

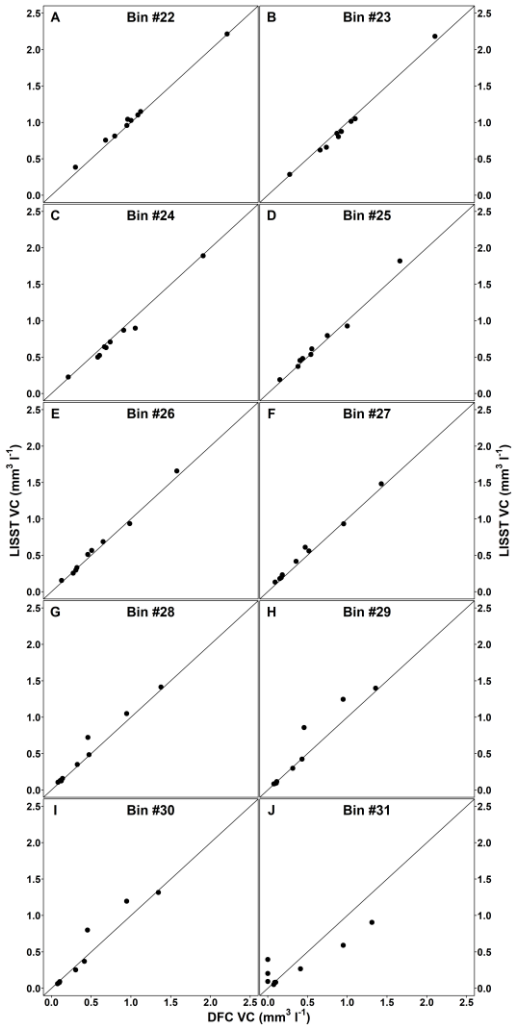

Figure S1. Relationships between the volume concentration (VC) from the LISST and corrected VC from the camera.

(A-J): volume concentration for each of the ten overlapping size bins used during the merging procedure (#22–31). Bins size classes description are provided in Supplemental Table S2.

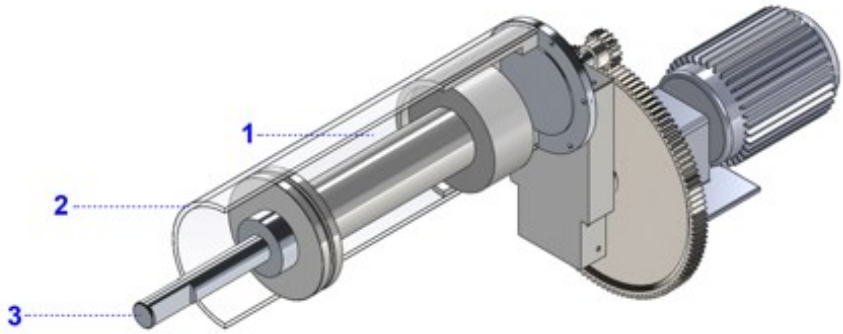

Figure S2. Schematic drawing of the Couette chamber used for aggregation of sediment under variable shear rate.
(1) annular space of 2 cm; (2) rotating outer Plexiglas cylinder diameter of 12.5 cm; (3) Fixed inner cylinder diameter of 8.5 cm. Total working volume of 1.7 L.

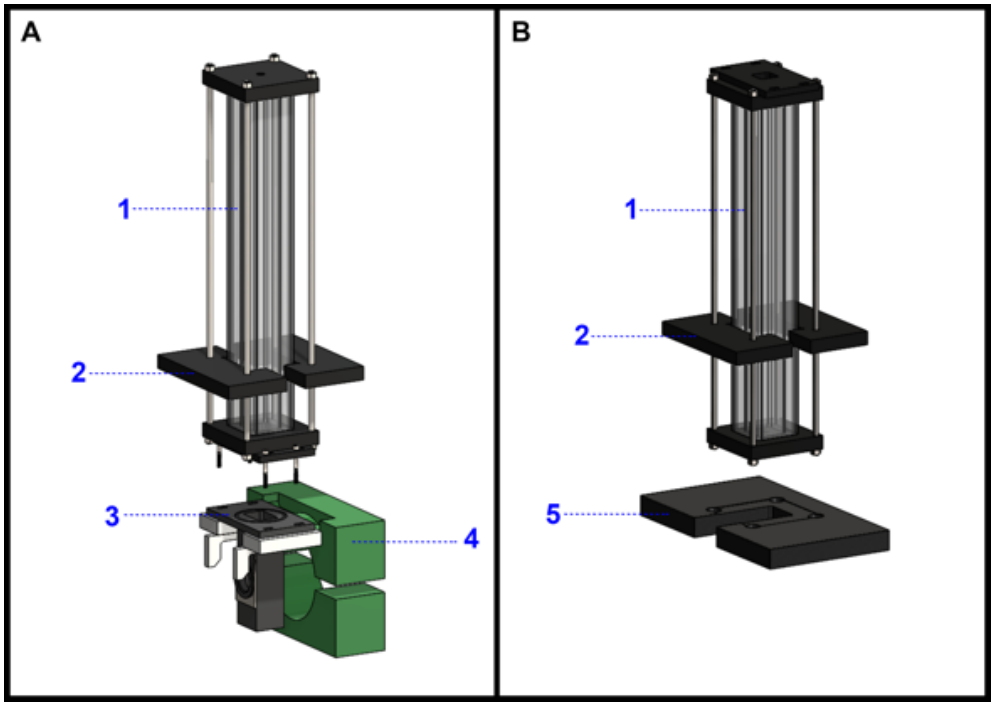

Figure S3. Schematic drawing of the settling column.
The design allows the column to be used either with the LISST-100X (**A**) or separately (**B**). (1) 50 cm high settling column; (2) light holder; (3) Measuring section of the LISST-100X; (4) LISST-100x fixation clamp; (5) Plate holder for separate use

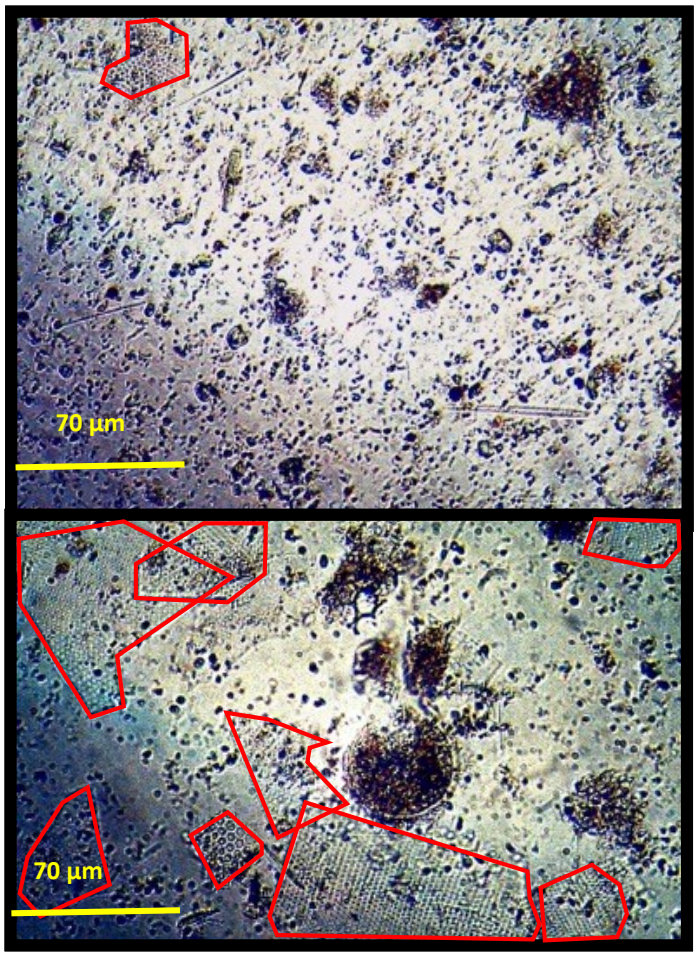

Figure S4. Microscopic pictures of sediment surface layer.
Top picture: sample 95 MUC located in a plain environment. Down picture: sample 106 MUC located next to a seamount. ■ Biogenic deposits including foraminiferal and diatom residues.

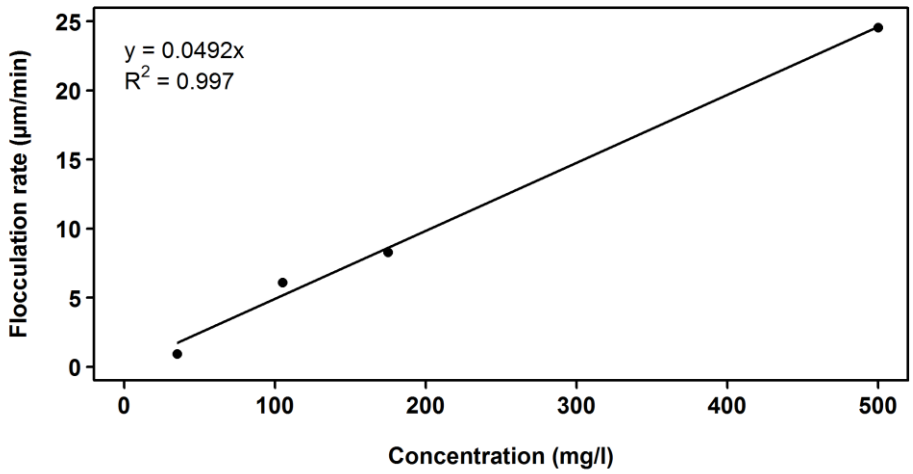

Figure S5. Comparison of flocculation rate against sediment plume concentration under differential settling (G = 0 s^{-1}).

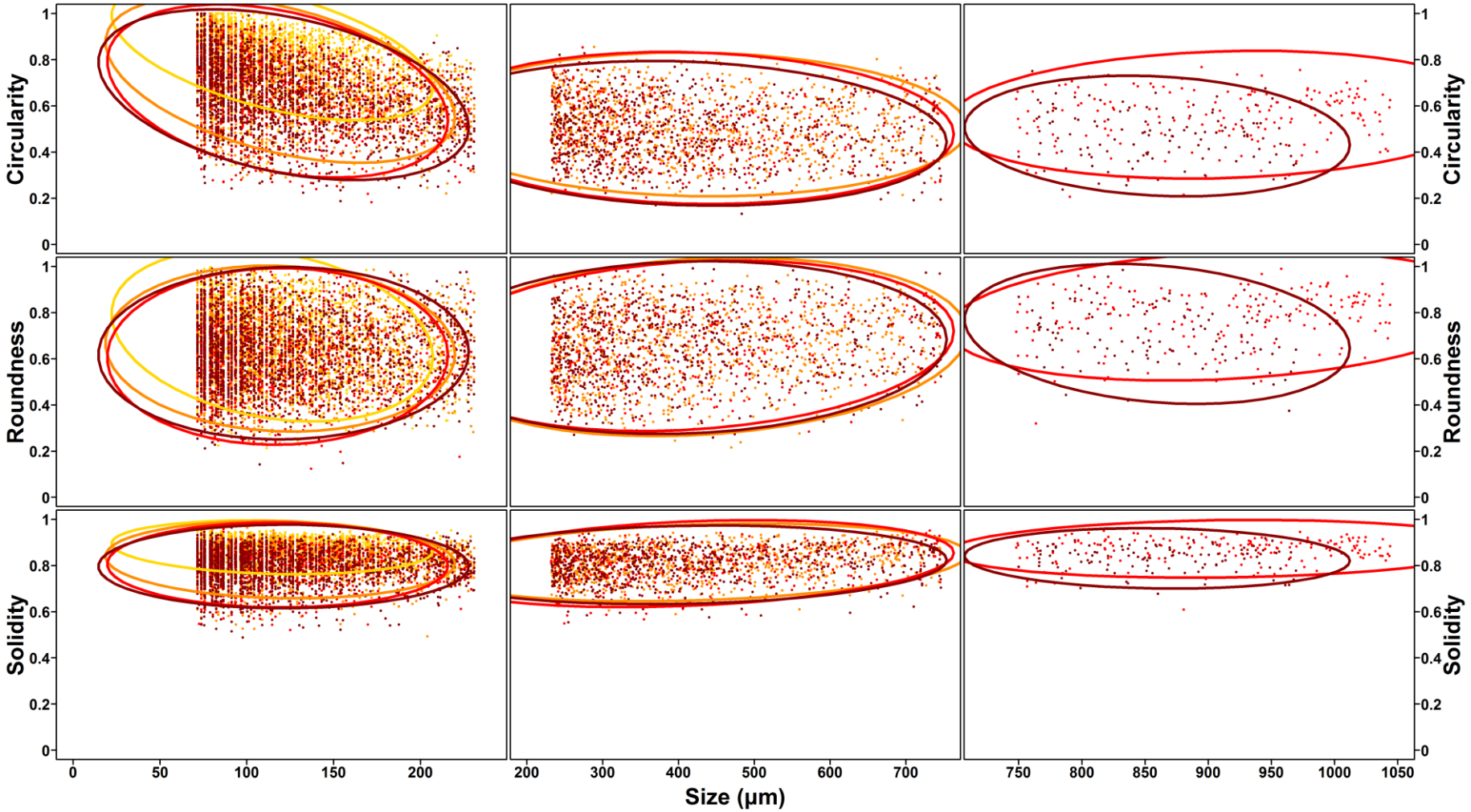

Figure S6. Morphological analysis of aggregates produced from variable sediment plume concentration under differential settling condition. Starting sediment plume concentration of: 35 mg L^{-1}; 105 mg L^{-1}; 175 mg L^{-1}; 500 mg L^{-1}. Ellipse shape represent 95 % of the data for each sediment concentration.

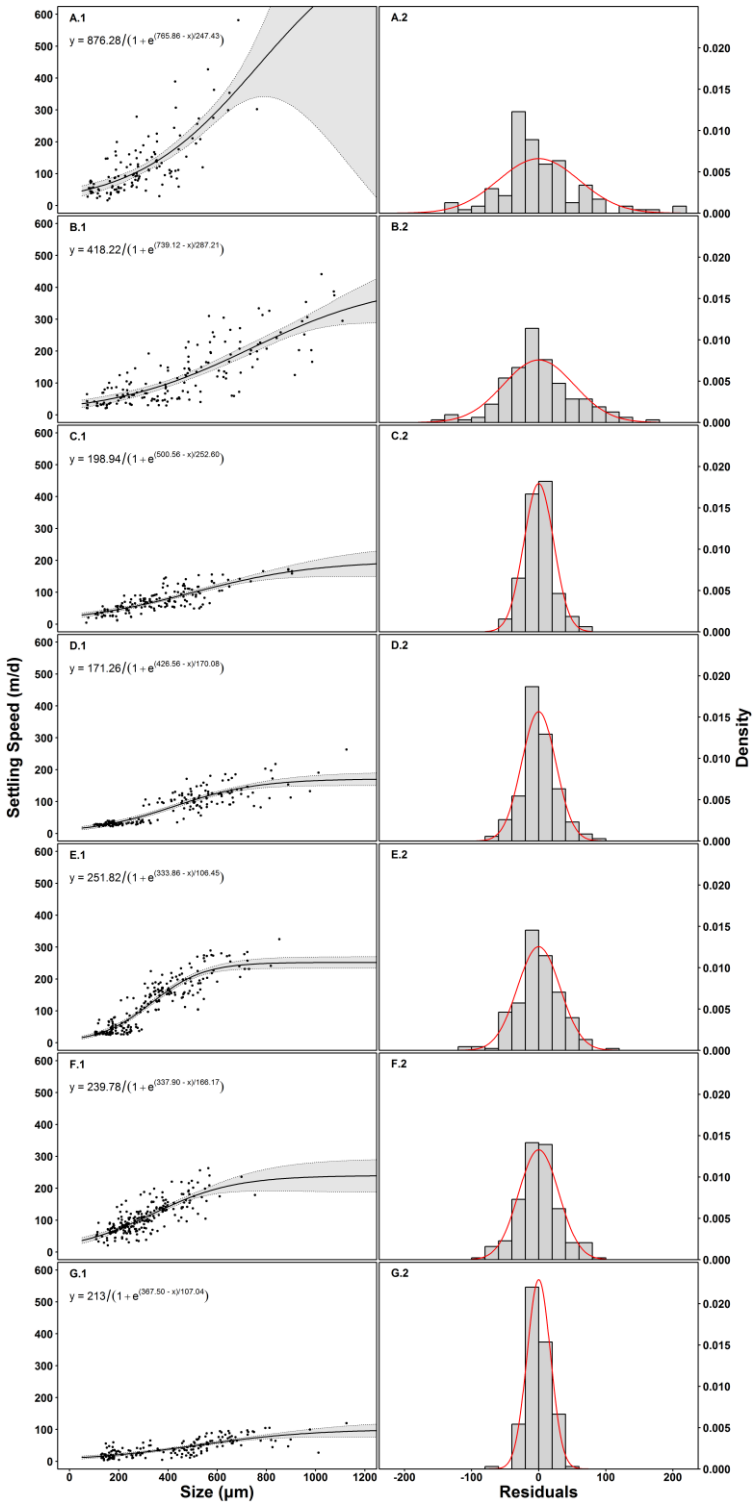

Figure S7. Fitted model equation of settling velocities from deep sea sediment plume aggregates. Settling velocities of aggregates produce under 0 G for a starting sediment plume concentration of: (**A**) 35 mg l^{-1}; (**B**) 105 mg l^{-1}; (**C**) 175 mg l^{-1}; (**D**) 500 mg l^{-1}. Settling velocities of aggregates produce under 2.4 G for a starting sediment plume concentration of: (**E**) 105 mg l^{-1}; (**F**) 175 mg l^{-1}; (**G**) 500 mg l^{-1}. Left column: (**.1**) combined raw data and predicted model curve with corresponding 95 % confidence interval. Right column: (**.2**) model residual histogram with plotted normal curve distribution.

Table S1. Location and description of 9 sediment push core used in this study.

Sample Nr. SO240	Working area	Date	Latitude	Longitude	Water depth	topography	Nodule coverage[1]	Nodule abundance
08 MUC	WA1	09.05.2015	13°10.524'N	118°06.708'W	4289 m	close to seamount	small	12.6 kg/m²
14 MUC	WA1	11.05.2015	13°10.528'N	118°10.108'W	4332 m	plain	large	14.8 kg/m²
18 MUC	WA1	12.05.2015	13°07.109'N	118°07.657'W	4318 m	plain	none	-
23 MUC	WA1	13.05.2015	13°10.526'N	118°08.186'W	4305 m	plain	large	18.6 kg/m²
34 MUC	WA2	07.05.2015	12°53.358'N	118°24.569'W	4287 m	plain	small	-
61 MUC	WA3	25.05.2015	12°56.109'N	119°08.871'W	4293 m	ridges	none	-
68 MUC	WA3	27.05.2015	12°40.307'N	119°11.514'W	4408 m	ridges	small	4.1 kg/m²
95 MUC	WA4	05.06.2015	11°49.262'N	117°13.197'W	4150 m	plain	large	-
106 MUC	WA4	07.06.2015	11°50.079'N	116°32.900'W	4351 m	close to seamount	none	-

[1] small nodules are < 4 cm in size; large nodules are > 4 cm in size

Table S2. Size classes boundaries for particles size analysis.

Size classes nbr. [A]	Lower limit (µm)	Upper limit (µm)	Median (µm)	Size classes nbr. [A]	Lower limit (µm)	Upper limit (µm)	Median (µm)
1	1.90	2.25	2.07	22	61.6	72.7	66.9
2	2.25	2.65	2.44	23	72.7	85.7	78.9
3	2.65	3.13	2.88	24	85.7	101	93.1
4	3.13	3.69	3.4	25	101	119	110
5	3.69	4.35	4.01	26	119	141	130
6	4.35	5.14	4.73	27	141	166	153
7	5.14	6.06	5.58	28	166	196	181
8	6.06	7.15	6.59	29	196	232	213
9	7.15	8.44	7.77	30	232	273	252
10	8.44	9.96	9.17	31	273	322	297
11	9.96	11.8	10.8	32	322	381	350
12	11.8	13.9	12.8	33	381	451	416
13	13.9	16	15.1	34	451	533	492
14	16	19.3	17.8	35	533	631	582
15	19.3	22.8	21	36	631	747	689
16	22.8	26.9	24.8	37	747	884	815
17	26.9	31.8	29.2	38	884	1046	965
18	31.8	37.5	34.5	39	1046	1238	1142
19	37.5	44.2	40.7	40	1238	1465	1351
20	44.2	52.2	48	41	1465	1734	1599
21	52.2	61.6	56.7	42	1734	2051	1892

[A] Lower limit, upper limit and median in microns for size classes 1 - 32 (LISST-100X) and size classes 22 - 42 (camera). The two instruments are overlapping in 10 classes, 22 - 32.

Table S3. Linear relationship between the Digital Floc Camera and the LISST-100X.

Sample Nr. SO240	Slope	Intercept	R squared	P value	Bins used
08 MUC	0,000172	0,000941	0,496	4,67E-02	22-28
14 MUC	0,000824	0,000072	0,990	1,76E-09	22-31
18 MUC	0,000703	0,000298	0,955	7,08E-07	22-31
23 MUC	0,000568	0,000085	0,982	1,62E-08	22-31
34 MUC	0,000656	0,000117	0,986	7,56E-09	22-31
61 MUC	0,000196	0,000073	0,900	1,75E-05	22-31
68 MUC	0,000172	0,000451	0,584	4,72E-02	22-27
95 MUC	0,000731	0,000377	0,955	7,40E-07	22-31
106 MUC	0,001143	0,001255	0,859	7,17E-05	22-31

Table S4. Modelled equations and coefficients of settling velocity.

Sediment concentration (mg L^{-1})	G (s^{-1})	Name [1]	Asym	xmid	scal	Equation
35	0	W_s	876.27	765.86	247.43	$W_s = 876.27/(1 + e^{(765.86 - x)/247.43})$
		CIL	203.36	1164.1	-33.95	$W_s = 203.36/(1 + e^{(1164.10 - x)/-33.95})$
		CIH	2113.27	1023.2	251.57	$W_s = 2113.27/(1 + e^{(1023.25 - x)/251.57})$
		PIL	126.59	1193.5	-21.51	$W_s = 126.59/(1 + e^{(1193.50 - x)/-21.51})$
		PIH	2548.4	1135.8	343.28	$W_s = 2548.45/(1 + e^{(1135.88 - x)/343.28})$
105	0	W_s	418.22	739.11	287.21	$W_s = 418.22/(1 + e^{(739.11 - x)/287.21})$
		CIL	299.72	595.02	212.25	$W_s = 299.72/(1 + e^{(595.02 - x)/212.25})$
		CIH	599.22	928.53	355.41	$W_s = 599.22/(1 + e^{(928.53 - x)/355.41})$
		PIL	235.38	789.82	124.41	$W_s = 235.38/(1 + e^{(789.82 - x)/124.41})$
		PIH	705.37	849.29	521.91	$W_s = 705.37/(1 + e^{(849.29 - x)/521.91})$
175	0	W_s	198.93	500.55	252.59	$W_s = 198.93/(1 + e^{(500.55 - x)/252.59})$
		CIL	151.50	393.13	185.28	$W_s = 151.50/(1 + e^{(393.13 - x)/185.28})$
		CIH	257.90	619.53	304.03	$W_s = 257.90/(1 + e^{(619.53 - x)/304.03})$
		PIL	129.00	560.68	138.66	$W_s = 129.00/(1 + e^{(560.68 - x)/138.66})$
		PIH	279.05	470.04	370.78	$W_s = 279.05/(1 + e^{(470.04 - x)/370.78})$
500	0	W_s	171.26	426.55	170.07	$W_s = 171.26/(1 + e^{(426.55 - x)/170.07})$
		CIL	151.33	406.15	143.24	$W_s = 151.33/(1 + e^{(406.15 - x)/143.24})$
		CIH	192.66	449.81	196.18	$W_s = 192.66/(1 + e^{(449.81 - x)/196.18})$
		PIL	113.45	532.72	94.19	$W_s = 113.45/(1 + e^{(532.72 - x)/94.19})$
		PIH	230.13	318.94	241.00	$W_s = 230.13/(1 + e^{(318.94 - x)/241.00})$
105	2,4	W_s	251.81	333.85	106.44	$W_s = 251.81/(1 + e^{(333.85 - x)/106.44})$
		CIL	234.31	329.17	96.47	$W_s = 234.31/(1 + e^{(329.17 - x)/96.47})$
		CIH	269.61	338.78	116.14	$W_s = 269.61/(1 + e^{(338.78 - x)/116.14})$
		PIL	184.26	396.32	66.61	$W_s = 184.26/(1 + e^{(396.32 - x)/66.61})$
		PIH	319.72	266.37	145.54	$W_s = 319.72/(1 + e^{(266.37 - x)/145.54})$
175	2,4	W_s	239.78	337.89	166.17	$W_s = 239.78/(1 + e^{(337.89 - x)/166.17})$
		CIL	190.57	278.61	120.35	$W_s = 190.57/(1 + e^{(278.61 - x)/120.35})$
		CIH	294.08	398.85	199.76	$W_s = 294.08/(1 + e^{(398.85 - x)/199.76})$
		PIL	159.68	403.58	94.64	$W_s = 159.68/(1 + e^{(403.58 - x)/94.64})$
		PIH	322.36	276.99	228.76	$W_s = 322.36/(1 + e^{(276.99 - x)/228.76})$
500	2,4	W_s	212.99	367.49	107.04	$W_s = 212.99/(1 + e^{(367.49 - x)/107.04})$
		CIL	197.30	362.84	98.60	$W_s = 197.30/(1 + e^{(362.84 - x)/98.60})$
		CIH	228.91	372.33	115.20	$W_s = 228.91/(1 + e^{(372.33 - x)/115.20})$
		PIL	158.49	426.40	67.78	$W_s = 158.49/(1 + e^{(426.40 - x)/67.78})$
		PIH	268.12	302.03	148.95	$W_s = 268.12/(1 + e^{(302.03 - x)/148.95})$

[1] W_s, settling velocity; CIL, Confidence Interval Lower limit; CIH, Confidence Interval Higher limit; PIL, Prediction Interval Lower limit; PIH, Prediction Interval Higher limit.

Table S5. Descriptive statistics analysis of sediment particle size distributions.

	MUC sediment sample								
Descriptive statistic	**106**	**95**	**68**	**61**	**34**	**23**	**18**	**14**	**08**
Median (μm)	52	29	22	15	20	20	23	21	30
Mode (μm)	67	21	21	15	21	21	21	21	21
10% (μm)	9	6	4	4	5	5	5	5	5
90% (μm)	252	130	130	48	79	79	93	79	181
< 10 μm (%)	12	20	31	37	28	28	24	25	23
10 - 63 μm (%)	41	53	46	55	57	56	56	59	46
> 63 μm (%)	47	27	23	8	15	16	20	16	31

Table S6. Raw data of re-calculated d_{50} settling velocities.

	Differential settling (0 s^{-1})				All shear Rates			
	Sediment concentration (mg L^{-1})				G (s^{-1})			
Descriptive statistic	**35**	**105**	**175**	**500**	**0**	**2.4**	**5.7**	**10.4**
Low whisker	27.64	25.57	20.42	27.01	17.18	7.04	13.02	31.77
Q 0.25	89.87	61.39	57.74	52.49	46.31	60.93	71.15	85.10
Q 0.5 (Median)	128.97	87.32	71.28	65.99	60.08	88.64	97.41	102.35
Mean	143.54	92.64	72.39	66.63	64.84	88.11	102.47	102.73
Q 0.75	177.43	111.00	89.30	81.20	75.96	111.44	129.99	120.92
High whisker	300.93	175.45	127.87	123.26	120.06	183.27	215.25	169.63

Table S7. Settling velocity statistical analysis results of aggregates produced under differential settling.

	z score			*p* value		
Sediment concentration (mg L^{-1})	35	105	175	35	105	175
105	6.13	-	-	2.68E-09	-	-
175	9.52	3.50	-	5.34E-21	0.001	-
500	11.43	5.51	2.03	8.89E-30	1.07E-07	0.13

Kruskal-Wallis x^2= 145.268, df = 3, $p < 2.2e^{-16}$

Table S8. Settling velocity statistical analysis results of aggregates produced under turbulent shear.

	z score			*p* value		
Shear rate (s^{-1})	**0**	**2.4**	**5.7**	**0**	**2.4**	**5.7**
2.4	-12.05	-	-	6.10E-33	-	-
5.7	-16.51	-5.39	-	1.01E-60	2.14E-07	-
10.4	-18.91	-7.82	-2.21	3.02E-79	1.61E-14	0.08

Kruskal-Wallis x^2= 411.468, df = 3, $p < 2.2e^{-16}$

2.2.13 References

Agrawal YC, Pottsmith HC. 2000. Instruments for particle size and settling velocity observations in sediment transport. *Mar Geol* **168**(1–4): 89–114. doi: 10.1016/S0025-3227(00)00044-X

Aleynik D, Inall ME, Dale A, Vink A. 2017. Impact of remotely generated eddies on plume dispersion at abyssal mining sites in the Pacific. *Sci Rep* **7**(1): 1–14. Springer US. doi: 10.1038/s41598-017-16912-2

Amon DJ, Ziegler AF, Dahlgren TG, Glover AG, Goineau A, Gooday AJ, Wiklund H, Smith CR. 2016. Insights into the abundance and diversity of abyssal megafauna in a polymetallic-nodule region in the eastern Clarion-Clipperton Zone. *Sci Rep* **6**(July): 1–12. Nature Publishing Group. doi: 10.1038/srep30492

Bianchi GG, McCave IN. 2000. Hydrography and sedimentation under the deep western boundary current on Bjorn and Gardar Drifts, Iceland Basin. *Mar Geol* **165**(1–4): 137–169. doi: 10.1016/S0025-3227(99)00139-5

Boetius A, Haecke M. 2018. Mind the seafloor. *Science (80-)* **359**(6371): 34–36. doi: 10.1126/science.aap7301

Camenen B, van Bang DP. 2011. Modelling the settling of suspended sediments for concentrations close to the gelling concentration. *Cont Shelf Res* **31**(10 SUPPL.). doi: 10.1016/j.csr.2010.07.003

Comeau LA, Vezina AF, Bourgeois M, Juniper K. 1995. Relationship between phytoplankton production and the physical structure of the water column near Coob Seamount Northeast Pacific. *Deep Res* **42**(6): 993–1005. Available at https://www.sciencedirect.com/science/article/pii/096706379500050G.

Coufort C, Bouyer D, Liné A. 2005. Flocculation related to local hydrodynamics in a Taylor-Couette reactor and in a jar. *Chem Eng Sci* **60**(8–9 SPEC. ISS.): 2179–2192. doi: 10.1016/j.ces.2004.10.038

Drapeau DT, Dam HG, Grenier G. 1994. An improved flocculation design for use in particle aggregation experiments. *Limnol Oceanogr* **39**: 723–729.

Van Duuren FA. 1968. Define velocity gradient model flocculator. *J Sanit Eng Div* **94**(4): 671–682.

Ferguson RI, Church M. 2004. A Simple Universal Equation for Grain Settling Velocity. *J Sediment Res* **74**(6): 933–937. Available at http://dx.doi.org/10.1306/051204740933.

Fukushima T. 1995. Overview"Japan Deep-Sea Impact Experiment = JET". First ISOPE Ocean Mining Symposium. Tsukuba, Japan: International Society of Offshore and Polar Engineers.

Gollner S, Kaiser S, Menzel L, Jones DOB, Brown A, Mestre NC, van Oevelen D, Menot L, Colaço A, Canals M, et al. 2017. Resilience of benthic deep-sea fauna to mining activities. *Mar Environ Res* **129**: 76–101. Elsevier Ltd. doi: 10.1016/j.marenvres.2017.04.010

Halbach P, Fellerer R. 1980. The metallic minerals of the Pacific Seafloor. *GeoJournal* **4**(5): 407–421. doi: 10.1007/BF01795925

Hein JR, Koschinsky A. 2013. Deep-Ocean Ferromanganese Crusts and Nodules. In: *Treatise on Geochemistry: Second Edition*2nd ed. Published by Elsevier Inc. p. 273–291. doi: 10.1016/B978-0-08-095975-7.01111-6

Hill PS, Boss E, Newgard JP, Law BA, Milligan TG. 2011. Observations of the sensitivity of beam attenuation to particle size in a coastal bottom boundary layer. *J Geophys Res Ocean* **116**(2): 1–14. doi: 10.1029/2010JC006539

Hughes DJ, Shimmield TM, Black KD, Howe JA. 2015. Ecological impacts of large-scale disposal of mining waste in the deep sea. *Sci Rep* **5**: 1–11. Nature Publishing Group. doi: 10.1038/srep09985

Iversen MH, Nowald N, Ploug H, Jackson GA, Fischer G. 2010. High resolution profiles of vertical particulate organic matter export off Cape Blanc, Mauritania: Degradation processes and ballasting effects. *Deep Res Part I Oceanogr Res Pap* **57**(6): 771–784. Elsevier. doi: 10.1016/j.dsr.2010.03.007

Jackson GA. 2015. Coagulation in a rotating cylinder. *Limnol Oceanogr Methods* **13**(4): 194–201. doi: 10.1002/lom3.10018

Jankowski JA, Zielke W. 1997. Data Support for Modelling of Deep-Sea Mining Impacts. Seventh Interational Offshore and Polar Engineering Conference **I**: 451–460. Available at http://citeseerx.ist.psu.edu/viewdoc/summary?doi=10.1.1.196.1886.

Jones DOB, Kaiser S, Sweetman AK, Smith CR, Menot L, Vink A, Trueblood D, Greinert J, Billett DSM, Arbizu PM, et al. 2017. Biological responses to disturbance from simulated deep-sea polymetallic nodule mining. *PLoS One* **12**(2). doi: 10.1371/journal.pone.0171750

Joshi S, Duffy GP, Brown C. 2014. Settling Velocity and Grain Shape of Maerl Biogenic Gravel. *J Sediment Res* **84**(8): 718–727. doi: 10.2110/jsr.2014.51

Kaiser S, Smith CR, Arbizu PM. 2017. Editorial: Biodiversity of the Clarion Clipperton Fracture Zone. *Mar Biodivers* **47**(2): 259–264. Marine Biodiversity. doi: 10.1007/s12526-017-0733-0

Khripounoff A, Caprais JC, Crassous P, Etoubleau J. 2006. Geochemical and biological recovery of the disturbed seafloor in polymetallic nodule fields of the Clipperton-Clarion Fracture Zone (CCFZ) at 5,000-m depth. *Limnol Oceanogr* **51**(5): 2033–2041. doi: 10.4319/lo.2006.51.5.2033

Klymak JM, Legg SM. 2010. A simple mixing scheme for models that resolve breaking internal waves. *Ocean Model* **33**(3–4): 224–234. Elsevier Ltd. doi: 10.1016/j.ocemod.2010.02.005

Kuhn T. 2015. Low- temperature fluid circulation at seamounts and hydrothermal pits: heat flow regime, impact on biogeochemical processes and its potential influence on the occurence and composition of manganese nodules in the NE Pacific. SO240 / FLUM Cruise Report. Bundesanstalt für Geowissenschaften und Rohstoffe (BGR). doi: 10.2312/cr_so240

Larsson AI, van Oevelen D, Purser A, Thomsen L. 2013. Tolerance to long-term exposure of suspended benthic sediments and drill cuttings in the cold-water coral Lophelia pertusa. *Mar Pollut Bull* **70**(1–2): 176–188. Elsevier Ltd. doi: 10.1016/j.marpolbul.2013.02.033

Lick W, Huang H, Jepsen R. 1993. Flocculation of fine-grained sediments due to differential settling. *J Geophys Res* **98**(C6): 10279–10288. doi: 10.1029/93JC00519

Lohrer AM, Thrush SF, Hewitt JE, Berkenbusch K, Ahrens M, Cummings VJ. 2004. Terrestrially derived sediment: Response of marine macrobenthic communities to thin terrigenous deposits. *Mar Ecol Prog Ser* **273**: 121–138. doi: 10.3354/meps273121

Manning AJ, Dyer KR. 1999. A laboratory examination of floc characteristics with regard to turbulent shearing. *Mar Geol* **160**(1–2): 147–170. doi: 10.1016/S0025-3227(99)00013-4

Marshall J, Adcroft A, Hill C, Perelman L, Heisey C. 1997. A finite-volume, incompressible Navier Stokes model for studies of the ocean on parallel computers. *J Geophys Res Ocean* **102**(C3): 5753–5766. doi: 10.1029/96JC02775

McCave IN. 1984. Size spectra and aggregation os suspended particles in the deep ocean. *Deep Sea Res* **31**(4): 329–352.

McCave IN, MANIGHETTI B, ROBINSON SG. 1995. Sortable Silt and Fine Sediment Size Composition Slicing - Parameters for Paleocurrent Speed and Paleoceanography. *Paleoceanography* **10**(3): 593–610. Available at http://apps.isiknowledge.com/InboundService.do?Func=Frame&product=WOS&action=retrieve&SrcApp=Papers&UT=A1995RG33700017&SID=4FoLPHP92OKagaMpJN%2540&Init=Yes&SrcAuth=mekentosj&mode=FullRecord&customersID=mekentosj&DestFail=http%253A%252F%252Faccess.isiprodu.

Mikkelsen OA, Hill PS, Milligan TG, Chant RJ. 2005. In situ particle size distributions and volume concentrations from a LISST-100 laser particle sizer and a digital floc camera. *Cont Shelf Res* **25**(16): 1959–1978. doi: 10.1016/j.csr.2005.07.001

Milligan TG, Hill PS. 1998. A laboratory assessment of the relative importance of turbulence, particle composition, and concentration in limiting maximal floc size and settling behaviour. *J Sea Res* **39**(3–4): 227–241. doi: 10.1016/S1385-1101(97)00062-2

Nakata K, Kubota M, Aoki S, Taguchi K. 1997. Dispersion of Resuspended Sediment by Ocean Mining Activity - Modelling Study -. Proceedings of the first International Symposium on Environmental Studies for Deep-Sea Mining, Tokyo, Japan: 169–186.

Nowald N, Fischer G, Ratmeyer V, Iversen M, Reuter C, Wefer G. 2009. In-situ sinking speed measurements of marine snow aggregates acquired with a settling chamber mounted to the Cherokee ROV. *Ocean '09 IEEE Bremen Balanc Technol with Futur*

Needs, in press. doi: 10.1109/OCEANSE.2009.5278186

Oebius HU, Becker HJ, Rolinski S, Jankowski JA. 2001. Parametrization and evaluation of marine environmental impacts produced by deep-sea manganese nodule mining. *Deep Res Part II Top Stud Oceanogr* **48**(17–18): 3453–3467. doi: 10.1016/S0967-0645(01)00052-2

Olsgard F, Hasle JR. 1993. Impact of waste from titanium mining on benthic fauna. *J Exp Mar Bio Ecol* **172**(1–2): 185–213. doi: 10.1016/0022-0981(93)90097-8

Pabortsava K, Purser A, Wagner H, Thomsen L. 2011. The influence of drill cuttings on physical characteristics of phytodetritus. *Mar Pollut Bull* **62**(10): 2170–2180. Elsevier Ltd. doi: 10.1016/j.marpolbul.2011.07.002

Porter ET, Sanford LP, Gust G, Porter FS. 2004. Combined water-column mixing and benthic boundary-layer flow in mesocosms: Key for realistic benthic-pelagic coupling studies. *Mar Ecol Prog Ser* **271**: 43–60. doi: 10.3354/meps271043

Ramirez-Llodra E, Trannum HC, Evenset A, Levin LA, Andersson M, Finne TE, Hilario A, Flem B, Christensen G, Schaanning M, et al. 2015. Submarine and deep-sea mine tailing placements: A review of current practices, environmental issues, natural analogs and knowledge gaps in Norway and internationally. *Mar Pollut Bull* **97**(1–2): 13–35. Elsevier Ltd. doi: 10.1016/j.marpolbul.2015.05.062

Ramirez-Llodra E, Tyler PA, Baker MC, Bergstad OA, Clark MR, Escobar E, Levin LA, Menot L, Rowden AA, Smith CR, et al. 2011. Man and the last great wilderness: Human impact on the deep sea. *PLoS One* **6**(8). doi: 10.1371/journal.pone.0022588

Roden GI. 1991. Mesoscale flow and thermohaline structure around Fieberling seamount. *J Geophys Res* **96**(C9): 16653. doi: 10.1029/91JC01747

Samadi S, Bottan L, Macpherson E, De Forges BR, Boisselier MC. 2006. Seamount endemism questioned by the geographic distribution and population genetic structure of marine invertebrates. *Mar Biol* **149**(6): 1463–1475. doi: 10.1007/s00227-006-0306-4

Sautya S, Ingole B, Ray D, Stöhr S, Samudrala K, Kamesh Raju KA, Mudholkar A. 2011. Megafaunal community structure of Andaman seamounts including the Back-Arc Basin - a quantitative exploration from the Indian Ocean. *PLoS One* **6**(1). doi: 10.1371/journal.pone.0016162

Serra T, Casamitjana X. 1998. Structure of the aggregates during the process of aggregation and breakup under a shear flow. *J Colloid Interface Sci* **206**(2): 505–511. doi: 10.1006/jcis.1998.5714

Shen X. 2016. Modeling Flocculation and Deflocculation Processes of Cohesive Sediments. The College of William and Mary.

Smith SDA, Rule MJ. 2001. The effects of dredge-spoil dumping on a shallow water soft-sediment community in the Solitary Islands Marine Park, NSW, Australia. *Mar Pollut Bull* **42**(11): 1040–1048. doi: 10.1016/S0025-326X(01)00059-5

Smith SJ, Friedrichs CT. 2011. Size and settling velocities of cohesive flocs and suspended sediment aggregates in a trailing suction hopper dredge plume. *Cont Shelf Res* **31**(10 SUPPL.): S50–S63. Elsevier. doi: 10.1016/j.csr.2010.04.002

Southard J. 1971. Experimental erosion of calcareous ooze. *J Geophys …* **76**(24): 5903–5909. Available at http://onlinelibrary.wiley.com/doi/10.1029/JC076i024p05903/full.

Sternberg RW, Berhane I, Ogston AS. 1999. Measurement of size and settling velocity of suspended aggregates on the northern California continental shelf. *Mar Geol* **154**(1–4): 43–53. doi: 10.1016/S0025-3227(98)00102-9

Sternberg RW, Ogston A, Johnson R. 1996. A video system for in situ measurement of size and settling velocity of suspended particulates. *J Sea Res* **36**(1–2): 127–130. Available

at http://www.sciencedirect.com/science/article/pii/S1385110196907820.
Sylvester Z. 2013. Exploring grain settling with Python. Available at https://hinderedsettling.com/2013/08/09/grain-settling-python/.
Thomsen L, Gust G. 2000. Sediment erosion thresholds and characteristics of resuspended aggregates on the western European continental margin. *Deep Res Part I Oceanogr Res Pap* **47**(10): 1881–1897. doi: 10.1016/S0967-0637(00)00003-0
Thomsen L, VanWeering T, Gust G. 2002. Processes in the benthic boundary layer at the Iberian continental margin and their implication for carbon mineralization. *Prog Oceanogr* **52**(2–4): 315–329. doi: 10.1016/S0079-6611(02)00013-7
Trannum HC, Nilsson HC, Schaanning MT, Øxnevad S. 2010. Effects of sedimentation from water-based drill cuttings and natural sediment on benthic macrofaunal community structure and ecosystem processes. *J Exp Mar Bio Ecol* **383**(2): 111–121. Elsevier B.V. doi: 10.1016/j.jembe.2009.12.004
Wedding LM, Reiter SM, Smith CR, Gjerde KM, Kittinger JN, Friedlander AM, Gaines SD, Clark MR, Thurnherr AM, Hardy SM, et al. 2015. Managing mining of the deep seabed: Contracts are being granted, but protections are lagging. *Science (80-)* **349**(6244): 144–145. doi: 10.1126/science.aac6647
White M, Bashmachnikov I, Arístegui J, Martins A. 2008. Physical processes and seamount productivity. In: *Seamounts: Ecology, Fisheries and Conservation*. p. 228–243.
Winterwerp JC. 2002. On the Flocculation and Settling Velocity of Esturine Mud. *Cont Shelf Res* **22**(October 2001): 1339–1360. doi: 10.1016/S0278-4343(02)00010-9
Zhu Z, Wang H, Yu J, Dou J. 2016. On the kaolinite floc size at the steady state of flocculation in a turbulent flow. *PLoS One* **11**(2): 1–16. doi: 10.1371/journal.pone.0148895

2.3 Manuscript III: Heavy-metal-resistant microorganisms in deep-sea sediments disturbed by mining activity: an application towards the development of experimental in vitro systems.

Benjamin Gillard[1, 2, *], Damianos Chatzievangelou[2], Laurenz Thomsen[2,] Matthias S. Ullrich[3]

[1]MARUM – Center for Marine Environmental Sciences, University of Bremen, Bremen, Germany

[2]Jacobs University Bremen, Department of Physics and Earth Science, Bremen, Germany

[3]Jacobs University Bremen, Department of Life Science and Chemistry, Bremen, Germany

Publish in: Frontiers in Marine Science, section Deep-Sea Environments and Ecology, DOI: 10.3389/fmars.2019.00462

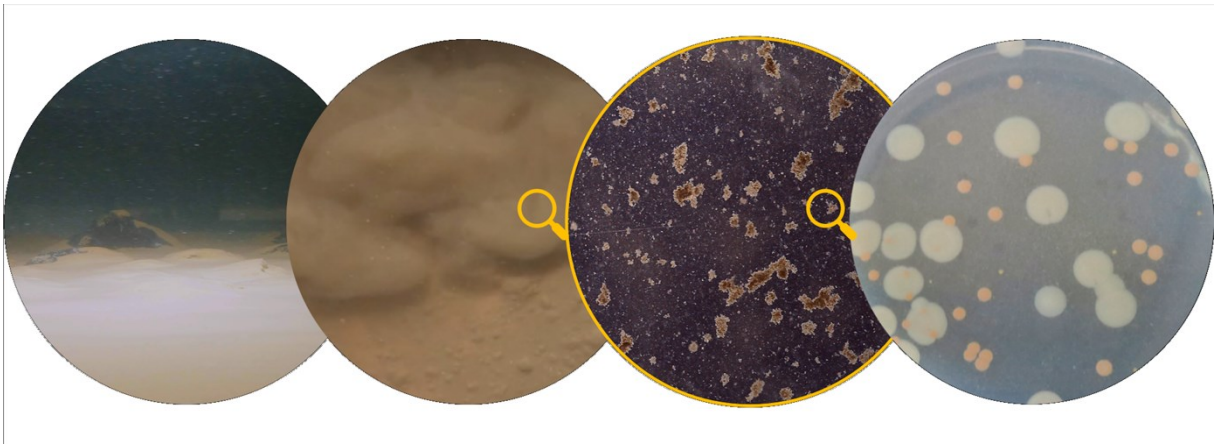

2.3.1 Abstract

Future mining of polymetallic nodules in the Clarion Clipperton Zone (Northeastern Pacific) is expected to affect all benthic ecosystems. The diversity, distribution, and environmental functions of microorganisms inhabiting abyssal sediments are barely understood. To understand consequences of deep-sea mining, experimental *in vitro* systems needs to be established to test hypotheses on the environmental impact of mining. For this, 40 bacterial strains, belonging to proteobacteria, actinobacteria and firmicutes were isolated from deep-sea sediments and nodules sampled at depths of ≥ 4000 m. Phenotypic characterization revealed a strong inter-species and moderate intra-species variability. Determination of metal minimum inhibitory concentrations indicated the presence of acute manganese-resistant bacteria such as *Rhodococcus erythropolis* [228.9 mM], *Loktanella cinnabarina* [57.2 mM], and *Dietzia maris* [14.3 mM] that might be suitable systems for testing the effects of release of microbes from nodules and their interactions with sediment particles in plumes generated during mining. Comparative genomic analysis indicated the presence of manganese efflux systems relevant for future transcriptomics or proteomics approaches with environmental samples and might serve in paving the way to develop model systems including representative organisms which are currently not cultivable. Monitoring deep-sea mining activity at abyssal depth is a challenge that has to be tackled. We proposed the use of API strips as a fast-on-board methodology for bacterial monitoring as an indicator for sediment plume dispersions within the water column.

2.3.2 Introduction

Deep-sea environments are considered the most remote, broad (95 % of ocean surface) and least understood ecosystems on Earth (Jørgensen and Boetius, 2007; Smith et al., 2008). Some deep-sea areas, however, contain considerably high amounts of mineral resources, which have recently received increasing attention from governments and private entities. Consequently, the Clarion Clipperton Zone (CCZ; NE equatorial Pacific; Figure 1), with an extent of 4.5 million km^2, has been the focus for polymetallic nodule exploration programs.

Polymetallic nodules are marine encrustations rich in precious metals such as manganese (Mn), nickel (Ni), copper (Cu), and cobalt (Co), as well as rare earth elements of both ecological and economical relevance (Fritz, 2016; Hein and Koschinsky, 2013).

Lying on the surface of abyssal plains at around 4000 m depth, their genesis is geologically slow and results from diagenetic and hydrogenetic processes that take place over a million years (Graham et al., 2004). Environmental conditions at the CCZ seafloor are characterized by cold temperature (2°C), clay siliceous ooze sediment with an oxygen penetration depth of around 2-3 m, a low sedimentation rate of 0.35 cm kyr^{-1}, and very low organic impact (Mewes et al., 2014).

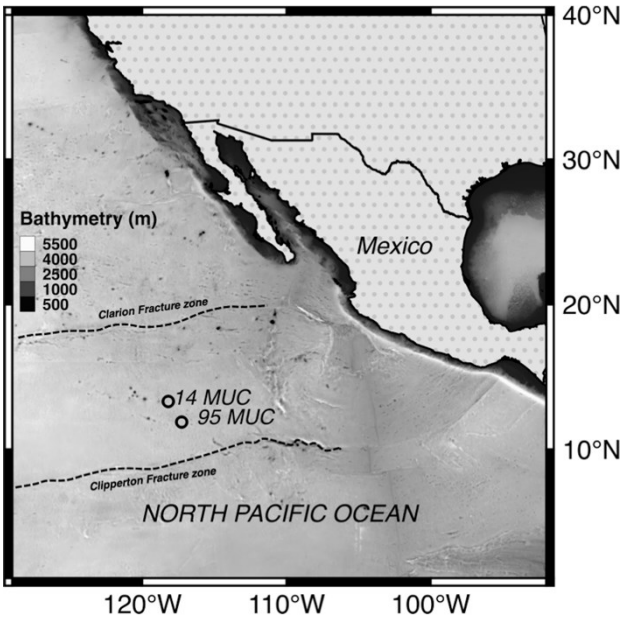

Figure 1. Study area and locations of sediment core sampling.

Nodule harvesting is expected to not only directly impact the mined surface, where the top sediment layer will be removed, but also a much wider area, as a result of the tailing of mined products (sediment plume and nodule debris) into the benthic boundary layer (Aleynik et al., 2017; Gillard et al., 2019; Oebius et al., 2001). This sediment plume, which is rich in manganese-oxide, may lead to potentially high sorption of trace metals in the water column (Koschinsky et al., 2003). To date, nothing is known about the role and interactions of microbial communities within the plume particles and the redeposited sediments that may influence the oxidation state, mobility and flux of metals. Heavy metals are essential elements for the maintenance of cellular functions in microorganisms. However, under elevated concentrations, those elements result in toxicity that is metal- and organism-dependent (Lemire et al., 2013). As such, the anticipated impact of mining activity is very difficult to estimate but will likely affect the entire regional deep-sea ecosystem. The extent to which this ecosystem will be affected is unknown and unpredictable (Ramirez-Llodra et al., 2011).

Although microbial diversity and ecology in most abyssal sediments have barely been investigated (Danovaro et al., 2014), the potential risks that these fragile ecosystems may encounter have forced the scientific community to increase efforts in describing the prokaryotic diversity in the CCZ area over the last few years (Parkes et al., 2014). Culture-independent approaches and the use of next generation sequencing technologies have revealed the high microbial diversity and complexity of bacterial assemblages inhabiting deep-sea sediments (Corinaldesi, 2015; Lindh et al., 2017; Shulse et al., 2016; Wu et al., 2013). In accompanying the efforts to explore the deep-sea with microbiological approaches and to broaden the understanding of gene activity for heavy metal resistance, a cultivation-based study was conducted herein.

It is hypothesized that isolation and characterization of heavy-metal-resistant and -sensitive bacterial strains from abyssal sediments of the CCZ may help to establish experimental *in vitro* system to study the dispersal of microorganisms during relocation of material in sediment plumes in dependence of diverse biotic and abiotic environmental factors. Such an *in vitro* system may complement omics-based microbial analysis, as well as mineralogical and hydrographical analyses, which would therefore shed light on ecosystem alterations caused by mining activities.

Our current research aims were to: (**1**) isolate and characterize of cultivable deep-sea microorganisms, (**2**) investigate heavy-metal-resistance and sensitivity of these microorganisms, (**3**) obtain any first insights on potential genes that confer manganese resistance in bacterial isolates.

2.3.3 Materials and methods

2.3.3.1 Study area and sampling

Abyssal sediments and polymetallic nodules were collected during the RV SONNE cruise SO-240, within the German license area for the exploration of polymetallic nodules in the CCZ (Figure 1). Samples were obtained at two different sites using a multicorer (MUC; samples 14 and 95; Supplementary Table S1 for details). The top water layer and 10 centimeters of sediment from one multicore (14 MUC) as well as surface nodules (95 MUC) were aseptically sampled, sliced in 1 cm intervals and stored at 4°C in the dark until further analysis in the laboratory.

2.3.3.2 Bacterial extraction and isolation

Sediments from every core layer were screened for fast growing aerobic bacteria. Aliquots of roughly 300 μg of sediment were resuspended in 1 mL of autoclaved North Sea water. Nodule samples were carefully rinsed several times with the same North Sea water prior to the extraction procedure. Bacterial cells were separated from sediment particles or nodules by three 10-minute vortexing intervals (Vortex 2 Genie, Scientific Industries, Bohemia, USA). Samples were centrifuged (Eppendorf 5418R; Eppendorf, Hamburg, Germany) at 750 x g for 10 minutes at 4°C (Dos Santos Furtado and Casper, 2000). After centrifugation, the supernatant was used for bacterial isolation.

Bacterial strain isolation was conducted using a serial dilution (up to 10^{-5}) plating on a marine broth (MB) agar medium (Sonnenschein et al., 2011). Samples were incubated in the dark at 18°C for 7 days to expedite microbial growth. Colonies with unique morphological features were re-streaked on the MB agar medium. Isolates were maintained on agar plates with regular re-streaking. A suspension of bacterial cells in 30 % (v/v) glycerol was prepared to store the bacterial strains for long term at -80°C.

2.3.3.3 Taxonomic characterization

The polymerase chain reaction (PCR) was conducted with a re-suspended single bacterial colony as a template in 100 μL of sterile water incubated at 95°C for 10 minutes prior to reaction. The corresponding 16S rRNA gene was amplified by PCR using the universal primers (5'- AGA GTT TGA TCC TGG CTC AG-3' and 5'- TAC GGY TAC CTT GTT ACG ACT T-3'; Alfaro-Espinoza and Ullrich 2014). The PCR reaction mix, with a final volume of 50 μL, consisted of 42.5 μL of target cell suspension (10-100 ng of DNA), 0.5 μL of each primer (50 pmol μL^{-1}), 1μL dNTP (2 μmol), 5 μL of 10X DreamTaq Green buffer, and 0.5 μL of DreamTaq DNA polymerase (5U μL^{-1}). All reagents were purchased from Thermo Fisher Scientific (Massachusetts, USA). The thermal cycling gradient program was as follows: initial denaturation (5 minutes at 94°C), subsequent denaturation (32 cycles of 15 seconds at 94°C), annealing (30 seconds at 55°C), extension (60 seconds at 72°C) and a final extension (72°C for 3 minutes). A negative control containing no DNA extract was conducted to account for any contamination.

The amplification of the 16S rRNA gene was confirmed by agarose (1 % (w/v)) gel electrophoresis (120 V, 30 minutes) and ethidium bromide staining (0.1 %). PCR products

were purified using a GeneJet PCR Purification Kit (Thermo Fisher Scientific, Massachusetts, USA). All 16S amplicons were sequenced by Eurofins Genomics (www.Eurofinsgenomics.eu). All nucleotides sequences were submitted to the NCBI 16S Microbial Database using the Basic Local Alignment Search Tool (BLAST; http://www.ncbi.nlm.nih.gov/blast) to determine whether they aligned with any closely related organisms. Sequence similarity was set to a threshold value of minimum 99 % for a positive match.

2.3.3.4 Morphological, biochemical and enzymatic characterization

Colony morphology, bacteria motility, and gram staining were examined using a phase contrast microscope (Axiostar plus, Zeiss). Biochemical characteristics and enzyme activity were determined using the API 20NE and API ZYM kits (BioMérieux, Marcy-l'Étoile, France). The protocol followed the manufacturer's instructions with the exception of the culture being suspended in autoclaved North Sea water (Kim et al., 2007; MacDonell et al., 1982). The incubation was done at 18°C for 24 hours.

Based on the corresponding phenotypical characteristics of the selected bacterial strains, single tests or combinations of tests providing a unique identification were performed in R (R Core Team 2016), thus providing the most effective identification path for each strain. Tests with results not in accordance with previously reported phenotypes were not considered. Cell or colony morphology was omitted from the analysis.

2.3.3.5 Minimum inhibitory concentration (MIC) of heavy metals

The MIC of heavy metal ions for bacteria isolated from deep-sea sediments or nodule surfaces was conducted in triplicate with a two-fold dilution assay in 96-well plates (Stahl et al., 2015). The heavy metals tested were: cadmium acetate ($Cd(CH_3CO_2)_2 \cdot 2H_2O$), cobalt chloride ($CoCl_2 \cdot H_2O$), cupric sulphate ($CuSO_4 \cdot 5H_2O$), zinc sulphate ($ZnSO_4 \cdot 7H_2O$) (Sigma-Aldrich, City, Germany), manganese (II)-sulphate ($MnSO_4 \cdot H_2O$) (Carl Roth, Karlsruhe, Germany) and nickel chloride ($NiCl_2 \cdot 6H_2O$) (AppliChem). The concentration of the metal stock solutions (1M) were confirmed by a Cyros Vision inductively coupled plasma optical emission spectrometry (ICP-OES) (SPECTRO Analytical Instruments Inc., Kleve, Germany). Cells were harvested in their exponential growth phase (OD_{600}= 0.5-1) and adjusted to ~ 2.85 x 10^6 cells mL^{-1} (OD_{600}= 0.001). The highest concentration of metal salt used was 0.5 M. Cells were incubated at

18°C for 96 hours. The MIC was defined as the lowest concentration of metal salt, which inhibited visible bacterial growth.

2.3.3.6 Genomic analysis of manganese resistance related genes

To our knowledge, only a few studies have investigated the differential gene expression mechanisms for Mn (II) efflux systems in several bacterial species over the last decade (Table 1). From the isolated bacterial strains, those showing the highest resistance to Mn as determined by MIC were selected for further analysis.

Table 1. Known bacterial manganese efflux systems and their regulators

	Bacteria species	Genes	Accession number	References
Cation diffusion facilitator (CDF)	*Streptococcus pneumoniae*	MntE	ABJ55467.1	Rosch *et al.* 2009
	Deinococcus radiodurans	MntE	AAF10804.1	Sun *et al.* 2010
	Escherichia coli	MntP	NP_416335.4	Waters, Sandoval and Storz 2011
	Xanthomonas oryzae	YebN	AEL04135.1	Li *et al.* 2011
	Bacillus subtilis	MneP/MneS	C0SP78.1; P46348.2	Huang *et al.* 2017
P-type ATPase	*Mycobacterium tuberculosis*	ctpC	NP_217787.1	Padilla-Benavides *et al.* 2013
Transcriptional regulators	*Bacillus subtillis*	MntR	P54512.2	Que and Helmann 2000
	Escherichia coli	MntR	NP_415338.1	Patzer and Hantke 2001
	Deinococcus radiodurans	DR2539	WP_010889164.1	Chen *et al.* 2010

Based on the availability of genome sequences from the literature, the search tool BlastP (protein-protein) was used to test for the presence of highly similar protein sequences from the tested bacterial species. Protein sequence homology was determined based on the following criteria: minimum sequence coverage of 90 %, bit score > 50 and sequence identity > 25 % (Pearson, 2014). Protein functional inference was based on the overall similarity, conserved active site domains and residues using the InterPro (Finn et al., 2017) and UniProtKB (Wu et al., 2006) databases. For every protein match, the length of identical DNA sequences was determined using TBlastn (protein-translated nucleotide).

2.3.4 Results

2.3.4.1 Bacterial extraction and isolation

The overall abundance of cultivable bacteria throughout the first 10 cm of sediment core 14 MUC delineates a multi-modal distribution pattern (Figure 2). Three peaks of elevated concentrations were observed at 2-3 cm (0.81 x 10^5 CFU g^{-1}), 4-5 cm (0.43 x 10^5 CFU g^{-1}), and 8-9 cm (0.68 x 10^5 CFU g^{-1}) depth.

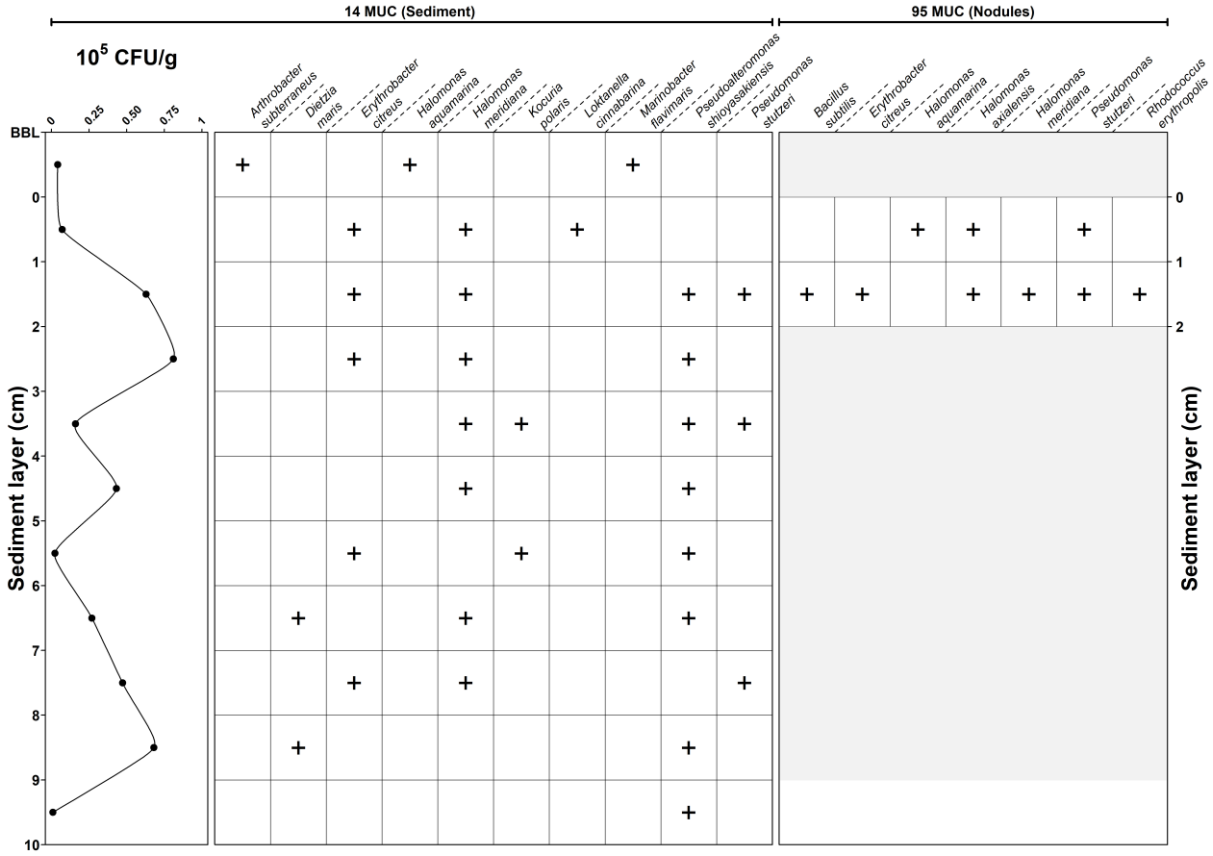

Figure 2. Depth profile and concentration of bacterial isolation.
(+) indicate positive isolation.

In total, 40 bacterial strains were isolated based on their distinguishing morphological characteristics. The amount of isolated strains per depth varied between one (10 cm depth) and six (nodule surface) strains. Species location revealed different trends of spatial distribution (Figure 2). The bottom boundary layer (BBL) representing the water in contact with the sediment core contained bacteria that were not present in the sediment (e.g. *Arthrobacter subterraneus*, *Marinobacter flavimaris*). Inside the sediment core, bacterial distribution occurred in three patterns: (1) widely spread (e.g. *Pseudoalteromonas shioyasakiensis*), (2) confined at certain depth (e.g. *Dietzia maris,*

Kocuria polaris) or (3) present at distinctive depth layers (e.g. *Erythrobacter citreus, Halomonas meridiana*).

2.3.4.2 Taxonomic characterization

BLASTN analysis results (Supplemental Table S2) based on partial 16S rRNA gene sequences indicated that the 40 bacterial isolates belonged to three distinctive phylogenetical groups (83 % proteobacteria, 15 % actinobacteria and 3 % firmicutes) and could be classified into 13 species (listed in Table 2). Sequences with similarities of > 99 % to sequences from taxonomically closely related species were deposited in GenBank (https://www.ncbi.nlm.nih.gov/genbank/) under the accession numbers MK254646-MK254685, demonstrating that all bacterial isolates from this study resembled species previously isolated from the marine environment and the marine benthos; the sole exception is *Marinobacter flavimaris*, which was previously only reported for bulk seawater.

Table 2. 16S rRNA Phylogenetic affiliations of isolated bacterial species.

	Bacteria species	Phylum	Isolate Nr.	Reported marine isolation	References [1]
1	*Arthrobacter subterraneus*	Actinobacteria	1	Sediment, deep water layer	Chang *et al.* 2007; Ettoumi *et al.* 2016
2	*Bacillus subtilis*	Firmicutes	1	Sediment, water column	Ivanova *et al.* 1999; Miranda, Martins and Clementino 2008; Nisha and Divakaran 2014
3	*Dietzia maris*	Actinobacteria	2	Sediment, hydrothermal field	Inagaki *et al.* 2003; Pathom-aree *et al.* 2006; Wang, Cai and Shao 2014; Gao *et al.* 2015
4	*Erythrobacter citreus*	Proteobacteria	6	Sediment, deep water layer	Gao *et al.* 2015; Kai *et al.* 2017; Li *et al.* 2018
5	*Halomonas aquamarina*	Proteobacteria	2	Sediment, water column, hypersaline pond	Wang *et al.* 2004; Xu *et al.* 2005; Mobberley *et al.* 2008; Ettoumi *et al.* 2010; Tang *et al.* 2011; Focardi *et al.* 2012
6	*Halomonas axialensis*	Proteobacteria	2	Sediment, hydrothermal vent	Kaye *et al.* 2004; Chen and Shao 2009; Ettoumi *et al.* 2010; Hirayama *et al.* 2015
7	*Halomonas meridiana*	Proteobacteria	8	Sediment, hydrothermal vent, surface water, coral mucus	Takami *et al.* 1999; Maruyama *et al.* 2000; Teske *et al.* 2000; Kaye *et al.* 2004; Ritchie 2006; Vraspir, Holt and Butler 2011
8	*Kocuria polaris*	Actinobacteria	2	Sediment, microbial mat	Reddy *et al.* 2003; Undabarrena *et al.* 2016
9	*Loktanella cinnabarina*	Proteobacteria	1	Sediment, surface water	Tsubouchi *et al.* 2013; Ma *et al.* 2017
10	*Marinobacter flavimaris*	Proteobacteria	1	Sea water	Yoon *et al.* 2004; Gärtner *et al.* 2011; Yuan *et al.* 2015; Cruz-López and Maske 2016
11	*Pseudoalteromonas shioyasakiensis*	Proteobacteria	8	Sediment, sponge, worm, biofilm	Matsuyama *et al.* 2014; Melnikova *et al.* 2017; Balqadi, Salama and Satheesh 2018; Bibi *et al.* 2018
12	*Pseudomonas stutzeri*	Proteobacteria	5	Sediment, seamount, surface water	Sudek *et al.* 2009; Bentzon-tilia *et al.* 2015; Catania *et al.* 2018; Zheng *et al.* 2018
13	*Rhodococcus erythropolis*	Actinobacteria	1	Sediment	Langdahl, Bisp and Ingvorsen 1996; Heald *et al.* 2001; Arias, Cisternas and Rivas 2017; Labonté *et al.* 2017

(1) The references column relates to the citation of research papers in which the given organism has been described in the marine ecosystem.

2.3.4.3 Phenotypic characterization

Based on the isolation depth profile and 16S rDNA sequence similarities, 16 bacterial strains were selected for further phenotypic characterization. Most strains were capable of using diverse substrates as sole carbon sources and synthesized a wide spectrum of hydrolytic enzymes (Table 3). The following tests were negative for all isolated bacterial strains: indole production, glucose fermentation, arginine dihydrolase, α-galactosidase, and α-fucosidase. After 24 hours of incubation, *Erythrobacter citreus* did not show any visible growth for any of the tested sole carbon sources. A similar result was observed for *Marinobacter flavimaris*, which could, however, utilize malic acid as its only carbon source. In the case of *Dietzia maris* and *Halomonas meridiana*, for which two strains each were isolated, biochemical analyses indicated high phenotypic similarity. In clear contrast, the two isolates of *Pseudoalteromonas shioyasakiensis* displayed substantial biochemical and enzymatic variability.

The applied identification path indicated that a combination of two phenotypical parameters allowed for the identification of 11 of the 13 species; for example, *Rhodococcus erythropolis* was distinguishable by its nitrate reduction and uptake of L-arabinose as its carbon source (Supplemental Table S3).

Table 3. Phenotypic characterization of type strains isolated from deep sea environment.

1. *Arthrobacter subterraneus (SO240BG01)*; **2.** *Bacillus subtilis (SO240BG32);* **3a.** *Dietzia maris (SO240BG03)*; **3b.** *Dietzia maris (SO240BG02)*; **4.** *Erythrobacter citreus (SO240BG08)*; **5.** *Halomonas aquamarina (SO240BG09)*; **6.** *Halomonas axialensis (SO240BG35)*; **7a.** *Halomonas meridiana (SO240BG14)*; **7b.** *Halomonas meridiana (SO240BG12)*; **8.** *Kocuria polaris (SO240BG17)*; **9.** *Loktanella cinnabarina (SO240BG19)*; **10.** *Marinobacter flavimaris (SO240BG20)*; **11a.** *Pseudoalteromonas shioyasakiensis (SO240BG28)*; **11b.** *Pseudoalteromonas shioyasakiensis (SO240BG21)*; **12.** *Pseudomonas stutzeri (SO240BG39)*; **13.** *Rhodococcus erythropolis (SO240BG40).*

API	Characteristics	1	2	3a	3b	4	5	6	7a	7b	8	9	10	11a	11b	12	13
	Morphology	RC	R	RC	RC	R	R	R	R	R	C	R	R	R	R	R	RC
	Pigmentation	PY	W	O	O	BY	C	W	W	W	LP	W	W	W	W	PY	LO
	Motility	-	+	-	-	-	+	+	+	+	-	-	+	+	+	+	-
	Gram	+	+	+	+	-	-	-	-	-	+	-	-	-	-	-	+
20NE																	
	Nitrite reduction	-	-	-	-	-	-	+[7]	-	+[6]	-	-	-	-	+	+	+
	Urease	-	-	-	-	-	-	-	-[6]	-[6]	-	-	-	-	-	-	+
	Hydrolysis of Esculin	+	+	-	-	-	-	-	-	-	+	+	-	+	+	+	+
	Hydrolysis of Gelatin	+	-	-	-	-	-	-	-	-	+[10]	+[11]	-	+	+	+	-
	D-glucose	+	+	+	+	-	+	+	+	+	+	+	-	+	+	+	+
	L-arabinose	+	-[2]	+[3]	+[3]	-	-[6]	+	+[7]	+[9]	+[10]	+	-	+	+	+	-
	D-mannose	+	-	+	+	-	-	+[7]	+[7]	-	+	-	-	-	+	-	-
	D-mannitol	+	+	+	+	-	-	+[7]	+	+	+[10]	+	-	+	+	+	+
	N-acetyl-glucosamine	-	-	+	+	-	+[6]	+	+[6]	-	+	-[11]	-	-[13]	+	-	+
	D-maltose	+	+	+	+	-	+	+	+	+	+	+	-	-	+	+	+
	Potassium gluconate	+	+	+	+	-	+	+	+	+	+	+	-	-	+	+	+
	Capric acid	-	+	-	-	-	+	-	-	-	-	+	-	-	-	+	+
	Adipic acid	-	+	+	+	-	+	+	+	+	+	+	-	-	+	+	+
	Malic acid	+	+	+	+	-	+	+	+	+	+	+	+	+	+	+	+
	Trisodium citrate	-	+	+	-	-	+	-	-	-	+	+	-	-	+	+	+
	Phenylacetic acid	-	-	-	-	-	-	-	-	-	-	-	-	-	-	-	+
ZYM																	
	Alkaline phosphatase	+[1]	-	+	+	+	+	+	-	-	+	-	+	+	+	+	+
	Esterase	-	+	+	+	+	+	+	-	-	+	-[11]	+	+	+	+	+
	Esterase lipase	-[1]	+	+	+	+	+	+	-	-	+	-[11]	+	+	+	+	+
	Lipase	-	-	-	-	-	+	-	-	-	-	-	+	-	+	+	+
	Leucine-arylamidase	+	+	+	+	+	+	+	+	+	+	-	+	+	+	+	+
	Valine arylamidase	+	+	+	-	+	+	+	+	+	+	+	-	+	+	+	+
	Cystine arylamidase	-	-	-	+	+	-	-	-	-	-	+	-	-	-	-	-
	Trypsin	-	-	-	-	-	+	+	+	-	-	+	-	-	-	-	-
	α-chymotripsin	-	-	-	-	-	-	-	-	-	-	+	-	+[13]	-	-	-
	Acid phosphatase	-	-	+	+	+	+	+	-	-	+	-	-	+	+	+	+
	ß-Galactosidase	-[1]	-	-	-	-	-	-	-	-	-	+	-	-	-	-	-
	ß-Glucuronidase	-	-	-	-	-	-	-	-	-	-	+	-	-	-	-	-
	α-Glucosidase	+	-	+	+	-	+	+	+	+	+	+	-	+	-[13]	-	+
	ß-Glucosidase	-	-	-	-	-	-	-	-	-	-	+	-	-	-	-	+
	N-acetyl-ß-glucosaminidase	-	-	-	-	-	-	+	-	-	-	+	+	+	-[13]	-	-
	α-Mannosidase	-	-	-	-	-	-	-	-	-	-	+	-	-	-	-	-

Morphology: R: Rod; C: Coccoid // **Pigmentation:** PY: pale yellow; W: white; O: orange; LO: light orange; BY: bright yellow; C: cream; LP: light pink // **(+)** positive; **(-)** negative // **Results that are not in accordance with previous description:** (1) Chang *et al.* 2007; (2) Miranda, Martins and Clementino 2008; (3) Koerner, Goodfellow and Jones 2009;(6) Guzmán *et al.* 2010; (7) Kaye *et al.* 2004; (9); (10) Reddy *et al.* 2003; (11) Tsubouchi *et al.* 2013; Kim, Srinivasan and Lee 2016; (13) Matsuyama *et al.* 2014

2.3.4.4 Determination of minimal inhibitory concentrations (MIC) of heavy metals

The multi-metal resistance of the 16 bacterial strains of interest in liquid medium was tested by determining the minimal inhibitory concentrations (MIC) following a two-fold dilution technique approach. High MIC values indicate high tolerance of the bacterial isolate towards the metal and vice-versa. Metal tolerance appeared to be heterogeneous; the results are listed in Table 4.

Table 4. Minimal inhibitory concentration of metal salt determined in liquid culture.

		Metal salt [mM]					
Species	**Culture Collection**	**Cu^{2+}**	**Cd^{2+}**	**Co^{2+}**	**Zn^{2+}**	**Ni^{2+}**	**Mn^{2+}**
Arthrobacter subterraneus	SO240BG01	5.7	0.3	1.3	0.6	3.0	1.8
Bacillus subtilis	SO240BG32	5.7	2.4	1.3	4.5	3.0	3.6
Dietzia maris	SO240BG03	2.8	0.6	1.3	2.2	3.0	**14.3**
Dietzia maris	SO240BG02	5.7	0.6	1.3	2.2	3.0	0.1
Erythrobacter citreus	SO240BG08	5.7	0.3	0.6	0.6	3.0	0.1
Halomonas axialensis	SO240BG35	5.7	1.2	1.3	4.5	3.0	7.2
Halomonas aquamarina	SO240BG09	5.7	1.2	1.3	2.2	3.0	7.2
Halomonas meridiana	SO240BG14	2.8	0.6	1.2	2.2	6.0	3.6
Halomonas meridiana	SO240BG12	2.8	0.6	0.6	2.2	3.0	0.4
Kocuria polaris	SO240BG17	2.8	1.2	2.6	2.2	**12.1**	1.8
Loktanella cinnabarina	SO240BG19	2.8	0.6	1.3	2.2	6.0	**57.2**
Marinobacter flavimaris	SO240BG20	5.7	0.3	0.6	1.1	3.0	0.9
Pseudoalteromonas shioyasakiensis	SO240BG28	5.7	0.3	0.6	1.1	6.0	0.4
Pseudoalteromonas shioyasakiensis	SO240BG21	5.7	0.3	0.3	4.5	3.0	0.4
Pseudomonas stutzeri	SO240BG39	5.7	1.2	0.3	4.5	3.0	1.8
Rhodococcus erythropolis	SO240BG40	5.7	1.2	1.3	2.2	6.0	**228.9**

Shaded: inter-species metal tolerance variabilities; **Bold**: highest metal resistance concentration.

The overall level of metal toxicity increased in the order of $Mn^{2+} < Cu^{2+} < Ni^{2+} < Zn^{2+} < Co^{2+} < Cd^{2+}$, corresponding to an average MIC of 20.6, 4.8, 4.3, 2.5, 1.1, and 0.8 Mm, respectively. As reported for the phenotypic characterization above, inter-species variability was observed for *Dietzia maris*, *Halomonas meridiana* and *Pseudoalteromonas shioyasakiensis*. The highest metal tolerance was found using manganese salt with *Dietzia maris* (MIC of 14.3 mM), *Loktanella cinnabarina* (MIC of 57.2 mM) and *Rhodococcus erythropolis* (MIC of 228.9 mM). *Kocuria polaris* also exhibited higher metal tolerance to nickel salt (12.1mM) as compared to the other tested bacterial strains.

2.3.4.5 Genomic analysis of manganese resistance related genes

As the deep-sea environment in focus is characterized by manganese nodules, the majority of isolated bacterial strains showed an elevated tolerance to Mn. Consequently, previously reported amino acid sequences of Mn efflux systems, P-type ATPase and Mn resistance-associated transcriptional regulators from relevant marine bacterial species were compared by sequence alignment (data not shown) and their functional conserved domains (CD) identified (Table 5). Protein similarity and domain architecture resulted in a functional classification of two cation diffusion facilitator family proteins (FieF and MntP), one P-type ATPase (ZntA) and one transcriptional regulator (MntR).

Table 5. Conserved domain identification of reported manganese efflux system and regulator.

Related To	CD	Reported genes	Accession	Description
Cation diffusion facilitator	FieF	MntE, MneP, MneS	COG0053	Divalent metal cation transporter
	MntP	MntP, YebN	COG1971	Putative Mn^{2+} efflux pump
P-type ATPase	ZntA	CtcP	COG2217	Cation transport ATPase
Transcriptional regulator	MntR	MntR	COG1321	Mn-dependent transcriptional regulator

The genomic analysis of *Dietzia maris*, *Loktanella cinnabarina* and *Rhodococcus erythropolis*), which exhibited the highest Mn^{2+} resistance, was conducted using Blast, InterPro and UniProtKB to give first hints on possible mechanisms of their metal tolerance. The published genomes of *D. maris* (LVFF00000000), *L. cinnabarina* (BATB00000000) and *R. erythropolis* (MDCH00000000) were retrieved from the Genbank database. The numbers of putative gene copies involved in Mn tolerance are presented in Table 6.

Table 6. Putative gene copies number involved in resistance to Mn^{2+}**.**

		Copies of genes		
Related To	**CD**	***D. maris***	***L. cinnabarina***	***R. erythropolis***
Cation diffusion facilitator (CDF)	FieF	1	3	5
	MntP	0	0	0
P-type ATPase	ZntA	1	3	4
Transcriptional regulator	MntR	1	1	1

Details of sequence identification are provided in Supplemental Table S4. Surprisingly, none of the investigated genomes possessed any copies of the putative Mn^{2+}

efflux pump MntP. In contrast, the divalent metal transporter FieF was found in one or more copies of the genomes of *D. maris*, *L. cinnabarina* and *R. erythropolis*. A similar situation was observed for the P-type ATPase, ZntA. Finally, only one copy of the transcriptional regulator MntR was found per genome investigated.

2.3.5 Discussion

The removal of surface sediment layers and subsequent dispersion of sediment plumes during a deep-sea mining operation is expected to disturb the benthic ecosystem to an unknown extent. The main aim of this study was to provide a pilot study for the development of an *in vitro* system containing metal-resistant and metal-sensitive bacterial organisms derived from deep-sea sediments. In the future, those organisms will allow a better assessment of heavy metal resistance, bacterial behaviour and bacterial dispersion during deep-sea mining in order to optimize comprehensive environmental monitoring in preparation for and during mining activities.

It must be admitted that *in vitro* cultivation of sub-seafloor microbial community representatives only reveals a very small fraction (less than 0.1%) of the total bacterial diversity (Hondt et al., 2004). However, our study is one of the first (Wang et al., 2018) in which cultivated deep-sea sediment bacteria from the CCZ were characterized in the laboratory in combination with assessment of their metals resistance and related gene repertoire. Comparable studies have been done in other deep-sea ecosystems such as hydrothermal vent or abyssal plain from different ocean in the world (Farias et al., 2015; Zhang et al., 2015).

Consequently, future studies on the development of a respective model system will complement ecosystem-wide 'omics studies (metagenomics and metatranscriptomics) and prokaryotic taxonomic diversity studies to ultimately provide a better understanding of the role of microbes and their interactions in the abyssal plain of the CCZ ecosystems during disruptive anthropogenic processes.

Under aerobic and nutrient-rich conditions, the composition of our cultivatable samples was dominated by proteobacteria over actinobacteria and much less firmicutes. The presence of representatives of the genera *Halomonas* (35 %), *Pseudomonas*, (13 %) and *Pseudoalteromonas* (20 %) in our samples is in agreement with previously reported predominant isolate groups from other deep-sea sediment locations (da Silva et al., 2013; Kobayashi et al., 2008; Parkes et al., 2014; Xu et al., 2005). This result is not surprising, as

those genera are among the most cultivatable ones from the marine environment (Giovannoni and Rappé, 2000). Even if those genera were certainly not the major microbial players in benthic microbial communities, their detection and simple 'on-board' monitoring could help to better understand the dispersion and microbial dissemination processes that occur during deep-sea mining activities.

The vertical distribution of species revealed a marked difference between the surface water (e.g. *Marinobacter flavimaris*, *Arthrobacter subterraneus*) and the sediment microbial communities. Another interesting bacterium is *Rhodococcus erythropolis,* which was isolated from the nodule's surface. A similar relation was previously reported in prokaryotic diversity studies conducted in the Clarion Clipperton Zone (Lindh et al., 2017; Shulse et al., 2016), where there were distinct microbial populations within the sediments, nodules and ambient water. The species richness and biomass of marine sediments are primarily related to organic degradation rates (electron donor diversity) and trace metal elements like Mn, Fe and Co, which act as micronutrients (Gillan et al., 2012; Walsh et al., 2016). Unfortunately, as of yet, no geochemical record has been retrieved from the sediment cores investigated here.

Heterotrophic bacteria are dominant players in the remineralization of organic material and carbon cycling in deep-sea environments (Lochte, 1992). The availability, composition and distribution of organic substrates in the sediment are directly related to the bacterial production and diversity of hydrolytic enzymes (Boetius, 1995; Hoppe et al., 2002). The phenotypic characterization of the 16 herein isolated bacterial strains revealed a strong inter-species and moderate intra-species variability. Surprisingly, our data for the two *Pseudoalteromonas shioyasakiensis* isolates displayed numerous inconsistencies in comparison to each other and the literature data (Matsuyama et al., 2014). Either this observation may indicate that both strains evolved independently over time, which is unlikely, or that the 16S rRNA molecular marker (99.93 % similarity) was not sufficiently sensitive to differentiate two closely related species.

All isolated bacterial strains were able to express at least three hydrolytic and proteolytic enzymes (e.g., *Halomonas meridiana*), with a maximum of 10 such enzymes in *Loktanella cinnabarina*. The most commonly detected enzyme activities were leucine-arylamidase (94%), valine-arylamidase (88%), alkaline phosphatase (75%), esterase (75%), esterase-lipase (75%), α-glucosidase (69%) and acid phosphatase (63%). The revealed ratios for the occurrence of such enzymes was characteristic of a typical activity spectrum for marine sediment bacteria (Arnosti, 2014; Boetius, 1995; Li et al., 2017; Liu

et al., 2018; Turley, 2000). The vertical distribution did not indicate any specific trends in enzymes utilization. This observation could be explained by the lack of information from the uncultivated bacteria, yet might also reveal a rich diversity within the micro-environment, in which species are adapted to certain ecological niches.

The results of the API strip analysis conducted here provide only very limited information on the enzymatic activity spectra and are not reflective for their intensities under deep-sea conditions, such as low temperatures and high pressure. For instance, exposure to higher hydrostatic pressure (>100 bar) might limit microbial growth, disrupt protein homeostasis, and conformational change in ribosomes structure (Gayán et al., 2017). Reaching environmental conditions for experimental *in vitro* study is crucial but rarely feasible in the case of deep-sea conditions (e.g., the hydrostatic pressure of min 400 bar). However, our results are relevant for the establishment of an *in vitro* system and therefore enhance the general knowledge of degradation processes for organic matter in the deep sea.

The use of fast-growing organisms combined with API strip assays is an inexpensive and reliable tool, which can easily be implemented on research vessels at sea for impact assessment studies during deep-sea mining activities. Partial enrichment media, designed based on the results of this study (Supplemental Table S3) could be used to select for potential indicator organisms related to either sediment (i.e. *Dietzia maris*, *Pseudoalteromonas shioyasakiensis*), nodules (i.e. *Rhodococcus erythropolis*) or water environments (i.e. *Marinobacter flavimaris*), with the aim of monitoring the plume propagation over distance and time. Such on-board studies could be easily further combined with metal tolerance or sensitivity assessments using MIC determination, as shown in our current study.

Multi-metal tolerance of isolated bacteria was increased in the order of Mn^{2+} < Cu^{2+} < Ni^{2+} < Zn^{2+} < Co^{2+} < Cd^{2+}. All strains delineate a similar trend in their metal tolerance with the exception of the strongest tolerance level from *Kocuria polaris* (Ni^{2+}: 12.1 mM), *Dietzia maris* (Mn^{2+}: 14.3 mM), *Loktanella cinnabarina* (Mn^{2+}: 57,2 mM) and *Rhodococcus erythropolis* (Mn^{2+}: 228.9 mM). The intra-species variabilities observed for *Dietzia maris* and *Halomonas meridiana* might suggest evolution and adaptation of those strains to cope with higher metal concentrations that are related directly to their micro-environment. It is important to note that the general response to a combined effect of cold temperature and higher hydrostatic pressure on heavy metal resistance may vary between organism but also from the metal tested (Brown et al., 2017).

As the main metal constituent of polymetallic nodules (Hein and Koschinsky, 2013), Mn^{2+} was selected to reveal the potential resistance pathway using a simple genomic analysis of the most tolerant bacterial strains: *Dietzia maris*, *Loktanella cinnabarina* and *Rhodococcus erythropolis*. The results here suggest that all strains possess at least one gene copy with high sequence similarity to previously described cation diffusion facilitator (FieF), P-type ATPase, ZntA and the transcriptional regulator, MntR. Such gene copies might be indicative of additional functions or denote a redundancy, which would indicate a need of these efflux systems in the corresponding environment. Interestingly, *Rhodococcus erythropolis*, which was isolated on the nodule's surface, exhibits the highest resistance to manganese salt and additionally has a remarkable sequence redundancy of homologous Mn^{2+} efflux systems. Furthermore, higher Mn resistance did not lead to other higher metal resistances, which might imply the specificity of those efflux systems.

2.3.6 Conclusions

This study has suggested a microbial cultivation-based approach for the broadening of our knowledge of deep-sea microorganisms. In total, 13 fast-growing bacterial species were identified, from which one to three potential organisms could be selected in future studies. Intra-species variabilities were not only found in phenotypic profiles but also in heavy metal tolerance although the taxonomic marker 16s rRNA sequences were almost identical. We propose the use of API strips and partial-enrichment media that can easily be implemented on-board for a rapid and inexpensive monitoring of deep-sea mining plume dispersion using microbial dissemination analyses. In this context, a heavy-metal resistance analysis provides a new scope for future research on Mn^{2+} resistance pathways and their role in microbial dispersion from anthropogenic impacts on deep-sea environments. Our genomic analysis indicated the presence of a potential efflux system(s), which could be subject to future transcriptomics or proteomics investigations.

2.3.7 Author Contributions

BG, LT, MU contributed conception and design of the study; BG acquires, analyzed and organized the database; DC performed the statistical analysis; BG wrote the first draft

of the manuscript; All authors contributed to manuscript revision, read and approved the submitted version.

2.3.8 Acknowledgments

The Authors would like to thank the scientific staff from BGR Hannover, crew members of the Sonne 240 and particularly Annemiek Vink for providing samples. We are also grateful for the proof reading of our manuscript done by Charlotte Kleint and Song Wang.

2.3.9 Funding

We acknowledge BGR Hannover for co-financing this study. B.G. is supported by JPI Oceans2 project “EcoMining-DEU – Ecological Aspects of Deep-Sea Mining”. This publication is supported by the HGF Young Investigator Group SeaPump “Seasonal and regional food web interactions with the biological pump”: VH-NG-1000 and by the OceanLab of Jacobs University.

2.3.10 Conflict of Interest

The authors declare that the research was conducted in the absence of any commercial or financial relationships that could be construed as a potential conflict of interest.

2.3.11 Data Availability Statement

All datasets generated for this study are included in the manuscript and the supplementary files.

2.3.12 Supplementary Material

Table S1. Sampling location details

Probe Nr.	Date (UTC)	Latitude (N)	Longitude (W)	Water depth (m)	Core length (cm)
SO240-14MUC	11.05.15	13°10,528'	118°10,108'	4332	10
SO240-95MUC	05.06.15	11°49,262'	117°13,197'	4150	-

Table S2. 16S rRNA BLASTN analysis results

Sample	Laboratory Reference	GenBank accession Nr.	Isolation depth (cm)	Closest phylogenetic relative (Accession no., organism)	Homology (%)
14 MUC	SO240BG01	MK254646	Water	*NR_043546.1, Arthrobacter subterraneus* strain M1406	99
	SO240BG02	MK254647	6 -7	*NR_116685.1, Dietzia maris* strain DSM 43672	99
	SO240BG03	MK254648	8 - 9		99
	SO240BG04	MK254649	0 - 1	*NR_028741.1, Erythrobacter citreus* strain RE35F/1	99
	SO240BG05	MK254650	1 - 2		99
	SO240BG06	MK254651	2 - 3		99
	SO240BG07	MK254652	5 - 6		99
	SO240BG08	MK254653	7 - 8		99
	SO240BG09	MK254654	Water	NR_042063.1, *Halomonas aquamarina* strain DSM 30161	99
	SO240BG10	MK254655	0 - 1	NR_042066.1, *Halomonas meridiana* strain DSM 5425	99
	SO240BG11	MK254656	1 - 2		99
	SO240BG12	MK254657	2 - 3		99
	SO240BG13	MK254658	3 - 4		99
	SO240BG14	MK254659	4 - 5		99
	SO240BG15	MK254660	6 - 7		99
	SO240BG16	MK254661	7 - 8		99
	SO240BG17	MK254662	3 - 4	NR_028924.1, *Kocuria polaris* strain CMS 76or	99
	SO240BG18	MK254663	5 - 6		99
	SO240BG19	MK254664	0 - 1	NR_114307.1, *Loktanella cinnabarina* strain LL-001	99
	SO240BG20	MK254665	Water	NR_025799.1, *Marinobacter flavimaris* isolate: D1-1M	99
	SO240BG21	MK254666	1 - 2	NR_125458.1, *Pseudoalteromonas shioyasakiensis* strain SE3	99
	SO240BG22	MK254667	2 - 3		99
	SO240BG23	MK254668	3 - 4		99
	SO240BG24	MK254669	4 - 5		99
	SO240BG25	MK254670	5 - 6		99
	SO240BG26	MK254671	6 - 7		99
	SO240BG27	MK254672	8 - 9		99
	SO240BG28	MK254673	9 -10		99
	SO240BG29	MK254674	1 - 2	NR_041715.1, *Pseudomonas stutzeri* strain 13635O	99
	SO240BG30	MK254675	3 - 4		99
	SO240BG31	MK254676	7 - 8		99
95 MUC	SO240BG32	MK254677	Nodule 1 - 2	AM110948.1, *Bacillus subtilis* isolate B-3141	99
	SO240BG33	MK254678	Nodule 1 - 2	*NR_028741.1, Erythrobacter citreus* strain RE35F/1	99
	SO240BG34	MK254679	Nodule 0 - 1	NR_042063.1, Halomonas aquamarina strain DSM 30161	99
	SO240BG35	MK254680	Nodule 0 - 1	NR_027219.1, Halomonas axialensis strain Althf1	99
	SO240BG36	MK254681	Nodule 1 - 2		99
	SO240BG37	MK254682	Nodule 1 - 2	NR_042066.1, Halomonas meridiana strain DSM 5425	99
	SO240BG38	MK254683	Nodule 0 - 1	NR_041715.1, Pseudomonas stutzeri strain ATCC 17588	99
	SO240BG39	MK254684	Nodule 1 - 2		99
	SO240BG40	MK254685	Nodule 1 - 2	KU904404.1, Rhodococcus erythropolis strain JA30	99

Table S3. Combinations of phenotypical test giving a unique bacterial identification

Test	Arthrobacter subterraneus (SO240BG6)	Bacillus subtilis (SO240BG40)	Dietzia Maris (SO240BG8)	Dietzia Maris (SO240BG10)	Erythrobacter citreus (SO240BG22)
General	Motility & Pigmentation Gram & Pigmentation	Gram & Pigmentation Gram & Motility			Pigmentation
API-20NE					Malic acid
API-20NE + general	Nitrite reduction & Pigmentation D-mannose & Pigmentation Capric acid & Pigmentation Adipic acid & Pigmentation Trisodium citrate & Pigmentation				D-glucose & Motility D-mannitol & Motility D-maltose & Motility Potassium gluconate & Motility
API-ZYM		Esterase/ Alkaline phosphatase α-Glucosidase & Alkaline phosphatase Esterase lipase & Alkaline phosphatase		Valine arylamidase & N-acetyl-glucosamine Cystine arylamidase & N-acetyl-glucosamine Valine arylamidase & Lipase Cystine arylamidase & Valine arylamidase Acid phosphatase & Valine arylamidase α-Glucosidase & Valine arylamidase N-acetyl-β-glucosaminidase & Valine arylamidase	α-Glucosidase & Cystine arylamidase N-acetyl-β-glucosaminidase & Potassium gluconate
API-ZYM + general	Esterase &Pigmentation Lipase & Pigmentation α-Glucosidase & Pigmentation Adipic acid & Gram Esterase & Gram	Alkaline phosphatase & Gram α-Glucosidase & Gram	Trisodium citrate & Pigmentation Valine arylamidase & Pigmentation Cystine arylamidase & Pigmentation	Valine arylamidase & Pigmentation Cystine arylamidase & Pigmentation Valine arylamidase & Motility Valine arylamidase & Gram Cystine arylamidase & Gram	α-Glucosidase & Motility
20NE +ZYM	N-acetyl-glucosamine & D-mannose Adipic acid & D-mannose Adipic acid & D-maltose Adipic acid & Potassium gluconate Esterase & Adipic acid			Valine arylamidase & D-glucose Valine arylamidase & D-mannose Cystine arylamidase & D-mannose Valine arylamidase & D-mannitol Valine arylamidase & D-maltose Valine arylamidase & Potassium gluconate Valine arylamidase & Adipic acid Trisodium citrate & Pigmentation	Lipase & D-glucose Valine arylamidase & D-glucose Cystine arylamidase & D-glucose Acid phosphatase & D-glucose N-acetyl-β-glucosaminidase & D-glucose Cystine arylamidase & L-arabinose Lipase & D-mannitol Cystine arylamidase & D-mannitol Cystine arylamidase & D-maltose/Potassium gluconate Cystine arylamidase & Adipic acid

Table S3. Continued

Test	Halomonas aquamarina (SO240BG31)	Halomonas axialensis (SO240BG23)	Halomonas meridiana (SO240BG3)	Halomonas meridiana (SO240BG14)	Kocuria polaris (SO240BG21)	Loktanella cinnabarina (SO240BG12)
General	Pigmentation				Pigmentation	Motility & Pigmentation
API-20NE	D-mannitol & D-glucose Capric acid & Hydrolysis of Esculin D-maltose & D-mannitol Capric acid & D-mannitol Adipic acid & D-mannitol Trisodium citrate & D-mannitol					
API-20NE + general						
API-ZYM	Trypsin & Lipase					Leucine-arylamidase α-Mannosidase β-Glucuronidase β-Glucosidase & Lipase β-Galactosidase Trypsin & Cystine arylamidase α-chymotripsin & Cystine arylamidase Acid phosphatase & Cystine arylamidase β-Glucosidase & Cystine arylamidase α-chymotripsin & Trypsin β-Glucosidase & Trypsin Acid phosphatase & α-chymotripsin β-Glucosidase & α-chymotripsin β-Glucosidase & Acid phosphatase
API-ZYM + general						Cystine arylamidase & Pigmentation β-Glucosidase & Gram Cystine arylamidase & Pigmentation β-Glucosidase & Pigmentation Alkaline phosphatase & Motility Trypsin & Motility α-chymotripsin & Motility
20NE +ZYM	Trypsin & L-arabinose Trypsin & D-mannitol α-Glucosidase & D-mannitol			Alkaline phosphatase & Nitrite reduction Esterase/Esterase lipase & Nitrite reduction Acid phosphatase & Nitrite reduction		β-Glucosidase & Nitrite reduction Cystine arylamidase & Hydrolysis of Esculin Trypsin & Hydrolysis of Esculin β-Glucosidase & L-arabinose Cystine arylamidase & Capric acid α-chymotripsin & Capric acid α-chymotripsin & Adipic acid Cystine arylamidase & Trisodium citrate α-chymotripsin & Trisodium citrate β-Glucosidase & Urease β-Glucosidase & Phenylacetic acid

Table S3. Continued

Test	Marinobacter flavimaris (SO240BG9)	Pseudoalteromonas shioyasakiensis (SO240BG4)	Pseudoalteromonas shioyasakiensis (SO240BG20)	Pseudomonas stutzeri (SO240BG43)	Rhodococcus erythropolis (SO240BG28)
General				Motility & Pigmentation Gram & Pigmentation	Pigmentation
API-20NE	Malic acid & D-glucose	D-maltose & Hydrolysis of Esculin D-maltose & Hydrolysis of Gelatin D-maltose & D-glucose D-maltose & L-arabinose D-maltose & D-mannitol			Urease Phenylacetic acid L-arabinose & Nitrite reduction
API-20NE + general	D-glucose & Pigmentation D-mannitol & Pigmentation D-glucose & Motility			Nitrite reduction & Pigmentation D-mannose & Pigmentation Capric acid & Pigmentation Adipic acid & Pigmentation Trisodium citrate & Pigmentation	Nitrite reduction & Motility Lipase & Motility Nitrite reduction & Gram
API-ZYM	D-glucose & Pigmentation D-mannitol & Pigmentation D-glucose & Motility Acid phosphatase & Lipase N-acetyl-β-glucosaminidase & Lipase Cystine arylamidase & Valine arylamidase Acid phosphatase & Valine arylamidase α-Glucosidase & Valine arylamidase N-acetyl-β-glucosaminidase & Valine arylamidase N-acetyl-β-glucosaminidase & α-Glucosidase	α-chymotripsin & Leucine-arylamidase α-chymotripsin & α-Mannosidase α-chymotripsin & β-Glucuronidase α-chymotripsin & β-Galactosidase α-chymotripsin & Cystine arylamidase α-chymotripsin & Trypsin Acid phosphatase & α-chymotripsin β-Glucosidase & α-chymotripsin α-chymotripsin & Alkaline phosphatase α-chymotripsin & Esterase α-chymotripsin & Esterase lipase	α-Glucosidase & N-acetyl-glucosamine		β-Glucosidase & N-acetyl-glucosamine β-Glucosidase & Alkaline phosphatase β-Glucosidase & Esterase β-Glucosidase & Esterase lipase β-Glucosidase & Lipase β-Glucosidase & Leucine-arylamidase β-Glucosidase & α-Mannosidase β-Glucosidase & β-Glucuronidase β-Glucosidase & β-Galactosidase β-Glucosidase & Cystine arylamidase β-Glucosidase & Trypsin β-Glucosidase & α-chymotripsin β-Glucosidase & Acid phosphatase N-acetyl-β-glucosaminidase & β-Glucosidase
API-ZYM + general	Valine arylamidase & Pigmentation Valine arylamidase & Motility Valine arylamidase & Gram	α-chymotripsin & Motility		Esterase/Esterase lipase & Pigmentation Lipase & Pigmentation Acid phosphatase & Pigmentation α-Glucosidase & Pigmentation	Lipase & Motility Lipase & Gram β-Glucosidase & Gram
20NE +ZYM	Lipase & D-glucose Valine arylamidase & D-glucose Cystine arylamidase & D-glucose Acid phosphatase & D-glucose N-acetyl-β-glucosaminidase & D-glucose Valine arylamidase & L-arabinose N-acetyl-β-glucosaminidase & L-arabinose Valine arylamidase & D-mannose Valine arylamidase & D-mannitol Acid phosphatase & D-mannitol N-acetyl-β-glucosaminidase & D-mannitol Lipase & Adipic acid Valine arylamidase & Adipic acid Lipase & Trisodium citrate	α-chymotripsin & Capric acid α-chymotripsin & Adipic acid α-chymotripsin & Trisodium citrate α-chymotripsin & D-maltose	Lipase & D-mannose α-Glucosidase & D-mannose		β-Glucosidase & Nitrite reduction β-Glucosidase & Hydrolysis of Gelatin β-Glucosidase & L-arabinose

2.3.13 References

Aleynik, D., Inall, M. E., Dale, A., and Vink, A. (2017). Impact of remotely generated eddies on plume dispersion at abyssal mining sites in the Pacific. *Sci. Rep.* 7, 1–14. doi:10.1038/s41598-017-16912-2.

Alfaro-Espinoza, G., and Ullrich, M. S. (2014). Marinobacterium mangrovicola sp. nov., a marine nitrogen-fixing bacterium isolated from mangrove roots of Rhizophora mangle. *Int. J. Syst. Evol. Microbiol.* 64, 3988–3993. doi:10.1099/ijs.0.067462-0.

Arias, D., Cisternas, L. A., and Rivas, M. (2017). Biomineralization of calcium and magnesium crystals from seawater by halotolerant bacteria isolated from Atacama Salar (Chile). *Desalination* 405, 1–9. doi:10.1016/j.desal.2016.11.027.

Arnosti, C. (2014). Patterns of Microbially Driven Carbon Cycling in the Ocean: Links between Extracellular Enzymes and Microbial Communities. *Adv. Oceanogr.* 2014, 1–12. doi:10.1155/2014/706082.

Balqadi, A. A., Salama, A. J., and Satheesh, S. (2018). Microfouling development on artificial substrates deployed in the central Red Sea. *Oceanologia* 60, 219–231. doi:10.1016/j.oceano.2017.10.006.

Bentzon-tilia, M., Severin, I., Hansen, L. H., and Riemann, L. (2015). Genomics and Ecophysiology of Heterotrophic Nitrogen-Fixing Bacteria Isolated from Estuarine Surface Water. *MBio* 6, 1–11. doi:10.1128/mBio.00929-15.Editor.

Bibi, F., Alvi, S. A., Al-sofyani, A., Yasir, M., Kensarah, E. A., and Azhar, E. I. (2018). Two marine sponges-associated cultivable bacteria : Diversity and biological activities. *Genet. Mol. Res.* 17. doi:10.4238/gmr16039910.

Boetius, A. (1995). Microbial hydrolytic enzyme activities in deep-sea sediments. *Helgoländer Meeresuntersuchungen* 49, 177–187. doi:10.1007/BF02368348.

Brown, A., Thatje, S., and Hauton, C. (2017). The Effects of Temperature and Hydrostatic Pressure on Metal Toxicity: Insights into Toxicity in the Deep Sea. *Environ. Sci. Technol.* 51, 10222–10231. doi:10.1021/acs.est.7b02988.

Catania, V., Cappello, S., Di Giorgi, V., Santisi, S., Di Maria, R., Mazzola, A., et al. (2018). Microbial communities of polluted sub-surface marine sediments. *Mar. Pollut. Bull.* 131, 396–406. doi:10.1016/j.marpolbul.2018.04.015.

Chang, H.-W., Bae, J.-W., Nam, Y.-D., Kwon, H.-Y., Park, J. R., Shin, K.-S., et al. (2007). Arthrobacter subterraneus sp. nov., isolated from deep subsurface water of the South Coast of Korea. *J. Microbiol. Biotechnol.* 17, 1875–9. Available at: http://www.ncbi.nlm.nih.gov/pubmed/18092474.

Chen, H., Wu, R., Xu, G., Fang, X., Qiu, X., Guo, H., et al. (2010). DR2539 is a novel DtxR-like regulator of Mn/Fe ion homeostasis and antioxidant enzyme in Deinococcus radiodurans. *Biochem. Biophys. Res. Commun.* 396, 413–418. doi:10.1016/j.bbrc.2010.04.106.

Chen, S., and Shao, Z. (2009). Isolation and diversity analysis of arsenite-resistant bacteria in communities enriched from deep-sea sediments of the Southwest Indian Ocean Ridge. *Extremophiles* 13, 39–48. doi:10.1007/s00792-008-0195-1.

Corinaldesi, C. (2015). New perspectives in benthic deep-sea microbial ecology. *Front. Mar. Sci.* 2, 1–12. doi:10.3389/fmars.2015.00017.

Cruz-López, R., and Maske, H. (2016). The vitamin B1 and B12 required by the marine dinoflagellate Lingulodinium polyedrum can be provided by its associated bacterial community in culture. *Front. Microbiol.* 7, 1–13. doi:10.3389/fmicb.2016.00560.

da Silva, M. A. C., Cavalett, A., Spinner, A., Rosa, D. C., Jasper, R. B., Quecine, M. C., et al. (2013). Phylogenetic identification of marine bacteria isolated from deep-sea sediments of the eastern South Atlantic Ocean. *Springerplus* 2, 1–10.

doi:10.1186/2193-1801-2-127.
Danovaro, R., Snelgrove, P. V. R., and Tyler, P. (2014). Challenging the paradigms of deep-sea ecology. *Trends Ecol. Evol.* 29, 465–475. doi:10.1016/j.tree.2014.06.002.
Dos Santos Furtado, A. L., and Casper, P. (2000). Different methods for extracting bacteria from freshwater sediment and a simple method to measure bacterial production in sediment samples. *J. Microbiol. Methods* 41, 249–257. doi:10.1016/S0167-7012(00)00163-9.
Ettoumi, B., Bouhajja, E., Borin, S., Daffonchio, D., Boudabous, A., and Cherif, A. (2010). Gammaproteobacteria occurrence and microdiversity in Tyrrhenian Sea sediments as revealed by cultivation-dependent and -independent approaches. *Syst. Appl. Microbiol.* 33, 222–231. doi:10.1016/j.syapm.2010.02.005.
Ettoumi, B., Chouchane, H., Guesmi, A., Mahjoubi, M., Brusetti, L., Neifar, M., et al. (2016). Diversity, ecological distribution and biotechnological potential of Actinobacteria inhabiting seamounts and non-seamounts in the Tyrrhenian Sea. *Microbiol. Res.* 186–187, 71–80. doi:10.1016/j.micres.2016.03.006.
Farias, P., Santo, C. E., Branco, R., Francisco, R., Santos, S., Hansen, L., et al. (2015). Natural hot spots for gain of multiple resistances: Arsenic and antibiotic resistances in heterotrophic, aerobic bacteria from marine hydrothermal vent fields. *Appl. Environ. Microbiol.* 81, 2534–2543. doi:10.1128/AEM.03240-14.
Finn, R. D., Attwood, T. K., Babbitt, P. C., Bateman, A., Bork, P., Bridge, A. J., et al. (2017). InterPro in 2017-beyond protein family and domain annotations. *Nucleic Acids Res.* 45, D190–D199. doi:10.1093/nar/gkw1107.
Focardi, S., Pepi, M., Landi, G., Gasperini, S., Ruta, M., Di Biasio, P., et al. (2012). Hexavalent chromium reduction by whole cells and cell free extract of the moderate halophilic bacterial strain Halomonas sp. TA-04. *Int. Biodeterior. Biodegrad.* 66, 63–70. doi:10.1016/j.ibiod.2011.11.003.
Fritz, J.-S. (2016). Commentary: Threatened by mining, polymetallic nodules are required to preserve abyssal epifauna. *Front. Mar. Sci.* 3. doi:10.1038/srep26808.
Gao, X., Gao, W., Cui, Z., Han, B., Yang, P., Sun, C., et al. (2015). Biodiversity and degradation potential of oil-degrading bacteria isolated from deep-sea sediments of South Mid-Atlantic Ridge. *Mar. Pollut. Bull.* 97, 373–380. doi:10.1016/j.marpolbul.2015.05.065.
Gärtner, A., Blümel, M., Wiese, J., and Imhoff, J. F. (2011). Isolation and characterisation of bacteria from the Eastern Mediterranean deep sea. *Antonie van Leeuwenhoek, Int. J. Gen. Mol. Microbiol.* 100, 421–435. doi:10.1007/s10482-011-9599-5.
Gayán, E., Govers, S. K., and Aertsen, A. (2017). Impact of high hydrostatic pressure on bacterial proteostasis. *Biophys. Chem.* 231, 3–9. doi:10.1016/j.bpc.2017.03.005.
Gillan, D. C., Baeyens, W., Bechara, R., Billon, G., Denis, K., Grosjean, P., et al. (2012). Links between bacterial communities in marine sediments and trace metal geochemistry as measured by in situ DET/DGT approaches. *Mar. Pollut. Bull.* 64, 353–362. doi:10.1016/j.marpolbul.2011.11.001.
Gillard, B., Purkiani, K., Chatzievangelou, D., Vink, A., Iversen, M. H., and Thomsen, L. (2019). Physical and hydrodynamic properties of deep sea mining-generated , abyssal sediment plumes in the Clarion Clipperton Fracture Zone (eastern-central Pacific). *Elem. Sci. Anthr.* doi:https://doi.org/10.1525/elementa.343.
Giovannoni, S. J., and Rappé, M. (2000). "Evolution, diversity, and molecular ecology of marine prokaryotes," in *Microbial ecology of the Oceans*, ed. D. L. Kirchman (Wiley-Blackwell), 47–84.
Graham, I. J., Dichburn, R. G., and Zondervan, A. (2004). Beryllium isotope dating of ferromanganese nodules and crusts. *New Zeal. Sci. Rev.* 36, 57–61.
Guzmán, D., Quillaguamán, J., Muñoz, M., and Hatti-Kaul, R. (2010). Halomonas andesensis

sp. nov., a moderate halophile isolated from the saline lake Laguna Colorada in Bolivia. *Int. J. Syst. Evol. Microbiol.* 60, 749–753. doi:10.1099/ijs.0.014522-0.

Heald, S. C., Brandão, P. F. B., Hardicre, R., and Bull, A. T. (2001). Physiology, biochemistry and taxonomy of deep-sea nitrile metabolising Rhodoccus strains. *Antonie van Leeuwenhoek, Int. J. Gen. Mol. Microbiol.* 80, 169–183. doi:10.1023/A:1012227302373.

Hein, J. R., and Koschinsky, A. (2013). "Deep-Ocean Ferromanganese Crusts and Nodules," in *Treatise on Geochemistry: Second Edition* (Published by Elsevier Inc.), 273–291. doi:10.1016/B978-0-08-095975-7.01111-6.

Hirayama, H., Abe, M., Miyazaki, J., Sakai, S., Nagano, Y., and Takai, K. (2015). Data report: cultivation of microorganisms from basaltic rock and sediment cores from the North Pond on the western flank of the Mid-Atlantic Ridge, IODP Expedition 336. doi:10.2204/iodp.proc.336.204.2015.

Hondt, S. D., Jørgensen, B. B., Miller, D. J., Batzke, A., Blake, R., Cragg, B. A., et al. (2004). Distributions of Microbial Activities in Deep Subseafloor Sediments. *Science (80-.).* 306, 2216–2222.

Hoppe, H.-G., Arnosti, C., and Herndl, G. F. (2002). "Ecological significance of bacterial enzymes in marine environment," in *Microbial Enzymes in the Environment Activity, Ecology and Application*, eds. R. G. Burns and R. P. Dick (New York Basel: Marcel Dekker), 73.

Huang, X., Shin, J. H., Pinochet-Barros, A., Su, T. T., and Helmann, J. D. (2017). Bacillus subtilis MntR coordinates the transcriptional regulation of manganese uptake and efflux systems. *Mol. Microbiol.* 103, 253–268. doi:10.1111/mmi.13554.

Inagaki, F., Suzuki, M., Takai, K., Oida, H., Sakamoto, T., Aoki, K., et al. (2003). Microbial Communities Associated with Geological Horizons in Coastal Subseafloor Sediments from the Sea of Okhotsk. *Appl. Environ. Microbiol.* 69, 7224–7235. doi:10.1128/AEM.69.12.7224.

Ivanova, E. P., Vysotskii, M. V., Svetashev, V. I., Nedashkovskaya, O. I., Gorshkova, N. M., Mikhailov, V. V., et al. (1999). Characterization of Bacillus strains of marine origin. *Int. Microbiol.* 2, 267–271. doi:10943423.

Jørgensen, B. B., and Boetius, A. (2007). Feast and famine - Microbial life in the deep-sea bed. *Nat. Rev. Microbiol.* 5, 770–781. doi:10.1038/nrmicro1745.

Kai, W., Peisheng, Y., Rui, M., Wenwen, J., and Zongze, S. (2017). Diversity of culturable bacteria in deep-sea water from the South Atlantic Ocean. *Bioengineered* 8, 572–584. doi:10.1080/21655979.2017.1284711.

Kaye, J. Z., Márquez, M. C., Ventosa, A., and Baross, J. A. (2004). Halomonas neptunia sp. nov., Halomonas sulfidaeris sp. nov., Halomonas axialensis sp. nov. and Halomonas hydrothermalis sp. nov.: Halophilic bacteria isolated from deep-sea hydrothermal-vent environments. *Int. J. Syst. Evol. Microbiol.* 54, 499–511. doi:10.1099/ijs.0.02799-0.

Kim, H., Choo, Y. J., Song, J., Lee, J. S., Lee, K. C., and Cho, J. C. (2007). Marinobacterium litorale sp. nov. in the order Oceanospirillales. *Int. J. Syst. Evol. Microbiol.* 57, 1659–1662. doi:10.1099/ijs.0.64892-0.

Kim, K., Srinivasan, S., and Lee, S.-S. (2016). Loktanella aquimaris sp. nov., Isolated from Seawater. *Curr. Microbiol.* 72, 228–233. doi:10.1007/s00284-015-0945-0.

Kobayashi, T., Koide, O., Mori, K., Shimamura, S., Matsuura, T., Miura, T., et al. (2008). Phylogenetic and enzymatic diversity of deep subseafloor aerobic microorganisms in organics- and methane-rich sediments off Shimokita Peninsula. *Extremophiles* 12, 519–527. doi:10.1007/s00792-008-0157-7.

Koerner, R. J., Goodfellow, M., and Jones, A. L. (2009). The genus Dietzia: A new home for

some known and emerging opportunist pathogens. *FEMS Immunol. Med. Microbiol.* 55, 296–305. doi:10.1111/j.1574-695X.2008.00513.x.

Koschinsky, A., Winkler, A., and Fritsche, U. (2003). Importance of different types of marine particles for the scavenging of heavy metals in the deep-sea bottom water. *Appl. Geochemistry* 18, 693–710. doi:10.1016/S0883-2927(02)00161-0.

Labonté, J. M., Lever, M. A., Edwards, K. J., and Orcutt, B. N. (2017). Influence of igneous basement on deep sediment microbial diversity on the eastern Juan de Fuca Ridge flank. *Front. Microbiol.* 8, 1–18. doi:10.3389/fmicb.2017.01434.

Langdahl, B. R., Bisp, P., and Ingvorsen, K. (1996). Nitrile hydrolysis by Rhodococcus erythropolis BLI, an acetonitrile-tolerant strain isolated from a marine sediment. *Microbiology* 142, 145–154.

Lemire, J. A., Harrison, J. J., and Turner, R. J. (2013). Antimicrobial activity of metals: Mechanisms, molecular targets and applications. *Nat. Rev. Microbiol.* 11, 371–384. doi:10.1038/nrmicro3028.

Li, C., Tao, J., Mao, D., and He, C. (2011). A novel manganese efflux system, YebN, is required for virulence by xanthomonas oryzae pv. oryzae. *PLoS One* 6. doi:10.1371/journal.pone.0021983.

Li, L., Ding, F., Sang, L., Liu, J., Mao, D., Liu, X., et al. (2018). Study on the oxygen reduction reaction catalyzed by a cold-tolerant marine strain phylogenetically related to Erythrobacter citreus. *Bioelectrochemistry* 119, 51–58. doi:10.1016/j.bioelechem.2017.08.011.

Li, Y., Wu, C., Zhou, M., Wang, E. T., Zhang, Z., Liu, W., et al. (2017). Diversity of cultivable protease-producing bacteria in Laizhou Bay sediments, Bohai Sea, China. *Front. Microbiol.* 8, 1–10. doi:10.3389/fmicb.2017.00405.

Lindh, M. V., Maillot, B. M., Shulse, C. N., Gooday, A. J., Amon, D. J., Smith, C. R., et al. (2017). From the surface to the deep-sea: Bacterial distributions across polymetallic nodule fields in the clarion-clipperton zone of the Pacific Ocean. *Front. Microbiol.* 8, 1–12. doi:10.3389/fmicb.2017.01696.

Liu, Q., Fang, J., Li, J., Zhang, L., Xie, B. Bin, Chen, X. L., et al. (2018). Depth-resolved variations of cultivable bacteria and their extracellular enzymes in the water column of the new britain trench. *Front. Microbiol.* 9, 1–10. doi:10.3389/fmicb.2018.00135.

Lochte, K. (1992). "Bacterial Standing Stock and Consumption of Organic Carbon in The Benthic Boundary Layer of The Abyssal North Atlantic," in *Deep-Sea Food Chains and the Global Carbon Cycle*, eds. G. T. Rowe and V. Pariente (Dordrecht: Springer Netherlands), 1–10. doi:10.1007/978-94-011-2452-2_1.

Ma, R., Wang, J., Wang, Q., Ma, Z., Li, J., and Chen, L. (2017). Draft Genome Sequence of Loktanella cinnabarina Strain XM1 Isolated from Coastal Surface Water. *Am. Soc. Microbiol.* 5, 4–6. doi:https://doi.org/10.1128/genomeA.00504-17.

MacDonell, M. T., Singleton, F. L., and Hood, M. A. (1982). Diluent composition for use of API 20E in characterizing marine and estuarine bacteria. *Appl. Environ. Microbiol.* 44, 423–427.

Maruyama, A., Honda, D., Yamamoto, H., Kitamura, K., and Higashihara, T. (2000). Phylogenetic analysis of psychrophilic bacteria isolated from the Japan Trench, including a description of the deep-sea species Psychrobacter pacificensis sp. nov. *Int. J. Syst. Evol. Microbiol.* 50, 835–846. doi:10.1099/00207713-50-2-835.

Matsuyama, H., Sawazaki, K., Minami, H., Kasahara, H., Horikawa, K., and Yumoto, I. (2014). Pseudoalteromonas shioyasakiensis sp. nov., a marine polysaccharide-producing bacterium. *Int. J. Syst. Evol. Microbiol.* 64, 101–106. doi:10.1099/ijs.0.055558-0.

Melnikova, D. I., Beleneva, I. A., Tyunin, A. P., and Magarlamov, T. Y. (2017). The taxonomic composition, characteristics, and neurotoxic activities of ribbon worm-associated

bacteria from the Sea of Japan. *Russ. J. Mar. Biol.* 43, 383–391. doi:10.1134/S1063074017050066.

Mewes, K., Mogollón, J. M., Picard, A., Rühlemann, C., Kuhn, T., Nöthen, K., et al. (2014). Impact of depositional and biogeochemical processes on small scale variations in nodule abundance in the Clarion-Clipperton Fracture Zone. *Deep. Res. Part I Oceanogr. Res. Pap.* 91, 125–141. doi:10.1016/j.dsr.2014.06.001.

Miranda, C. A. C., Martins, O. B., and Clementino, M. M. (2008). Species-level identification of Bacillus strains isolates from marine sediments by conventional biochemical, 16S rRNA gene sequencing and inter-tRNA gene sequence lengths analysis. *Antonie van Leeuwenhoek, Int. J. Gen. Mol. Microbiol.* 93, 297–304. doi:10.1007/s10482-007-9204-0.

Mobberley, J. M., Authement, R. N., Segall, A. M., and Paul, J. H. (2008). The Temperate Marine Phage HAP-1 of Halomonas aquamarina Possesses a Linear Plasmid-Like Prophage Genome. *J. Virol.* 82, 6618–6630. doi:10.1128/JVI.00140-08.

Nisha, N. S., and Divakaran, J. (2014). Optimization of alkaline protease production from Bacillus subtilis NS isolated from sea water. *African J. Biotechnol.* 13, 1707–1713. doi:10.5897/AJB2014.13652.

Oebius, H. U., Becker, H. J., Rolinski, S., and Jankowski, J. A. (2001). Parametrization and evaluation of marine environmental impacts produced by deep-sea manganese nodule mining. *Deep. Res. Part II Top. Stud. Oceanogr.* 48, 3453–3467. doi:10.1016/S0967-0645(01)00052-2.

Padilla-Benavides, T., Long, J. E., Raimunda, D., Sassetti, C. M., and Argüello, J. M. (2013). A novel P1B-type Mn2+-transporting ATPase is required for secreted protein metallation in mycobacteria. *J. Biol. Chem.* 288, 11334–11347. doi:10.1074/jbc.M112.448175.

Parkes, R. J., Cragg, B., Roussel, E., Webster, G., Weightman, A., and Sass, H. (2014). A review of prokaryotic populations and processes in sub-seafloor sediments, including biosphere: Geosphere interactions. *Mar. Geol.* 352, 409–425. doi:10.1016/j.margeo.2014.02.009.

Pathom-aree, W., Stach, J. E. M., Ward, A. C., Horikoshi, K., Bull, A. T., and Goodfellow, M. (2006). Diversity of actinomycetes isolated from Challenger Deep sediment (10,898 m) from the Mariana Trench. *Extremophiles* 10, 181–189. doi:10.1007/s00792-005-0482-z.

Patzer, S. I., and Hantke, K. (2001). Dual Repression by Fe 2+ -Fur and Mn 2+ -MntR of the mntH Gene , Encoding an NRAMP-Like Mn 2+ Transporter in Escherichia coli. *J. Bacteriol.* 183, 4806–4813. doi:10.1128/JB.183.16.4806.

Pearson, W. R. (2014). An Introduction to Sequence and Series. *Int. J. Res.* 1, 1286–1292. doi:10.1002/0471250953.bi0301s42.An.

Que, Q., and Helmann, J. D. (2000). Manganese homestasis in Bacillus subtilis is regulated by MntR, a bifunctional regulator related to the diphtheria toxin repressor family of proteins. *Mol. Microbiol.* 35, 1454–1468. doi:10.1046/j.1365-2958.2000.01811.x.

Ramirez-Llodra, E., Tyler, P. A., Baker, M. C., Bergstad, O. A., Clark, M. R., Escobar, E., et al. (2011). Man and the last great wilderness: Human impact on the deep sea. *PLoS One* 6. doi:10.1371/journal.pone.0022588.

Reddy, G. S. N., Prakash, J. S. S., Prabahar, V., Matsumoto, G. I., Stackebrandt, E., and Shivaji, S. (2003). Kocuria polaris sp. nov., an orange-pigmented psychrophilic bacterium isolated from an Antarctic cyanobacterial mat sample. *Int. J. Syst. Evol. Microbiol.* 53, 183–187. doi:10.1099/ijs.0.02336-0.

Ritchie, K. B. (2006). Regulation of microbial populations by coral surface mucus and mucus-associated bacteria. *Mar. Ecol. Prog. Ser.* 322, 1–14.

doi:10.3354/meps322001.
Rosch, J. W., Gao, G., Ridout, G., Wang, Y. D., and Tuomanen, E. I. (2009). Role of the manganese efflux system mntE for signalling and pathogenesis in Streptococcus pneumoniae. *Mol. Microbiol.* 72, 12–25. doi:10.1111/j.1365-2958.2009.06638.x.
Shulse, C. N., Maillot, B., Smith, C. R., and Church, M. J. (2016). Polymetallic nodules, sediments, and deep waters in the equatorial North Pacific exhibit highly diverse and distinct bacterial, archaeal, and microeukaryotic communities. *Microbiologyopen* 6, 1–16. doi:10.1002/mbo3.428.
Smith, C. R., De Leo, F. C., Bernardino, A. F., Sweetman, A. K., and Arbizu, P. M. (2008). Abyssal food limitation, ecosystem structure and climate change. *Trends Ecol. Evol.* 23, 518–528. doi:10.1016/j.tree.2008.05.002.
Sonnenschein, E. C., Gärdes, A., Seebah, S., Torres-Monroy, I., Grossart, H. P., and Ullrich, M. S. (2011). Development of a genetic system for Marinobacter adhaerens HP15 involved in marine aggregate formation by interacting with diatom cells. *J. Microbiol. Methods* 87, 176–183. doi:10.1016/j.mimet.2011.08.008.
Stahl, A., Pletzer, D., Mehmood, A., and Ullrich, M. S. (2015). Marinobacter adhaerens HP15 harbors two CzcCBA efflux pumps involved in zinc detoxification. *Antonie van Leeuwenhoek, Int. J. Gen. Mol. Microbiol.* 108, 649–658. doi:10.1007/s10482-015-0520-5.
Sudek, L. A., Templeton, A. S., Tebo, B. M., and Staudigel, H. (2009). Microbial Ecology of Fe (hydr)oxide Mats and Basaltic Rock from Vailulu'u Seamount, American Samoa. *Geomicrobiol. J.* 26, 581–596. doi:10.1080/01490450903263400.
Sun, H., Xu, G., Zhan, H., Chen, H., Sun, Z., Tian, B., et al. (2010). Identification and evaluation of the role of the manganese efflux protein in Deinococcus radiodurans. *BMC Microbiol.* 10, 319. doi:10.1186/1471-2180-10-319.
Takami, H., Kobata, K., Nagahama, T., Kobayashi, H., Inoue, A., and Horikoshi, K. (1999). Biodiversity in deep-sea sites located near the south part of Japan. *Extremophiles* 3, 97–102. doi:10.1007/s007920050104.
Tang, J., Zheng, A. P., Bromfield, E. S. P., Zhu, J., Li, S. C., Wang, S. Q., et al. (2011). 16S rRNA gene sequence analysis of halophilic and halotolerant bacteria isolated from a hypersaline pond in Sichuan, China. *Ann. Microbiol.* 61, 375–381. doi:10.1007/s13213-010-0137-x.
Teske, a, Brinkhoff, T., Muyzer, G., Moser, D. P., Rethmeier, J., and Jannasch, H. W. (2000). Diversity of Thiosulfate-Oxidizing Bacteria from Marine Sediments and Hydrothermal Vents. *Appl. Environ. Microbiol.* 66, 3125–3133. doi:10.1128/AEM.66.8.3125-3133.2000.Updated.
Tsubouchi, T., Shimane, Y., Mori, K., Miyazaki, M., Tame, A., Uematsu, K., et al. (2013). Loktanella cinnabarina sp. nov., isolated from a deep subseafloor sediment, and emended description of the genus Loktanella. *Int. J. Syst. Evol. Microbiol.* 63, 1390–1395. doi:10.1099/ijs.0.043174-0.
Turley, C. (2000). Bacteria in the cold deep-sea benthic boundary layer and sediment-water interface of the NE Atlantic. *FEMS Microbiol. Ecol.* 33, 89–99. doi:10.1111/j.1574-6941.2000.tb00731.x.
Undabarrena, A., Beltrametti, F., Claverias, F. P., Gonzalez, M., Moore, E. R. B., Seeger, M., et al. (2016). Exploring the diversity and antimicrobial potential of marine actinobacteria from the comau fjord in Northern Patagonia, Chile. *Front. Microbiol.* 7, 1–16. doi:10.3389/fmicb.2016.01135.
Vraspir, J. M., Holt, P. D., and Butler, A. (2011). Identification of new members within suites of amphiphilic marine siderophores. *BioMetals* 24, 85–92. doi:10.1007/s10534-010-9378-1.

Walsh, E. A., Kirkpatrick, J. B., Pockalny, R., Sauvage, J., Spivack, A. J., Murray, R. W., et al. (2016). Relationship of bacterial richness to organic degradation rate and sediment age in subseafloor sediment. *Appl. Environ. Microbiol.* 82, 4994–4999. doi:10.1128/AEM.00809-16.

Wang, F., Wang, P., Chen, M., and Xiao, X. (2004). Isolation of extremophiles with the detection and retrieval of Shewanella strains in deep-sea sediments from the west Pacific. *Extremophiles* 8, 165–168. doi:10.1007/s00792-003-0365-0.

Wang, W., Cai, B., and Shao, Z. (2014). Oil degradation and biosurfactant production by the deep sea bacterium Dietzia maris As-13-3. *Front. Microbiol.* 5, 1–11. doi:10.3389/fmicb.2014.00711.

Wang, X., Lin, D., Jing, X., Zhu, S., Yang, J., and Chen, J. (2018). Complete genome sequence of the highly Mn(II) tolerant Staphylococcus sp. AntiMn-1 isolated from deep-sea sediment in the Clarion-Clipperton Zone. *J. Biotechnol.* 266, 34–38. doi:10.1016/j.jbiotec.2017.12.004.

Waters, L. S., Sandoval, M., and Storz, G. (2011). The Escherichia coli MntR miniregulon includes genes encoding a small protein and an efflux pump required for manganese homeostasis. *J. Bacteriol.* 193, 5887–5897. doi:10.1128/JB.05872-11.

Wu, C. H., Apweiler, R., Bairoch, A., Natale, D. A., Barker, W. C., Boeckmann, B., et al. (2006). The Universal Protein Resource (UniProt): an expanding universe of protein information. *Nucleic Acids Res.* 34, D187–D191. doi:10.1093/nar/gkj161.

Wu, Y. H., Liao, L., Wang, C. S., Ma, W. L., Meng, F. X., Wu, M., et al. (2013). A comparison of microbial communities in deep-sea polymetallic nodules and the surrounding sediments in the Pacific Ocean. *Deep. Res. Part I Oceanogr. Res. Pap.* 79, 40–49. doi:10.1016/j.dsr.2013.05.004.

Xu, M., Wang, P., Wang, F., and Xiao, X. (2005). Microbial diversity at a deep-sea station of the Pacific nodule province. *Biodivers. Conserv.* 14, 3363–3380. doi:10.1007/s10531-004-0544-z.

Yoon, J. H., Yeo, S. H., kim, I. G., and Oh, T. K. (2004). Marinobacter flavimaris sp. nov. and Marinobacter daepoensis sp. nov., slightly halophilic organisms isolated from sea water of the Yellow Sea in Korea. *Int. J. Syst. Evol. Microbiol.* 54, 1799–1803. doi:10.1099/ijs.0.63151-0.

Yuan, J., Lai, Q., Sun, F., Zheng, T., and Shao, Z. (2015). The diversity of PAH-degrading bacteria in a deep-sea water column above the southwest Indian ridge. *Front. Microbiol.* 6, 1–12. doi:10.3389/fmicb.2015.00853.

Zhang, D. C., Liu, Y. X., and Li, X. Z. (2015). Characterization of bacterial diversity associated with deep sea ferromanganese nodules from the South China Sea. *J. Microbiol.* 53, 598–605. doi:10.1007/s12275-015-5217-y.

Zheng, R., Wu, S., Ma, N., and Sun, C. (2018). Genetic and physiological adaptations of marine bacterium Pseudomonas stutzeri 273 to mercury stress. *Front. Microbiol.* 9, 1–14. doi:10.3389/fmicb.2018.00682.

3 GENERAL DISCUSSION

The overall aim of this cumulative thesis project was to investigate the impact of deep-sea mining activities on the benthic-pelagic coupling environment (**Manuscript I, II, III**). Due to the remote location, the extreme environment of the deep-sea, and the fact that deep-sea mining has not been initiated yet, only sparse data are available. It is still today, extremely challenging to assess the magnitude of such an ecological impact accurately.

The CCZ has the highest nodule concentration observed so far. However, if or when mining for those nodules will take place the mining activity will affect the environment, e.g. via sediment plumes released into the water column and dredging of the seafloor. This will have large implications for the pelagic communities and the distribution and export of organic matter in the water column. To improve full water-depth modelling, we assessed the regional oceanographic settings of the eastern German licensed area (**Manuscript I**). Our findings denoted the particular significance of the area, which was identified as a productive transitional zone with the formation of a chlorophyll front during the winter season. In the marine ecosystem, frontal systems always played a major role by sustaining primary producers and a wide range of pelagic organisms (Ayers and Lozier, 2010; Constable et al., 2014; Polovina et al., 2001). Due to the high productivity of the German lincence area compared to other regions in the CCZ, it is important to keep in mind the mining activity in this area will have a large impact on the food web. This finding should, therefore, be considered for future mining regulation by recommending a specific mining frame period.

Despite a relatively constant primary productivity in the surface ocean throughout all seasons, as observed via satellite imagery (**Manuscript I**), we still know very little about the phytoplankton community composition in the German licensed area. Taxonomic phytoplankton and zooplankton identifications in the CCZ have only been addressed during the '70s and '80s (Fryxell et al., 1979; Venrick, 1988) and need to be revised to have a baseline before the mining activities are initiated. This is especially important since rising of ocean temperature (Vinnikov and Gordy, 2003) and ocean acidification (Caldeira and Wickett, 2003) seem to have had a global impact on phytoplankton composition and the whole ecosystem structure and functioning (Winder and Sommer, 2012). As an example, the ocean acidification is predicted to lower the amount of carbonate ion

available for calcifying organisms. In the CCZ, calcifying organisms were previously found to represent up to 50% of the planktonic community (e.g., Cocolithophorids, Fryxell, Taguchi and El-Sayed, 1979), suggesting that the importance of calcifying organism in the CCZ may have changed during the past three to four decades since the last assessment. Calcifying organisms may ballast marine snow aggregates, hence, if they are reduced in abundance it is expected that marine aggregates (Iversen and Ploug, 2010) will have lower settling velocities and, as a result, lower carbon export to the deep-sea (Orr et al., 2005).

Global ocean changes affect not only the surface ocean but also the OMZ, which is a key feature of the Pacific Ocean (Fernández-Álamo and Färber-Lorda, 2006). It has shown to play an essential role in the transportation and the alteration of particulate matters (**Manuscript I**). Expansion of the OMZ and declining oxygen concentration (Pierce et al., 2012) will cause behavioural changes of planktonic organisms by diminishing their grazing and carbon remineralization rates (Cavan et al., 2017).

We found that the combination of small aggregate size, strong bottom currents, and slow seafloor consolidation might explain the extremely low sedimentation rate reported in the CCZ. These conditions has allowed polymetallic nodules to form as a result of the low sedimentation rate (< 10 mm/Kyr; Gollner *et al.*, 2017). Interestingly, the highest nodule concentrations seem to be in the CCZ areas which has much higher POC flux to the seafloor than e.g. the North Pacific gyre system, which is a system with only few nodules (Lutz et al., 2007) (See Introduction Fig. 7). The possible reason for this disparity could be due to increased POC flux to the seafloor enhancing rapid bacterial turnover and remineralization (Kanzog et al., 2009), which in turn seem to trigger diagenetic growth of the nodules (up to 250 mm/myr; Von Stackelberg, 2000).

Currently, scientific efforts have focused on environmental impacts from mining collectors on the seabed, we therefore need to characterize the consequences of sediment plume releases (deliberately or accidentally) for both the benthic and pelagic environments. An investigation of the effects of plume release (**Manuscript II**) on the settling of organic matter (**Manuscript I**) from the euphotic zone should be made and included as a requirement for an environmental impact assessment study of deep-sea mining activities. During the SONNE cruise 262 (May-June 2018), an onboard experiment was carried out using marine snow particles that were exposed to variable sediment plume concentrations (**Manuscript in preparation I**). The aim was to analyze the aggregation and transformation processes occurring during the scavenging of sediment

plume by the settling aggregates (Figure 8, size, settling velocity, degradation rate, oxygen diffusion boundary layer, bacterial count, and CN analysis).

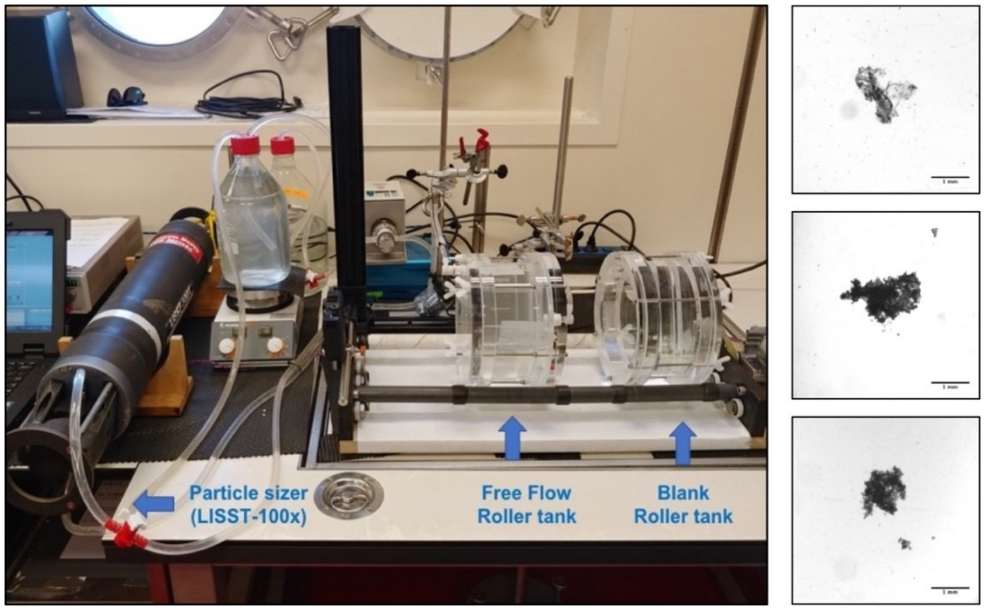

Figure 8. (**Left**) Onboard laboratory setup used for investigating the sediment plume effect on marine snow aggregates. (**Right**)Marine snow aggregates produced under a variable sediment plume concentration. From top to bottom: 0 - 17,5 and *35 mg/L*.

We found that the sticky nature of the marine snow caused high scavenging of deep-sea sediment particles (D_{50} = 20 μm; Fig. 8 right) when they were introduced to ambient water. The porous structure of the aggregates might become clogged over time and could result in the development of suboxic to anoxic conditions inside the aggregates, especially in the OMZ (Ploug and Bergkvist, 2015). Bacterial community shifts due to environmental changes might also affect the degradation rate of organic matter. Overall, increased aggregate density by scavenging lithogenic particles will increase the aggregate settling velocities and, thus, may increase carbon flux to the seafloor. Our preliminary results and observations seem in a good agreement with the ballasting effect observed from mineral clay when scavenged by phytoplankton aggregates (Iversen and Robert, 2015).

Apart from the direct impact on the seafloor from mining collectors (Paul et al., 2018; Stratmann et al., 2018; Vanreusel et al., 2016) the most critical parameter to assess is the sediment plume released back into the marine environment after the nodules have been removed. Extensive efforts are currently being undertaken by the industry to start mining activities very soon. Limiting the related plume dispersal as much as possible will become a pivotal factor to prevent a widespread and ecological impact on the

environment. The purpose of **Manuscript II** was to characterize the abyssal sediments of the CCZ and to study the formation of sediment plume under variable current regimes.

Since a mining trial has not yet been carried out, we do not know the impact from different discharge rates of the plume sediment. As an example, discharge from drill cutting operation in Norwegian water was fixed at maximum 175 mg L^{-1} (Pabortsava et al., 2011). Those plume concentrations have been used as a reference in our study case (**Manuscript II**) which also included a higher concentration up to 500 mg L^{-1}. Our findings suggested that the use of a higher sediment discharge (500 mg L^{-1}) under turbulent shear rates ≥ 2.4 s^{-1} which can be expected in the wake of the mining collector, allowed the most rapid sediment flocculation and rapid sedimentation. Those results were quite surprising in terms of aggregation efficiency (≈10 min; Manuscript II Fig.3) in comparison to lower discharge concentration used by drilling regulation (Pabortsava et al., 2011) which resulted in the same time in plume of small sediment particles that would travel much further before they sedimented.

To date, the impact assessment of deep-sea mining plume behaviour relies mostly on modelling techniques that have to be balanced between spatial resolution and computational requirements (Jankowski and Zielke, 1997). Due to the complexity of model developments, the cohesive properties, aggregation potential, and different settling processes of the deep-sea sediments are still not fully considered (Aleynik et al., 2017; Jankowski et al., 1996). Our results suggested a clear difference (one order of magnitude) between size-specific settling velocities of plume aggregates and typical model-based calculations using either Stokes or the recalculated settling velocity of Ferguson & Church (Ferguson and Church, 2004). Not taking those data into account generate a strong bias that will either over estimate (without aggregation processes) or underestimate (higher particle size or increased settling velocity) the spread of the mining plume. Our modeling results (four days simulation), based on optimized aggregation process, indicated that mining under "normal" flow conditions (3-4 cm s^{-1}) resulted in a relatively fast deposition of particles from the plume (up to 4 km downstream), thus restricting the blanketing effect to a relatively small fall-out area. As model reliability depends on the quality of the input parameters, we performed direct measurements of a wide range of the input parameters for the model (**Manuscript II).** This data set is freely available to everyone and will hopefully be of help for future model and regulation studies.

Transparency for operational parameters from mining companies are rare, but estimation of the correct plume discharge concentration is a primary factor to allow an accurate estimation of the plume spread. Release of the Environmental impact statement by GSR (DEME, 2018) indicated an expected outflow from the collector ranging from 34–170 g L^{-1}, which were much higher than previously predicted. Even if those concentrations will dilute relatively fast, a completely different type of plume behaviours will have to be considered for the near-field plume discharge scenario.

When the concentration of particles inside a sediment suspension become high enough (few g L^{-1}) settling particles start to hinder each other and collide in a process call "hinderer settling" (Fig. 9; Scott, 1984; Winterwerp, 2002; Dankers and Winterwerp, 2007). This reduce aggregate settling velocities and increases their residence time in the water column. A longer residence time of the sediment plume in the water column means that the predicted impacted area from the plume might increase. When the concentration of suspended sediment further increases, they will reach a point where particles are in constant contact with other particle known as the "gelling point". The gelling point is dependent on the particles that compose the suspension (e.g. particle size and stickiness). Realistically, this flocculation phase won't occur during mining as the separation of the nodules from the sediment will require some dilution to be efficient.

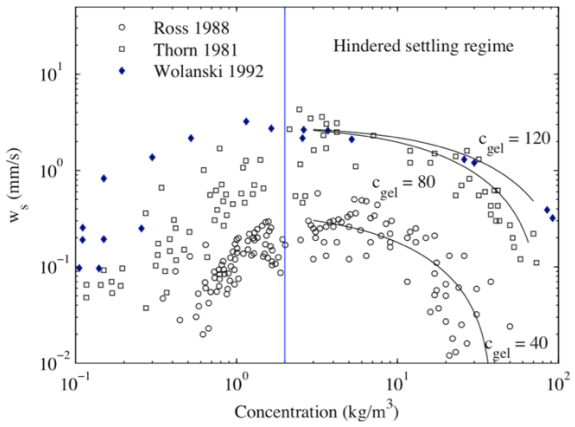

Figure 9. Hindered settling regime (Winterwerp, 1999)

Below the gelling point concentration, those high-density sediment suspensions will lead to the formation of a "mudflow", similar to those found in submarine canyons and deep-sea environment (Stevenson et al., 2014; Xu et al., 2013). Similar conditions can be achieved from a constant supply of sediment from the mining collector. This would cause the sediment to move as a gravity current toward the lowest topographical point. Though

it seems counter intuitive, high release of sediment might provide to be a better solution to confine the sediment plume within a small impact area. Based on a high-resolution bathymetry and currents regime surveys, it might be possible to predict the plume's dispersion and reduce the monitoring effort at the same time.

Once the sediment plume has settled, the buried nodules and benthic fauna associated with them is a key issue and is predicted to impact the ecosystem functioning (Gollner et al., 2017). Presently, no data are available concerning the resilience of deep-sea fauna in nodule fields to variable burial rate. Predicted to be less adapted than their counterparts of the continental margin (Larsson et al., 2013), they do provide excellent starting references. Studies of underwater mining disposal (Hughes et al., 2015; Lohrer et al., 2004; Smith and Rule, 2001; Trannum et al., 2010) indicated that immediate burial of 1 mm to threshold limit of 3 mm did not affect species richness or abundance. Until accurate measurements, using a precautionary approach, area predicted to reach up to 1mm of blanketing should be consider as primarily impacted area during mining regulation.

Presently, no study has allowed a proper estimation of the hydrodynamic behaviour and blanketing effect on nodule fields at the bottom boundary layer under normal conditions or after settling of the sediment plumes on nodules. For instance, the evaluation of the bottom roughness is often inaccurate and nodule flow fields are neglected during modelization (Fig. 10; **manuscript in preparation II**).

Figure 10. Nodule flow fields investigation experimental setup.

The presence of polymetallic nodules on the seafloor has been an essential factor for epifaunal development. Increased nodule concentrations have been linked to an increased amount of sponges, corals, as well as associated biodiversity (Amon et al., 2016). Except for their importance as providing hard substrate, we suggest that hydrodynamic flow generated around nodules might result in resuspension and turbulent flow that will sustain higher food supply for filter feeders. After a blanketing event (Figure 9), depending on the plume's concentration, nodules field topography will become smoother resulting in an increased current velocity for resuspension event to occur.

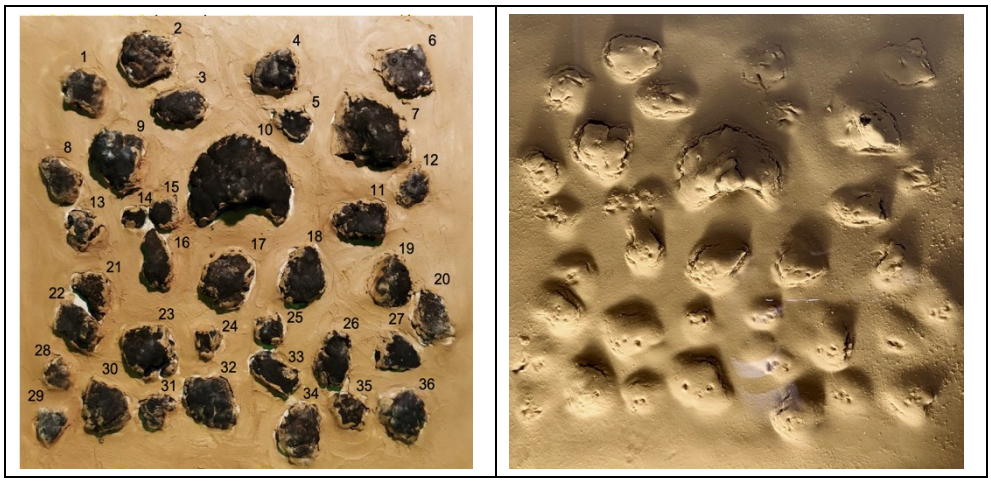

Figure 9. Top view of test section in the flume (0.5 m^2) showing left: artificial sediment floor before plume release, Right: after ≈ 12 hours of sedimentation of 0.5 g L^{-1} from a 1 m water column under zero flow.

The role of microbes during deep-sea mining has not been studied so far. Bacterial assemblage and distribution differ throughout the water column and appear even more distant from the seafloor community, but do share common species, likely arriving at seafloor with sedimentation of phytodetritus. Sinking marine aggregates are considered nutrient hotspot in the ocean (Azam and Long, 2001) where the bacterial concentrations can be one to four orders of magnitude higher when associated with aggregates in comparison to the ambient water column. Their colonization mainly occur in the surface ocean during aggregates formation, which correlate with the maximum chlorophyll depth bacterial community (Thiele et al., 2015).

In **Manuscript III**, 40 bacterial strain belonging to 13 species have been isolated from the deep-sea sediment in the CCZ and characterized. Three potential species (Dietzia maris, Rhodococcus erythropolis, Marinobacter flavimaris) belonging to different ecological niches (sediment, nodule, and water column) have been proposed for a future environmental monitor of mining or metal resistance studies. The release of sediment

plumes (**Manuscript II**) into the water column (**Manuscript I**) will inject a tremendous amount of sediment-associated bacteria (**Manuscript III**) and might alter the ecosystem functioning to an unknown extent depending on the considered depth of exhaust of sediment plumes from mining activities.

Even if *in vitro* cultivation of microbes only reveals a very small fraction (less than 0.1%) of the total bacterial diversity (Hondt et al., 2004), fast-growing conditions (18°C) has allowed the isolation of deep-sea bacteria (**Manuscript III**). Those strains were not affected either by the pressure change or the increased temperature and might be well suited for proliferation in the surface water. A competition assay should, therefore, be considered to investigate the fitness of interacting bacteria associated with the water column and the deep-sea sediment (Patin et al., 2016; Yawata et al., 2014).

In the unlikely event of a mining plume release in the surface water, where normal ocean aggregates are formed, supplement of lithogenic matter and associated-bacteria will alter the aggregate primary composition, reduce aggregate sizes and increase their size-specific settling speed (Hamm, 2002). On the other hand, marine aggregate sinking through a cloud of sediment particles in the water column (**Manuscript in preparation I**) appear to have little to no scavenging of the sediment particles (Iversen and Robert, 2015, van der Jagt et al., 2018). This suggest that we still need more investigation to understand the interactions between settling aggregates and sediment plumes release due to mining activities.

Of another concern, is the release of dissolved heavy metal such as Mn, Co, Fe and Cu from the sediment plume during mining operations. Under oxic conditions, those metals are bonded in the solid phase of the sediment and are unlikely to be released into the surrounding water (Koschinsky, 2001). Under anoxic conditions, such as found inside the OMZ or large marine snow with low porosities, e.g. ballasted by sediment particles, those metals (dissolved or particulate) could potentially become toxic for the environment (Hauton et al., 2017). The specific characteristic of OMZ in the CCZ has been shown to play a significant role in the particulate matter alteration and act as a border separating the surface water from the deep ocean (**Manuscript I**). The release and settling of sediment plumes inside the OMZ will have drastic consequence for the environment by reshaping the OMZ ecosystem (e.g., diel migration, bacterial composition) with the formation of toxic metal layers. Under those conditions, heavy-metal resistant deep-sea bacteria (**Manuscript III**) could use these advantages and repopulate this empty ecological niche.

In the context of heavy-metal resistance, our analysis provided new scope for future research on Mn^{2+} resistance pathways. Our genomic analysis indicated the presence of a potential efflux system(s), which could be subject to future transcriptomic or proteomic investigations. Gene expression and regulation should be addressed in the future and will provide a significant improvement in our understanding of how those organisms can cope with such an elevated manganese concentration.

The use of molecular method to assess the microbial communities could help in monitoring the extent of the plume dispersion. Often classic oceanographic tools such as hydroacoustics maybe not be able to detect low concentrations of sediment plume. We, therefore, propose the use of API strips to monitor the spreading of heavy metal resistant bacteria. API strips can easily be implemented to on-board studies for rapid and inexpensive monitoring using microbial dissemination analyses. Since the last decades, API strips have been used in routine studies in many hospital laboratories as a fast and reliable methodology for identification of potential pathogens. Some studies use them for proxy studies in the for marine environment (MacDonell et al., 1982).

4 OUTLOOK

During the PhD project I identified several research areas which would improve the impact assessments from deep-sea mining activity. I will here present the most urgent research we need to carry out before we can make regulations for deep-sea mining.

Optimization of the sediment plume aggregation during mining activity has proven to be an efficient way of reducing the mining-impacted area (**Manuscript II**). As discussed previously, the investigation of hindered settling plumes (≈ 2 g L^{-1}) and mudflow (≈ 10-100 g L^{-1}) hydrodynamic behavior under varying flow regime will drastically improve the near field modeling of mining activity. Such investigation will require the use of measuring tools adapted for extremely high sediment plume concentration (e.g., high-resolution conductivity probe, close-up camera system in combination with laser sheet).

The design of the collector exhaust muffler could also be improved (e.g., orientation, flexible 3D structure for variable shear rate) to allow an optimum shear rate resulting in an ideal sediment flocculation. Soon, the trial of DEME mining collector will be repeated and might provide an excellent opportunity for scientists to further test new developed equipment and monitoring strategies. After a successful mining trial, evaluation of environmental monitoring technologies, as well as a management program concept, will pave the way for precise regulation of future activity from deep-sea mining.

It is essential to include long-term flux studies in the CCZ in order to obtain a better understanding of the impacts from mining activity on the biological carbon pump and degradation rates of organic matter settling over the entire water column in the area of the nodule field. Furthermore, the use of camera system profiling (**Manuscript I**) and short term deployment of sediment traps in the upper water column and near the seafloor will allow detailed reconstruction of the particulate matter transport and help identifying export and attenuation processes (Iversen et al., 2010; Karakaş et al., 2009).

The impact of sediment plume release into the OMZ and ecological advantages from deep-sea bacteria should be considered *in vitro* by using free flow roller tank, variable oxygen concentration (based on *in situ* CTD profiles; **Manuscript I**), sediment plumes **(Manuscript II)**, and heavy metal resistant/sensitive bacteria isolated during this work **(Manuscript III)**. The bacterial composition and metals concentration overtime should be monitor using classic microbiological approach and ICP-OES for metal content. Response from marine snow and degradation rate change should also be considered.

5 CONCLUDING REMARKS

This doctoral thesis has attempted to draw a comprehensive picture of the anticipated impacts from sediment plume dispersion caused by deep-sea mining activities. Based on multi-disciplinary research approaches, this work has described the particularities of the nodules belt area in the Pacific using general oceanographic concepts followed by microscale resolution methods characterizing particulate matter distribution, sediment aggregation processes and cultivable microbes. The optimization of sediment aggregation processes has proven to be an efficient way to reduce the impacted area from the mining plume. We further proposed the use of sediment-derived cultivable microbes to monitor the residual suspension of the sediment plumes once it is becoming undetectable by current technologies. The research carried out during this project as allowed the development and implementation of instruments that are both utilizable *in-situ* and *ex-situ* for future environmental monitoring study. The results of this thesis complement the scientific effort made in describing the deep-sea environment and contribute to developpe tools to minimize the impact from a potential mining activity.

One question was repeatedly asked of me during this project, "*Do you think deep-sea mining should be carried out*? "

The answer is complex and resides in a combination of multiple factors. Economically thinking, deep-sea mining will allow countries to find an alternative to the current market monopolies from China. What would happen when the supplies stop or the cost become too expensive? In terms of ecological impact, deep-sea mining will remove irreplaceable resources for marine life. However, the next mining generations have high standards and regulations in order to minimize the ecological impacts. Finally, the social economical aspect of mining will require trained personnel, which will reduce, to a certain extent, the human exploitation of third world countries. As a scientist, I believe mining should not happen. We should preserve what is left of our planet's prestine ecosystems and focus on restoring environments instead of destroying them. Overall, we might not be able to prevent deep-sea mining and we should therefore anticipate and be prepared to advise appropriate industrial practices to limit the ecological impacts on fragile environments exposed to mining activities. These practices could be such as those

outlined in the discussion, e.g. the use of an optimize sediment discharge (high sediment concentration and turbulence); sediment plume release as close as possible to the seafloor; limitation of the mining period to avoid high productivity season; adapted contingency plan to avoid any sediment release into the upper 400 m (no influence on primary productivity or OMZ contamination).

Reference

Aleynik, D., Inall, M. E., Dale, A., and Vink, A. (2017). Impact of remotely generated eddies on plume dispersion at abyssal mining sites in the Pacific. *Sci. Rep.* 7, 1–14. doi:10.1038/s41598-017-16912-2.

Amon, D. J., Ziegler, A. F., Dahlgren, T. G., Glover, A. G., Goineau, A., Gooday, A. J., et al. (2016). Insights into the abundance and diversity of abyssal megafauna in a polymetallic-nodule region in the eastern Clarion-Clipperton Zone. *Sci. Rep.* 6, 1–12. doi:10.1038/srep30492.

Ayers, J. M., and Lozier, M. S. (2010). Physical controls on the seasonal migration of the North Pacific transition zone chlorophyll front. *J. Geophys. Res. Ocean.* 115, 1–11. doi:10.1029/2009JC005596.

Azam, F., and Long, R. A. (2001). Sea snow microcosms. *Nature* 414, 495–496. doi:10.1080/08940889508602814.

Caldeira, K., and Wickett, M. E. (2003). Anthropogenic carbon and ocean pH. *Nature* 425, 365. doi:10.1038/425365a.

Cavan, E. L., Trimmer, M., Shelley, F., and Sanders, R. (2017). Remineralization of particulate organic carbon in an ocean oxygen minimum zone. *Nat. Commun.* 8, 1–9. doi:10.1038/ncomms14847.

Constable, A. J., Melbourne-Thomas, J., Corney, S. P., Arrigo, K. R., Barbraud, C., Barnes, D. K. A., et al. (2014). Climate change and Southern Ocean ecosystems I: How changes in physical habitats directly affect marine biota. *Glob. Chang. Biol.* 20, 3004–3025. doi:10.1111/gcb.12623.

Dankers, P. J. T., and Winterwerp, J. C. (2007). Hindered settling of mud flocs: Theory and validation. *Cont. Shelf Res.* 27, 1893–1907. doi:10.1016/j.csr.2007.03.005.

Ferguson, R. I., and Church, M. (2004). A Simple Universal Equation for Grain Settling Velocity. *J. Sediment. Res.* 74, 933–937. Available at: http://dx.doi.org/10.1306/051204740933.

Fernández-Álamo, M. A., and Färber-Lorda, J. (2006). Zooplankton and the oceanography of the eastern tropical Pacific: A review. *Prog. Oceanogr.* 69, 318–359. doi:10.1016/j.pocean.2006.03.003.

Fryxell, G. A., Taguchi, S., and El-Sayed, S. Z. (1979). "Vertical distribution of diverse phytoplankton communities in the central Pacific," in *Marine geology and oceanography of the Pacific manganese nodule province*, ed. by J. L. B. and D. Z. Piper (Plenum Publishing Corporation), 203–239. doi:https://doi.org/10.1007/978-1-4684-3518-4_6.

Gollner, S., Kaiser, S., Menzel, L., Jones, D. O. B., Brown, A., Mestre, N. C., et al. (2017). Resilience of benthic deep-sea fauna to mining activities. *Mar. Environ. Res.* 129, 76–101. doi:10.1016/j.marenvres.2017.04.010.

Hamm, C. E. (2002). Interactive aggregation and sedimentation of diatoms and clay-sized lithogenic material, Limnol.Oceanogr..pdf. *Limnol. Oceanogr.* 47, 1790–1795.

Hauton, C., Brown, A., Thatje, S., Mestre, N. C., Bebianno, M. J., Martins, I., et al. (2017). Identifying Toxic Impacts of Metals Potentially Released during Deep-Sea Mining - A Synthesis of the Challenges to Quantifying Risk. *Front. Mar. Sci.* 4, 1–13. doi:10.3389/fmars.2017.00368.

Hondt, S. D., Jørgensen, B. B., Miller, D. J., Batzke, A., Blake, R., Cragg, B. A., et al. (2004). Distributions of Microbial Activities in Deep Subseafloor Sediments. *Science (80-.).* 306, 2216–2222.

Hughes, D. J., Shimmield, T. M., Black, K. D., and Howe, J. A. (2015). Ecological impacts of large-scale disposal of mining waste in the deep sea. *Sci. Rep.* 5, 1–11.

doi:10.1038/srep09985.
Iversen, M. H., and Robert, M. L. (2015). Ballasting effects of smectite on aggregate formation and export from a natural plankton community. *Mar. Chem.* 175, 18–27. doi:10.1016/j.marchem.2015.04.009.
Jankowski, J. A., Malcherek, A., and Zielke, W. (1996). Numerical modeling of suspended sediment due to deep-sea mining. *J. Geophys. Res. C Ocean.* 101, 3545–3560. doi:10.1029/95JC03564.
Jankowski, J. A., and Zielke, W. (1997). Data Support for Modelling of Deep-Sea Mining Impacts. in *Seventh Interational Offshore and Polar Engineering Conference*, 451–460. Available at: http://citeseerx.ist.psu.edu/viewdoc/summary?doi=10.1.1.196.1886.
Kanzog, C., Ramette, A., Quéric, N. V., and Klages, M. (2009). Response of benthic microbial communities to chitin enrichment: An in situ study in the deep Arctic Ocean. *Polar Biol.* 32, 105–112. doi:10.1007/s00300-008-0510-4.
Koschinsky, A. (2001). Heavy metal distributions in Peru Basin surface sediments in relation to historic, present and disturbed redox environments. *Deep. Res. Part II Top. Stud. Oceanogr.* 48, 3757–3777. doi:10.1016/S0967-0645(01)00066-2.
Larsson, A. I., van Oevelen, D., Purser, A., and Thomsen, L. (2013). Tolerance to long-term exposure of suspended benthic sediments and drill cuttings in the cold-water coral Lophelia pertusa. *Mar. Pollut. Bull.* 70, 176–188. doi:10.1016/j.marpolbul.2013.02.033.
Lohrer, A. M., Thrush, S. F., Hewitt, J. E., Berkenbusch, K., Ahrens, M., and Cummings, V. J. (2004). Terrestrially derived sediment: Response of marine macrobenthic communities to thin terrigenous deposits. *Mar. Ecol. Prog. Ser.* 273, 121–138. doi:10.3354/meps273121.
Lutz, M. J., Caldeira, K., Dunbar, R. B., and Behrenfeld, M. J. (2007). Seasonal rhythms of net primary production and particulate organic carbon flux to depth describe the efficiency of biological pump in the global ocean. *J. Geophys. Res. Ocean.* 112. doi:10.1029/2006JC003706.
MacDonell, M. T., Singleton, F. L., and Hood, M. A. (1982). Diluent composition for use of API 20E in characterizing marine and estuarine bacteria. *Appl. Environ. Microbiol.* 44, 423–427.
Orr, J. C., Fabry, V. J., Aumont, O., Bopp, L., Doney, S. C., Feely, R. A., et al. (2005). Anthropogenic ocean acidification over the twenty-first century and its impact on calcifying organisms. *Nature* 437, 681–686. doi:10.1038/nature04095.
Pabortsava, K., Purser, A., Wagner, H., and Thomsen, L. (2011). The influence of drill cuttings on physical characteristics of phytodetritus. *Mar. Pollut. Bull.* 62, 2170–2180. doi:10.1016/j.marpolbul.2011.07.002.
Patin, N. V., Duncan, K. R., Dorrestein, P. C., and Jensen, P. R. (2016). Competitive strategies differentiate closely related species of marine actinobacteria. *ISME J.* 10, 478–490. doi:10.1038/ismej.2015.128.
Paul, S. A. L., Gaye, B., Haeckel, M., Kasten, S., and Koschinsky, A. (2018). Biogeochemical Regeneration of a Nodule Mining Disturbance Site: Trace Metals, DOC and Amino Acids in Deep-Sea Sediments and Pore Waters. *Front. Mar. Sci.* 5, 1–17. doi:10.3389/fmars.2018.00117.
Pierce, S. D., Barth, J. A., Shearman, R. K., and Erofeev, A. Y. (2012). Declining Oxygen in the Northeast Pacific. *J. Phys. Oceanogr.* 42, 495–501. doi:10.1175/jpo-d-11-0170.1.
Ploug, H., and Bergkvist, J. (2015). Oxygen diffusion limitation and ammonium production within sinking diatom aggregates under hypoxic and anoxic conditions. *Mar. Chem.* 176, 142–149. doi:10.1016/j.marchem.2015.08.012.
Polovina, J. J., Howell, E., Kobayashi, D. R., and Seki, M. P. (2001). The transition zone

chlorophyll front, a dynamic global feature defining migration and forage habitat for marine resources. *Prog. Oceanogr.* 49, 469–483. doi:10.1016/S0079-6611(01)00036-2.

Resources, G. S. M. (2018). Environmental Impact Statement. Available at: https://www.deme-group.com/gsr/news/gsr-publishes-its-prior-environmental-impact-statement-relating-2019-patania-ii-disturbance.

Scott, K. (1984). "Hindered settling of a suspension of spheres : critical evaluation of equations relating settling rate to mean particle diameter and suspension concentration.," in *CSIR report, CENG 497*, ed. Pretoria, 98.

Simon, M., Grossart, H. P., Schweitzer, B., and Ploug, H. (2002). Microbial ecology of organic aggregates in aquatic ecosystems. *Aquat. Microb. Ecol.* 28, 175–211. doi:10.3354/ame028175.

Smith, S. D. A., and Rule, M. J. (2001). The effects of dredge-spoil dumping on a shallow water soft-sediment community in the Solitary Islands Marine Park, NSW, Australia. *Mar. Pollut. Bull.* 42, 1040–1048. doi:10.1016/S0025-326X(01)00059-5.

Stevenson, C. J., Talling, P. J., Sumner, E. J., Masson, D. G., Frenz, M., and Wynn, R. B. (2014). On how thin submarine flows transported large volumes of sand for hundreds of kilometres across a flat basin plain without eroding the sea floor. *Sedimentology* 61, 1982–2019. doi:10.1111/sed.12125.

Stratmann, T., Van Oevelen, D., Lins, L., Purser, A., Marcon, Y., Rodrigues, C. F., et al. (2018). Abyssal plain faunal carbon flows remain depressed 26 years after a simulated deep-sea mining disturbance. *Biogeosciences* 15, 4131–4145. doi:10.5194/bg-15-4131-2018.

Thiele, S., Fuchs, B. M., Amann, R., and Iversen, M. H. (2015). Colonization in the photic zone and subsequent changes during sinking determine bacterial community composition in marine snow. *Appl. Environ. Microbiol.* 81, 1463–1471. doi:10.1128/AEM.02570-14.

Trannum, H. C., Nilsson, H. C., Schaanning, M. T., and Øxnevad, S. (2010). Effects of sedimentation from water-based drill cuttings and natural sediment on benthic macrofaunal community structure and ecosystem processes. *J. Exp. Mar. Bio. Ecol.* 383, 111–121. doi:10.1016/j.jembe.2009.12.004.

Vanreusel, A., Hilario, A., Ribeiro, P. A., Menot, L., and Arbizu, P. M. (2016). Threatened by mining, polymetallic nodules are required to preserve abyssal epifauna. *Sci. Rep.* 6, 1–6. doi:10.1038/srep26808.

Venrick, E. L. (1988). The vertical distributions of chlorophyll and phytoplankton species in the North Pacific central environment. *J. Plankton Res.* 10, 987–998. doi:10.1093/plankt/10.5.987.

Vinnikov, K. Y., and Gordy, C. (2003). Global Warming Trend of Mean Tropospheric Temperature Observed by Satellites. *Science (80-.).* 302, 269–272. doi:10.1126/science.1087910.

Von Stackelberg, U. (2000). "Manganese nodules of the Peru basin," in *Handbook of Marine Mineral Deposits (Marine Science)*, ed. D. S. Cronan (CRC Press), 197–238.

Winder, M., and Sommer, U. (2012). Phytoplankton response to a changing climate. *Hydrobiologia* 698, 5–16. doi:10.1007/s10750-012-1149-2.

Winterwerp, J. C. (2002). On the Flocculation and Settling Velocity of Esturine Mud. *Cont. Shelf Res.* 22, 1339–1360. doi:10.1016/S0278-4343(02)00010-9.

Xu, J. P., Barry, J. P., and Paull, C. K. (2013). Small-scale turbidity currents in a big submarine canyon. *Geology* 41, 143–146. doi:10.1130/G33727.1.

Yawata, Y., Cordero, O. X., Menolascina, F., Hehemann, J.-H., Polz, M. F., and Stocker, R. (2014). Competition-dispersal tradeoff ecologically differentiates recently speciated

marine bacterioplankton populations. *Proc. Natl. Acad. Sci.* 111, 5622–5627. doi:10.1073/pnas.1318943111.

APPENDIX

Author contributions

Manuscript I

Gillard, B., Purkiani, K., Chatzievangelou, D., Vink, A., Iversen, M.H. and Thomsen, L., 2019. Physical and hydrodynamic properties of deep sea mining-generated, abyssal sediment plumes in the Clarion Clipperton Fracture Zone (eastern-central Pacific).

Specific contribution to manuscript (% of BG's to the total workload)

BG (50%), KP, LT designed the study. BG (70%), KP, AV, DC and MIH performed experimental work, and data analysis. BG (40%) and DC prepared figures and tables. BG (60%), KP, DC, AV, MIH, LT wrote the manuscript. AV procured the environmental samples. KP was responsible for the modelling section.

Manuscript II

Gillard, B., Chatzievangelou, D., Thomsen, L., Ullrich, M. S. Heavy-metal-resistant microorganisms in deep-sea sediments disturbed by mining activity: an application towards the development of experimental in vitro systems.

Specific contribution to manuscript (% of BG's to the total workload)

BG (80%), LT, MU designed the study. BG (100%) performed experimental work, and data analysis. BG (40%) and DC prepared figures and tables. BG (70%), DC, LT, MU wrote the manuscript.

Manuscript III

Gillard, B., Harbour, R. P., Nowald, N., Thomsen, L., Iversen, M.H., From the surface to the seafloor, vertical profile of particulate matter in the Clarion Clipperton fracture zone (eastern-central Pacific).

Specific contribution to manuscript (% of BG's to the total workload)

BG (60%), NW, LT and IMH designed the study. BG (75%), HRP and IMH performed experimental work, and data analysis. BG (100%) prepared figures and tables. BG (70%), HRP, NW, LT and IMH wrote the manuscript.

Appendix

Additional co-author contributions

The numerical analysis of sediment transport induced by deep sea mining activity in the northeastern tropical Pacific Ocean

Kaveh Purkiani[a,*], André Paul[a], Benjamin Gillard[a,b], Annemiek Vink[c], Michael Schulz[a], Laurenz Thomsen[b], Maren Walter[d]

[a] *Center for Marine Environmental Sciences and Faculty of Geosciences, University of Bremen, Germany*
[b] *Jacobs University of Bremen, Germany*
[c] *Federal Institute for Geosciences and Natural Resources, Hannover, Germany*
[d] *Institute for Environmental Physics, University of Bremen, Germany*

In preparation for submission to Deep sea research Part II

Abstract

A numerical modeling study is conducted in the German license area in the northeastern tropical Pacific Ocean to investigate the environmental impact of mining exploitation. A nested model approach using the MITgcm (Massachusetts In-stitute of Technology general circulation model) is applied, further developed, and validated against oceanographic measurements obtained in this region. Two different flow conditions for determination of the disturbances were introduced in our study; i) a high energetic flow from March to June and ii) a low energetic condition from September to November. While the sediment deposition under normal benthic flow condition is mainly driven by the predominant east to southeast flow, higher deep-sea flow condition has a significant impact on the pattern and amount of sediment deposition in the deep ocean. The sediment are drifted for a few kilometers from the release point following the main current direction. The height of resettled sediment in low energetic condition follows a linear trend. Whereas, at high energetic flow condition no clear pattern could be identified. Analysis of sediment deposition indicated that deposition height and pattern are generally controlled by the local current properties, particle sinking velocity and sediment supply availability in the model. The model results shows that as long as the sediment is supplied to the system, a closely linear trend of deposition rate is obtained in the normal benthic regime condition, while a parabolic trend with the higher values is taken during the benthic eddy condition. New evidences of nonlinear deep-sea sediment transport mechanism have been revealed by a series of sensitivity analysis in our study. With applying the similar amount of sediment mass undergoes with identical benthic flow condition, the model results reveal different pattern of depositions when only various

mass release strategies were employed. In contrast to ex-situ analysis carried out with similar hydrodynamic condition in deep ocean, the results of numerical simulations do not show a natural seabed erosion in neither of flow conditions. Unfortunately, the predictions for industrial sediment discharges must still be treated with caution due to the insufficient amount of support data

Versicherung an Eides Statt / *Affirmation in lieu of an oath*

gem. § 5 Abs. 5 der Promotionsordnung vom 18.06.2018 /
according to § 5 (5) of the Doctoral Degree Rules and Regulations of 18 June, 2018

Ich / I, Benjamin Gillard, Lange Reihe 39, 28219, Bremen
(Vorname / First *Name*, Name / *Name*, Anschrift / *Address*, ggf. Matr.-Nr. / *student ID no., if applicable)*

versichere an Eides Statt durch meine Unterschrift, dass ich die vorliegende Dissertation selbständig und ohne fremde Hilfe angefertigt und alle Stellen, die ich wörtlich dem Sinne nach aus Veröffentlichungen entnommen habe, als solche kenntlich gemacht habe, mich auch keiner anderen als der angegebenen Literatur oder sonstiger Hilfsmittel bedient habe und die zu Prüfungszwecken beigelegte elektronische Version (PDF) der Dissertation mit der abgegebenen gedruckten Version identisch ist. / *With my signature I affirm in lieu of an oath that I prepared the submitted dissertation independently and without illicit assistance from third parties, that I appropriately referenced any text or content from other sources, that I used only literature and resources listed in the dissertation, and that the electronic (PDF) and printed versions of the dissertation are identical.*

Ich versichere an Eides Statt, dass ich die vorgenannten Angaben nach bestem Wissen und Gewissen gemacht habe und dass die Angaben der Wahrheit entsprechen und ich nichts verschwiegen habe. / *I affirm in lieu of an oath that the information provided herein to the best of my knowledge is true and complete.*

Die Strafbarkeit einer falschen eidesstattlichen Versicherung ist mir bekannt, namentlich die Strafandrohung gemäß § 156 StGB bis zu drei Jahren Freiheitsstrafe oder Geldstrafe bei vorsätzlicher Begehung der Tat bzw. gemäß § 161 Abs. 1 StGB bis zu einem Jahr Freiheitsstrafe oder Geldstrafe bei fahrlässiger Begehung. / *I am aware that a false affidavit is a criminal offence which is punishable by law in accordance with § 156 of the German Criminal Code (StGB) with up to three years imprisonment or a fine in case of intention, or in accordance with § 161 (1) of the German Criminal Code with up to one year imprisonment or a fine in case of negligence.*

Bremen,
Ort / *Place*, Datum / *Date*

Unterschrift / *Signature*